NTNU

Norwegian University of
Science and Technology

Characterization of the airflow distribution in close proximity to a patient in operating rooms with laminar airflow at St. Olavs Hospital

Madeleine Charlotte Aviles Storås

NTNU

Norwegian University
of Science and Technology

Department of Energy
and Process Engineering

EPT-M-2017-84

MASTER THESIS

for

Student Madeleine Charlotte Aviles Storås

Spring 2017

Characterization of the airflow distribution in close proximity to a patient in operating rooms
with laminar airflow at St. Olavs Hospital

*Karakterisering av luftfordeling i umiddelbar nærhet til en pasient i en operasjonsstue med LAF
tak på St. Olavs Hospital*

Background and objective

In modern hospitals, among surgical patients surgical-site infections (SSIs) are the most common
hospital-acquired infections accounting for 36% of nosocomial infections. Tremendous efforts
have been made to understand the general and procedure-specific patient risk factors for the
development of postoperative surgical site infection. However, the nature of the turbulence
airflow and the complex dynamic biochemical process prevent the identification and
quantification of the effect of airflow on SSI. Ultra-clean ventilation systems and laminar air
flow ceilings have been used in ORs to improve the cleanliness of indoor air. However, another
individual study showed significantly higher severe SSI rates following knee prosthesis and
significantly higher SSI rates following hip prosthesis under laminar airflow conditions.

St. Olavs Hospital has 43 operating rooms and over 1000 patient bed. A recent internal study
completed in 2016 at St Olavs Hospital investigated 587 patients who have been operated at the
hospital and found the postoperative infection rate was 3.4%, which is higher than other type of
infections. This master project will carry out field measurements in two operating rooms at St.
Olavs Hosptial with laminar airflow and mixing ventilation systems, respectively.

The objective of this study is to characterise the airflow distribution in close proximity to a
patient in one operating room with a laminar airflow system at St Olavs Hosptial.

The following tasks are to be considered:

1. Literature review: state of the art analysis of the airflow distribution close to a patient in an
   operating room with a laminar airflow system.
2. Model the thermal plumes from a patient in an operating room.
3. Conduct experimental measurements of airflow distribution close to a patient in one
   operating room and the laboratory with a laminar airflow system.
4. Analyse the effect of thermal plumes on the airflow distribution in an operating room.
5. Provide suggestions and guidance to design the airflow distribution in operating rooms to
   avoid the transmission of the indoor airborne pollutants to operating sites.

Within 14 days of receiving the written text on the master thesis, the candidate shall submit a research plan for his project to the department.

When the thesis is evaluated, emphasis is put on processing of the results, and that they are presented in tabular and/or graphic form in a clear manner, and that they are analyzed carefully.

The thesis should be formulated as a research report with summary both in English and Norwegian, conclusion, literature references, table of contents etc. During the preparation of the text, the candidate should make an effort to produce a well-structured and easily readable report. In order to ease the evaluation of the thesis, it is important that the cross-references are correct. In the making of the report, strong emphasis should be placed on both a thorough discussion of the results and an orderly presentation.

The candidate is requested to initiate and keep close contact with his/her academic supervisor(s) throughout the working period. The candidate must follow the rules and regulations of NTNU as well as passive directions given by the Department of Energy and Process Engineering.
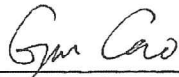
Risk assessment of the candidate's work shall be carried out according to the department's procedures. The risk assessment must be documented and included as part of the final report. Events related to the candidate's work adversely affecting the health, safety or security, must be documented and included as part of the final report. If the documentation on risk assessment represents a large number of pages, the full version is to be submitted electronically to the supervisor and an excerpt is included in the report.

Pursuant to "Regulations concerning the supplementary provisions to the technology study program/Master of Science" at NTNU §20, the Department reserves the permission to utilize all the results and data for teaching and research purposes as well as in future publications.

The final report is to be submitted digitally in DAIM. An executive summary of the thesis including title, student's name, supervisor's name, year, department name, and NTNU's logo and name, shall be submitted to the department as a separate pdf file. Based on an agreement with the supervisor, the final report and other material and documents may be given to the supervisor in digital format.

☐ Work to be done in lab (Water power lab, Fluids engineering lab, Thermal engineering lab)
☐ Field work

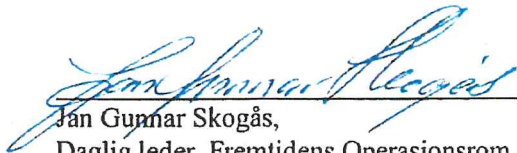Department of Energy and Process Engineering, March 1, 2017

Guangyu Cao
Academic Supervisor

Research Advisors:

Liv- Inger Stenstad,
Forskningskoordinator, Fremtidens Operasjonsrom, St. Olavs Hospital

Jan Gunnar Skogås,
Daglig leder, Fremtidens Operasjonsrom, St. Olavs Hospital

Preface

This master's thesis is written at Department of Energy and Process Engineering at The Norwegian University of Science and Technology during the spring semester of 2017. The thesis is written in collaboration with Fremtidens Operasjonsrom (FOR) at St. Olavs Hospital in Trondheim.

Madeleine Charlotte A. Storås
Trondheim, July 2017

Abstract

This master's thesis has investigated the airflow distribution in close proximity to a patient in a laminar airflow ventilated operating theatre. The assignment was divided into three different scenarios, that each consider an important aspect in the assignment. Scenario 1 considers the effect that warm surfaces close to an operating table has on the air distribution above the table. A thermal manikin was used to study thermal plume generated by both natural and forced convection. In Scenario 2 the plume above a thermal manikin is studied in a non-ventilated room and in Scenario 3 the interaction between a thermal plume generated by a patient and the laminar airflow ventilation system is investigated. All of the scenarios were investigated experimentally, and the majority of the results are presented as contour plots.

First it was investigated whether the airflow from the ceiling, laminar air supply diffuser was affected by the presence of warm surfaces around the operating table. Three heated cylinders and two surgical lamps were placed around the table and several different cases were studied. The obtained result was that the convective airflow had an impact on the air distribution above the operating table. The surgical lamps had the greatest impact on the air distribution above the table, as their placement between the air supply diffuser and the table hindered the airflow to reach the operating table. Lamps placed in horizontal position was discovered to block the airflow the most. The addition of surgical lamps also increased the turbulence level above the table to a much higher level. This indicate that the placement of the lamps above the surgical zone should be considered carefully before an operation. The first scenario did also show that the addition of thermal plumes can cause larger local temperature gradients and higher local air speeds above the operating table.

Velocity profiles above a thermal manikin in a non-ventilated room were obtained. The purpose of this was to investigate the potential the thermal plume has on the air distribution in a room. The experiment showed that the greatest plume was developed above the manikin's stomach, and the maximum velocity was 0.139 m/s. By the measured velocity profile above the stomach, two different approaches were used to suggest a mathematical equation for the plume development, and it was suggested to model it as a point source.

Lastly, the interaction between a thermal plume from a patient and clean airflow from the supply diffuser was investigated. It was shown that the convective airflow from the thermal manikin had an impact on the airflow from the ventilation system, which also was concluded by measurements performed on above a real human. This indicates that the human thermal plume should be considered when designing laminar airflow ventilation systems.

Several limitations made it challenging to solve the main objective of the master's thesis, and the conclusions from the experiments should therefore be looked deeper into. However, some observations were done that hopefully will contribute to the lack of previous studies on the field. The thesis does also give some observations that can be considered for design of ventilation systems.

Sammendrag

Denne oppgaven har studert luftfordelingen i nærheten av en pasient i en operasjonsstue ventilert av et LAF-tak. Oppgaven ble løst ved hjelp av tre forskjellige scenarier, som hver er med på å besvare formålet med oppgaven. I Scenario 1 ble det fokusert på å studere hvilke påvirkning varme flater rundt operasjonsbordet har på luftfordelingen over operasjonsbordet. En termisk dukke ble brukt til å analysere varmestrøm via både fri- og tvungen konveksjon. I Scenario 2 er det fokusert på hastighetsprofilen over den termiske dukken i et rom uten ventilasjon, mens i Scenario 3 er interaksjonen mellom den konvektive luftstrømmen som stiger fra den termiske dukken og luftstrømmene fra LAF-taket studert. Alle scenarioene er løst eksperimentelt, og resultatene er blant annet presentert som kontur-plots.

Det ble først analysert hvorvidt luftstrømmene fra LAF-taket ble påvirket av flere varme flater rundt operasjonsbordet. Tre oppvarmede sylindere og to lamper ble derfor plassert rundt pasienten. Resultatet var at det var tydelig at konvektiv luftstrøm generert av varme overflater påvirket luftstrømmen over pasienten. Det var plasseringen av de kirurgiske lampene som påvirket luftstrømmene mest, da luften ble mest blokkert når lampene var plassert horisontalt over bordet. Turbulensintensiteten over bordet økte også kraftig ved bruk av lamper. Dette indikerer at plasseringen av lampene bør vurderes nøye før en operasjon for å sikre at den rene luftstrømmen fra ventilasjonssystemet når ned til operasjonsfeltet. Scenario 1 viste også at konvektive luftstrømmer kan skape høye lokale temperaturgradienter og høyere lokale hastigheter over operasjonsbordet.

Hastigheter ble målt over en termisk dukke i et rom uten ventilasjon. Hensikten med dette var å finne ut hvor stort potensiale den konvektive luftstrømmen som genereres av dukken kan ha på luftfordelingen i et rom. Det ble funnet ut at det ble generert høyest hastigheter over dukkens mage, der den største hastigheten var på 0.139 m/s. Ut fra hastighetsprofilen over magen ble det foreslått to forskjellige linkninger for utviklingen av den konvektive luftstrømmen, der det ble foreslått å modellere magen som en punktkilde.

Til slutt var det ønskelig å studere samhandlingen mellom den kovektive luftstrømmen generert av dukken og luftstrømmene fra det laminære ventilasjonssystemet. Resultatet ble at luftstrømmene fra ventilasjonen ble redusert noe av tilstedeværelsen av en termisk dukke. Dette stemte overens med målinger gjort i nærhet av et ekte menneske, noe som indikerer at det bør tas hensyn til konvektive luftstrømmer ved utforming av slike ventilsjonsanlegg.

Det var flere begrensninger som førte til flere utfordringer knyttet til å løse oppgaven og det bør det knyttes noe tvil til resultatene. Likevel gir denne oppgaven et insikt i luftfordelingen i nærhet av pasienten, og kan forhåpentligvis bli brukt i arbeidet om å minke forekomsten av postoperative sårinfeksjoner. Oppgaven viser også viktigheten av å vurdere konvektive luftstrømmer ved dimensjonering av ventilasjonssystemer, for å sikre at ren luft når frem til sitt formål.

Contents

List of Figures

List of Tables

Nomenclature

A	Area	m^2
A_c	Convective surface area	m^2
β	Volumetric thermal expansion coefficient	K^{-1}
C	Constant	
C_b	Proportionality constant	
C_d	Discharge coefficient	
c_p	Specific heat capacity	$kJ/(kg \cdot K)$
clo	Clothing insulation	$m^2 \cdot K/W$
d	Diameter	m
DR	Draft rate	$\%$
E_0	Zero flow current output	mA
E_{FS}	Full scale current output	mA
E_{out}	Measured output current signal	mA
g	Gravitational Constant	$9.81 m/s^2$
H	Body height	cm
h_c	Heat transfer coefficient	$W/(m^2 \cdot K)$
i	Subscript, an integer ≥ 1	
$\dot{m}_p$	Mass flow rate, plume	kg/s
MET	Metabolic rate	W/m^2
n	Subscript, an integer ≥ 1	
N	Number of readings in a given location	
$\dot{Q}_c$	Convective heat output	kW
$\dot{Q}_k$	Convective heat output	W
$\dot{Q}_l$	Flow rate of plume above a heat source	m^3/h
q_z	Volume flow rate	m^3/s
R_a	Free area ratio	
R_t	Width of air temperature excess profile	m
R_v	With of air velocity profile	m
r	Radius distance for actual plume axis	m
ρ	Density	kg/m^3
S_v	Standard deviation	
T_0	Room temperature	K

T_a	Surface temperature	K
$t_{a,l}$	Local air temperature	$°C$
Tu	Turbulence intensity	$\%$
ΔT	Temperature difference	K
Δt_m	Maximum air temperature excess	K
U_0	Centerline velocity	m/s
U_m	Maximum velocity	m/s
U_o	Discharge velocity	m/s
U_{oc}	Discharge velocity based on core area	m/s
V	Velocity	m/s
V_{FS}	Full scale velocity	m/s
$\overline{v}$	Mean velocity	m/s
$\overline{v}_{a,l}$	Local mean air velocity	m/s
v_{zm}	Maximum vertical air velocity component	m/s
W	Body weight	kg
z	Cartesian coordinate in the vertical plane	m
z_0	Cartesian coordinate in the vertical plane, distance to virtual origin	m

Abbreviations

ADI	Approximate Distributions Integration
BCPs	Bacteria-carrying particles
BMS	Building management system
CFD	Computational fluid dynamics
CFU	Colony-forming units
DR	Draft rate
HEPA	High Efficiency Particulate Air
HTM	Health Technical Memoranda
LAF	Laminar airflow
mA	Milliampere
MCPs	Microbe-carrying particles
PIV	Particle Image Velocimetry
SD	Standard deviation
SSIs	Surgical site infections
TP	Thermal plume
TU	Turbulence intensity
UCV	Ultra-clean ventilation
UDAF	Unidirectional airflow
VariAC	Variable transformer unit

1   Introduction

1.1   Background and problem statement

Surgical site infections (SSIs) are a common problem at modern hospitals. The Norwegian Institute of Public Health reported that about 4.3% of surgical patients received an infection in the surgical site after selected surgical procedures in 2015, where 40% of these were deep infections [8]. SSIs influences mental, physical, social and financial aspects, and contributes to higher patient mortality, longer hospitalisation and imposes severe demands on health care services. And as antibiotic-resistance bacteria are developing, SSIs should be prevented and not cured.

Airborne bacteria can cause deep infections, and the main cause of SSIs comes from bacterial contamination in the operating room air, mainly emerged from skin squames shed by personnel [9]. Previous studies has revealed that the human microenvironment has a significantly higher content of microorganisms than ambient air, and that buoyancy-driven air flow around the human body is able to raise bacteria-carrying particles (BCPs) onto the critical wound [10, 11] The infection rate depends on several factors, and the cleanliness of air within the operation room is one of them, which includes the level of airborne bacteria in the air. Some types of surgery has a higher risk of infection than others (e.g. implant and orthopedic surgeries), and should be performed in an ultra-clean atmosphere [12]. But even though the current operating theatres use sterile air supplied through High Efficiency Particulate Air (HEPA) filters, SSIs are still remaining a problem. This leads to the need of a more throughout investigation of the airflow pattern in the operating theatre.

Laminar downflow ventilation systems are seen as the successor of mixing system, but research that correlates postoperative wound infections and type of ventilation system in use has not shown consistently that laminar airflow systems lead to fewer infections than mixing systems [13, 14]. From this it can be concluded that the airborne route does not play a significant role on the occurrence of wound infections, or that laminar flow systems does not perform in practice the way they should. In this master's thesis the air flow pattern from a laminar airflow (commonly abbreviated to LAF) system will be examined above the operating table, with focus on its performance in an environment with thermal plumes.

1.2   Objective of this study

The main objective of this study is to characterise the airflow distribution in close proximity to a patient in one operating room with a laminar airflow system. To ensure that the objective is reached, three sub-objectives were defined. These objectives were solved by three different scenarios which are briefly presented in the following:

- Scenario 1: Analyse the effect of thermal plumes on the airflow distribution

- Scenario 2: Study the thermal plume from a patient and suggest a mathematical formula

- Scenario 3: Study the interaction between the convective plume from the patient and the laminar airflow

1.3   Structure and methodology

Before starting on the master's thesis, a Gantt chart was developed to structure the time to ensure to reach the main objective on time. Most of the tasks went as planned, but there were spent much more time at the lab than predicted. This did of course cause less time for other important parts of the thesis. The structure of the master's thesis is divided into four main parts, which is a literature review, study of the human thermal plume, method for experimental setup and results.

The first part of this master's thesis consist of a theory and literature review. This is to give a better understanding of the state of art analysis of the airflow distribution in operating theatres and challenges regarding thermal plumes in the surgical zone. Unfortunately, previous studies from scientific articles have mainly focused on bacterial dispersion, and not directly of the airflow distribution in operating theatres. The ones that were found are mostly analysed by computational fluid dynamics (CFD) of airflow patterns and not studies based on actual experiments. This caused some challenges in the first part of the thesis.

The second part of the assignment will focus on the human thermal plume, and the development of a mathematical model will be presented. To reach the main objective of this master's thesis, three main scenarios were developed, where each of them will focus on fulfil point 2 to 4 in the assignment description. After the method and results for each scenario is presented and discussed, some suggestions to design the airflow distribution in operating rooms are provided. Lastly a conclusion is presented.

The fundamental theory used in this master's thesis is mainly obtained from books, and the university library has been useful. The scientific journal research papers usually do not explain the fundamental theory, so this was found in books. The scientific articles has been tracked down by use of databases as Scopus and Google Scholar, which are peer-reviewed databases that have been approved by real people. Other helpful databases were also found through oria.no.

1.4   Assumptions and limitations

It is important to make it clear that this master's thesis only focus is on the air distribution above the operating table in an operating theatre ventilated by LAF, and does not take into account the bacteria dispersion close to the patient. The thesis can therefore not be used to conclude whether there is a relation between SSIs and the used ventilation system. Still, the thesis does study relevant subjects which can contribute to the field, and to give some recommendations for the design of a LAF ventilation system. But the different aspects found in this study should be investigated further, as there were some assumptions and limitations in the work.

One of the main limitations in this following work is the absence of information found in previous studies. The articles found on the human thermal plume were mainly focusing on a sedentary or standing persons, and not on a lying persons. This made it challenging to suggest methods for the plume modelling, and discussion on whether the results were reliable or not. A lot of assumptions regarding the mathematical models had to be made, which should be considered again.

Another limitation were the time. As there were spent many weeks to construct both the thermal manikin and the LAF ceiling at the climate chamber at NTNU, did naturally cause time constraints in the work. The ceiling supply diffuser was tried to build as laminar by using both perforated plates and a honeycomb. As there were spent weeks at the climate

chamber, with no result of an evenly distributed airflow, it was chosen to do the measurements in the last scenario at St. Olavs Hospital. The thermal manikin was also shared with another master student, which because of her deadline had priority before me. This caused delay in the plume measurements, and of course restricted the amount of measurements which were performed at the climate chamber and at the hospital. It was not possible to obtain the direction of the airflow by using the omnidirectional anemometers. This did also cause limitations in the analysis of the results, which could have been even more examined.

2 Literature review

2.1 Hospital ventilation by laminar airflow

The main goal for a ventilation system of a hospital operating room is to provide a comfortable and healthy environment for the patient and the surgical team, and the provision of the ventilation system is crucial for protecting the patient and surgical staff against hazardous emissions [11]. The exchange of air carries several functions, and to reach an appropriate level of thermal comfort the ventilation system is used to control factors such as temperature, humidity, air circulation to minimise the migration of airborne bacteria, and dilution (preferably removal) of indoor pollutants (including waste anesthetic gases and odors from the surgical region). In this way we can provide a adequate movement of clean conditioned air to where surgery is performed, and where the sterile instruments and drapes are exposed. A goal is also to provide a comfortable working condition for the surgeons to facilitate their demanding work during an operation [9].

To prevent bacterial emission into the surgical area the ventilation air flow system must be designed carefully. An important factor that will affect the particle removal drastically is the air changes per hour. Air changes per hour is expressed as the volumetric airflow through the operating room divided by the volume of the room space [9]. However, even with the same particle source location and air changes per hour, different ventilation solutions have different particles removal efficiency.

There are mainly two different types of systems in use for ventilating operating rooms; laminar and mixing systems [13]. For mixing systems the concentration of contaminants is diluted, and a higher ventilation rate gives automatically a lower concentration of airborne contaminants, which includes bacteria and anaesthetic gases [15]. On the other hand, laminar systems are supposed to deliver clean air to critical areas before it mixes with the contaminated surrounding air. Laminar downflow systems are considered as more efficient than mixing ventilation, and Whyte et al. stated in 2015 that ventilation via laminar airflow would give substantially lower concentrations of microbe-carrying particles in operating rooms, compared to conventional ventilation [13, 16]. Chow et al. had some of the same approach and reported that the airborne infection risk can be reduced by the use of low-velocity laminar airflow, as it tends to direct the airborne contaminants toward the exhaust outlets [15]. However, research has not shown consistently that laminar airflow systems lead to fewer postoperative wound infections than mixing systems [13, 14]. It may therefore seem that either the airborne route can not be directly linked to the occurrence of wound infections or laminar flow systems do not work in practice the way they should. In this master's thesis the airflow from a laminar ventilation system will be investigated further.

In the early 1960s it was invented a new type of clean air ventilation called ”*laminar*” air flow, with low and uniform velocity. In laminar systems the airflow moves in parallel layers at constant velocity in a single direction, from the beginning to the end of the straight-line vector [17]. Hence the robust and uniform airflow will sweep particles away from the critical processing or testing area, and in this way control airborne particulate contamination. In reality the airflow does not fulfil the aerodynamic conditions of laminar flow, as there are small differences in velocities between individual perforations discharging air from the diffuser [15]. Linear or unidirectional airflow (commonly abbreviated to UDAF) is therefore a better alternative, as the actual air pattern of the flow is in parallel lines. But it is still chosen to refer to it as laminar ventilation throughout this master's thesis. It was after the second world war that ventilation in hospitals was introduced for contamination control, and High Efficiency Particulate Air (HEPA) filters were developed to achieve a low level of airborne contamination

in the supply airflow [18]. These HEPA filters ought to remove 99.97% of particles greater than $0.3\mu m$ [19, 20]. As the bacteria-carrying particles in operating rooms range in size from $5\mu m$ to $60\mu m$, and the bacteria itself from $1\mu m$ to $2\mu m$, implies that the supplied air through HEPA filters is sterile with regard to bacterial contamination [19]. Investigations on the filters shows that filters 87% efficient against the most penetrating particle size (as specified in EN 1822) is likely to have a removal efficiency against microbe-carrying particles (MCPs) of 99.995% [16]. An *ultraclean air system* was defined as the combination of LAF and HEPA filter, and this combination was patented in 1960 [19].

LAF systems are usually classified based on the position of the diffuser, and they can be vertical, horizontal or mobile. There have been performed several studies on which solution will give the best indoor conditions for operating rooms. Common for the studies was the disruption of the airflow by different hot surfaces (lamps, people etc.) in the operating room, and different solutions may be preferred in different situations. Air sampling must be carried out close to the surgical area to be representative of the concentration at the wound. Whyte investigated on if surgical lamps and operating room personnel would affect the ventilation airflow and cause higher bacterial concentrations in the wound area below, and found out that it was a relation between dispersion and penetration of particles from a source and hot surfaces [16]. Melhado et al. stated that vertical LAF systems are more efficient than horizontal, since the clean air in this case will directly supplied over the operating table [12]. Horizontal supplied LAF will usually get disrupted by the surgical team, and is therefore not the most practical solution. Pereira et al. found out that horizontal LAF ventilation has a higher degree of contamination compared to vertical LAF, which make them less common in surgical rooms [20].

Traditionally, the design of the vertical systems have included extra side-walls enclosing the core of the ultra-clean air as shown in Figure 1 [1]. The aim by creating this operating box is to prevent bacteria-carrying particles (BCPs) from being encountered in the air in the ultra-clean-zone. The main drawbacks of such enclosures are the decreased versatility and space for the operating team in the room [21]. Friberg et al. performed a study on operating boxes with three different lengths in order to evaluate the efficiency on elimination of BCPs during standard sham operations. In this way the entrainment of peripheral contaminated air from outside the ultra-clean zone could be prevented. The study showed that the ventilation efficiency was proved to be independent of the length of the enclosures [1]. The zone close to the side-walls are known as the semi-clean zone, which should be regarded as contaminated [19].
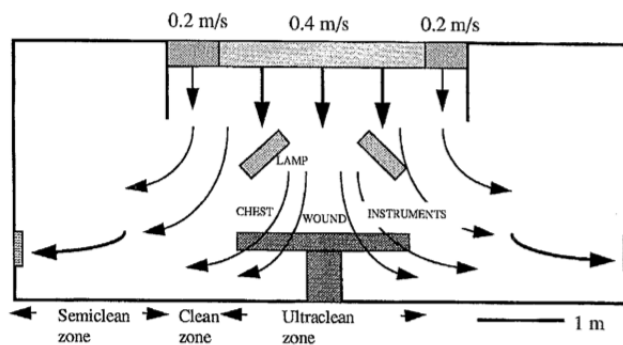
Figure 1: Airflow in a zoned vertical LAF unit with a short enclosure [1]

2.1.1 Design considerations for ventilation in healthcare premises

The Health Technical Memorandum (HTM) developed by the UK National Health Service Estates has made a design guidebook for ventilation in healthcare premises. A correspondingly guidebook was not found in the Norwegian Standard, so the HTM is used to provide some recommendations. In the guideline there is plenty of recommendations for ultra-clean ventilation (UCV) systems with supplied laminar airflow, and three specific factors that must be considered when designing a UCV is especially highlighted [22]:

- The discharge velocity from the supply unit is critical as convective up-currents from the surgical team, the operating lamp and buoyancy effects tends to counter the movement of the clean air towards the wound.

- The size of the ultra clean operating zone needs to be large enough to enclosure the operating site and instrument table. This leads to a large amount of air diffusion is required, to cover the large area of air distribution.

- The two previous mentioned considerations leads to a high discharge air volume. Recirculation of a considerably portion of this volume is essential to minimise operating costs.

The discharge velocity of the supply diffuser is crucial to ensure that sufficient air reach the operating table. In the guideline the minimum discharge velocities are discussed and dependent on the type of flow system. The minimum discharge velocity for vertical flow systems with fixed partial walls should have an average of 0.38 m/s [22]. The downward flow of clean air should provide a washing effect for removing particles in the surgical zone. Any contaminant into the air can be immediately removed by an airflow with minimum velocity of 0.2 m/s [22, 11]. Friberg et al. states that at an airflow of 0.4 m/s is optimal to remove airborne particles [19].

2.2 Laminar flow panels

Laminar flow panels are used in clean rooms, hospitals and laboratories where the supply air is required to have a low turbulence level. The panels can be either placed on a wall to produce side flow ventilation, or positioned at the ceiling to produce a downflow ventilation. Even though the flow panels are called laminar, the airflow produced by them are not completely laminar but a flow with a low amount of turbulence [4]. This type of airflow is achieved by the production of small air jets by a huge amount of perforations in the panel face. These small air jets are later merged together and form an uniform airflow. In clean rooms the panels are installed side by side to prevent entrainment of supply air with room air. In this way displacement ventilation is achieved with a low turbulence level, and the velocity remains almost constant in the room [4]. For less demanding applications, laminar flow panels may be mixed with perforated ceiling diffusers that produce conventional air jet supplies, hence the supply air from the laminar flow panels diffuses with room air as a normal jet.

For laminar, perforated flow panel outlets the core velocity can be calculated by Formula 1 [4].

$$U_c = 1.2 U_d \sqrt{C_d R_a} \tag{1}$$

In Equation 1 U_o is the velocity of the jet at the *vena contracta* of the perforations, hence $U_d = \frac{U_{oc}}{C_d R_a}$, where U_{oc} is the discharge velocity based on the core area. R_a is the ratio of free

area to gross or core area of the panel and C_d is the discharge coefficient.

For less demanding applications, laminar flow panels may be mixed with perforated ceiling diffusers that produce conventional air jet supplies. In that case the air supply from the laminar flow panels diffuses with room air as for a normal jet.

2.2.1 Air draught and turbulence intensity

Draught is defined by ISO 7730:2005 as unwanted local cooling due to air movement [23]. Air draught is a common problem for dissatisfaction due to local cooling or heating of particularly parts of the body. Experiments has been conducted to estimate the dissatisfaction due to draught for people in thermally neutral conditions. It was shown that both the relative velocity and the turbulence intensity had an impact on the occurrence of dissatisfaction [24]. This indicates that draft also can be caused by local fluctuating air velocities, and not only local cooling alone.

The draught rate (DR) express the percentage of people predicted to feel discomfort due to draught and is expressed by Formula 2 (model of draught) [23].

$$DR = (34 - t_{a,l})(\overline{v}_{a,l} - 0.05)^{0.62}(0.37 \cdot \overline{v}_{a,l} \cdot Tu + 3.14) \qquad (2)$$

Formula 2 applies for people in light, sedentary activity, and in the formula $t_{a,l}$ is the local air temperature in °C (from 20°C to 26°C), $\overline{v}_{a,l}$ is the local mean air velocity in m/s (< 0.5 m/s) and Tu is the local turbulence intensity in percent (10% to 60%).

The turbulence intensity, also known as the turbulence level, is defined as the standard deviation (S_v) of the air velocity divided by the average air velocity [24]. An expression for turbulence intensity (Tu) is given the following formula [25].

$$Tu = \frac{s_v}{\overline{v}} \cdot 100\% \qquad (3)$$

The standard deviation is given by Equation 4 [25].

$$s_v = \sqrt{\frac{1}{N-1} \sum_{i=1}^{N} (v_i - \overline{v})^2} \qquad (4)$$

In Equation 4 v_i is the velocity at each second, $\overline{v}$ is the mean velocity and N is the total numbers of sampling for the mean velocity. The mean velocity is found by equation 5 [25].

$$\overline{v} = \frac{1}{N} \cdot \sum_{i=1}^{N} v_i \qquad (5)$$

Fanger et. al. showed that periodically fluctuating airflow cause more discomfort than non-fluctuating (laminar) flow [26]. The magnitude of fluctuations in the air speed should therefore be kept below a given level. Fanger et al. proposes in their study that values for Tu<12% is a low level of turbulence, 20% < Tu <35% is a medium level of turbulence, while a Tu>55% is a high level of turbulence [26, 4]. For operating theatres, Karthikeyan et al.

denotes a turbulence level of 7.7% as a low turbulence level, and a turbulence level of 12.5% as high turbulence level [27].

2.3   Air distribution influenced by plumes

The air distribution in rooms is a result of complex interactions between forced flows generated by the ventilation system and convective flows generated by heat sources or warm- and cold surfaces within the room. As the development of low-power-consuming devices is carried out, the thermal plumes generated by lighting and equipment is assumed to decrease in the future. And for that reason the importance of plumes generated by humans will have a greater impact on the air distribution in a room [2].

As already mentioned, thermal plumes are one of the main factors to determine the air distribution in a room [5]. The plumes degree of influence on the air flow is dependent on the airflow distribution system. In published work, the effect of thermal plumes are usually discussed related to displacement ventilation, as its impact is more prominent compared to for example mixing ventilation. However, Chow et al. found that the impact of thermal plumes also is interesting to discuss related to mixing ventilation, as they can have a significant impact on the ceiling jet, and consequently the air movement in the room [28].

A thermal plume is created by a convective heat loss from a warm object, which will cause a convective boundary layer that will because of a buoyancy-effect rise and develop into a plume [4]. The buoyancy effect is the driving force of the flow, and is caused by a density difference, i.e. the temperature difference of the air in the plume and the ambient air. The larger the temperature difference between the heat source and the surroundings, the more powerful the plume will become. The geometry and power of the plume source gives knowledge of the developing vertical temperature and velocity profile in the room, and can consequently give information about thermal comfort and indoor air quality. The amount of air in the convection flow increase with height as shown in Figure 2. This is due to entrainment of surrounding air, and the amount of air transported by natural convection is dependent on the geometry and temperature of the heat source, and the temperature of the surrounding air.
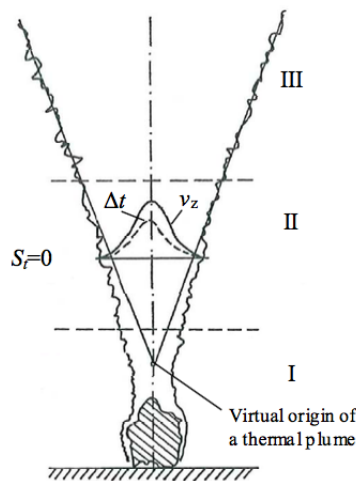
Figure 2: Sketch of flow regions in the plume above a heat source without thermal stratification ($S_t = 0$) [2]

In general, the thermal plume above a heat source can be distinguished in three regions, see Figure 2 [5]. The region closest to the heat source (the initial region) begins as a con-

vective boundary layer around the heat source. Then, the laminar flow becomes turbulent, and a thermal plumes forms. In this region, the air temperature- and velocity-profiles are not developed. The region of self-similarity of mean velocity is the second region. In this region, the plume is turbulent and axis-symmetrical with a Gaussian distributed velocity- and temperature-profile. The development of the plume in the third region is dependent on the thermal stratification of the environment and is therefore divided into two cases. If the surrounding environment does not contain thermal stratification, the plume is fully developed and spread linearly. The third region is then called the region of complete flow similarity and a sketch of this is shown in Figure 2. For plumes propagating in environments with thermal stratification, air flows out horizontally as a stratified layer where the maximum elevation is reached. This region is then called the region of the maximum plume rise. At a certain height above the heat source, most convective plumes become symmetrical, but the ceiling height is usually insufficient to allow the full development.

Figure 3 shows some characteristics for an axis-symmetric plume [3]. As seen from the figure, the highest velocity and temperature is at the centerline of the plume. The centerline velocity and temperature, denoted as u_0 and T_0 respectively, changes with height z as shown in Figure 3b. The figure also shows that both centerline velocity and temperature is decreasing with height, as more ambient air is entrained, which cools the plume. From the figure it is also shown how the mass flow rate, $\dot{m}_p$, is increasing with height.

(a) Sketch of velocity and temperature profile

(b) Development of centerline velocity and temperature
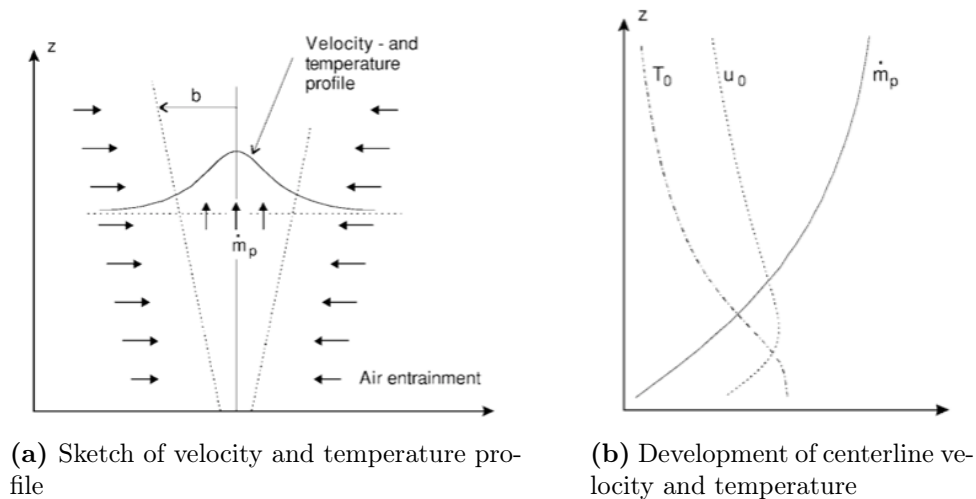
Figure 3: Some characteristics for a buoyant axis-symmetric plume [3]

2.4   The human thermal plume

Occupants are major pollution and heat sources in buildings, and the thermal flows generated by the human body have a significant impact on the room air distribution [29]. A temperature gradient between a human body surface and cooler surrounding air induces upward natural flow of the surrounding air, causing a convective boundary layer around the human body [30]. This convective boundary layer rises further developing into a thermal plume, which may disturb the LAF from supplying a particle free airflow to the surgical site at operating theatres [31].

It is important that the discharge velocity is large enough to control the thermal plume to maintain a laminar airflow in the ultra-clean zone. There were restricted amounts of articles on what is a sufficient air flow velocity to control a thermal plume generated by a lying human

body. One scientific article were found, in which was stated that a velocity above 0.2 m/s is sufficient to control the human thermal plume [31]. But this study were based on CFD and not on real experiments.

The convective heat loss from the human body is either caused by natural or forced convection [32, 33, 34]. The temperature gradient at the skin surface cause convective heat transfer in the case of natural convection. This heat transfer may be expressed non-dimensionally as the Nusselt number, which is dependent on the Grashof and Prandtl number. At forced convection a body is cooled by an airflow. In that case the heat loss is additionally dependent on Reynolds number. In both cases the convective heat loss is proportional to the temperature gradient at the skin surface. Studies show that the initial velocity in the rising plume are small, but accelerates upwards due to buoyancy [10, 35]. Upon reaching a maximum velocity, the mixing of surrounding air reduce the buoyancy-effect and decelerate the velocity.

2.4.1 Thermal manikin

Thermal manikins were originally developed to measure the thermal insulation of clothing, and have been used to simulate heat transfer between "human" and the environment for more than 60 years [36]. Today's manikins are getting more complex, where sweating and breathing mechanisms are included. This gives a better approach when analysing the thermal interface of the human body and its environment, and is useful to predict indoor environment and thermal comfort. An advantage by using thermal manikins for research is that convective, radiative and conductive heat loss can be measured over the whole surface in all directions [36]. The use of a thermal manikin is a quick, easily standardised and repeatable method, which can under the same exposure conditions measure the heat losses in a comparable, reliable and accurate way.

A manikin can be heated in several ways, and the heating system of the thermal manikin can either be placed at the outer- or inner surface of the manikin, or inside the space of the manikin (given a hollow manikin). Each of the methods have advantages and disadvantages. When using a heating system inside of the thermal manikin, high-conductivity materials such as copper and aluminium are often used for the shell to keep an uniform surface temperature [37].

There are mainly two control strategies used for the heating systems of thermal manikins. The first is to keep the heater temperature constant and the second is to keep the supply power constant. For manikins with constant power supply, temperature control may not be required. But for non-uniform environments the skin temperature can get unrealistically high or low and temperature control is therefore recommended. For a more realistic approach of a human body, almost all manikins today consists of several, independently controlled segments over the body surface. Most of the manikins consists of more than 15 segments [36]. This gives a more precise way to measure and control each part of the thermal manikin separately by a computer, and adjust the heating loads thereafter. Given steady-state conditions there has been found that heat supplied to the manikin's heating elements equals to the heat loss from the manikins outer surface [37]. The electricity consumption of each part of the manikin can therefore give the heat loss per unit skin surface area. This was used for the construction of the thermal manikin in this master's thesis.

3 Thermal plume generated by a lying human body

In this chapter, a model of the thermal plume generated by a person in supine position will be presented. There have been performed several studies of the thermal plume generated by humans, but most of them focus on a body posture in standing or sedentary position. Since there is a strongly restricted literature of studies on a person in supine position, an exact model is challenging to develop. Nevertheless, one previous article where the plume is suggested to develop as a line source were found. This formula, and other plume equations, are presented in Chapter 3.3.

The fundamental theory in this chapter is mainly found in "Ventilasjonsteknisk håndbok" by E. Skåret and "Ventilation of buildings" by H. B. Awbi. "Industrial ventilation design guidebook" by H. D. Goodfellow has also been helpful for knowledge about thermal plumes. In addition, scientific articles has been used to establish information of parts that should be considered for the model.

3.1 Mathematical model

In "Ventilasjonsteknisk håndbok" from 2000 Skåret derives formulas for plume development based on fundamental theory. In this chapter equations for plume development by a point- and a line heat source will be presented briefly. These formulas are considered at the basic theory that can be adapted based on results from my experimental measurements, and the steps for the empirical model are presented in the next sub-chapter.

According to authors like Skåret and Awbi, a thermal plume in a quiescent environment can be assumed to have a Gaussian distribution from its second region as explained in Chapter 2.3 [6, 4]. For a point source, the generated thermal plume for an axis-symmetric flow is shown in Figure 4. From the figure it is evident that air is entraining and the plume radius is increasing with height z.
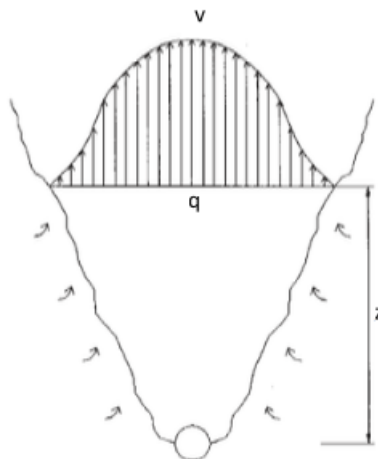
Figure 4: Sketch of thermal plume generated by a point heat source [4]

The formulas suggested by Skåret is given by Equation 6 and 7, which express the centerline velocity distribution in m/s and volume flow in m^3/s for a point source, respectively [6].

$$U_0 = \frac{1.63}{C_b^{2/3}} \cdot (\frac{g\beta}{\rho c_p})^{1/3} \cdot (\frac{\dot{Q}_c}{z + z_0})^{1/3} \tag{6}$$

$$q_z = 1.31 \cdot C_b^{4/3} \cdot (\frac{g\beta}{\rho c_p})^{1/3} \cdot \dot{Q}_c^{1/3}(z + z_0)^{5/3} \tag{7}$$

In Equation 6 and 7, the constants 1.63 and 1.31 are constants found by geometry for a point source. C_b is the proportionality constant, which is equal to tan of the spread angle of the plume, α. Skåret suggests a C_b equal to 0.238, which is based on a spread angle α equal to 13.4°. g is the gravitational acceleration in m/s^2, β is the volumetric thermal expansion coefficient given by $\frac{1}{T_{room}}$ $[\frac{1}{K}]$, ρ is the density of the fluid in kg/m^3, c_p is the specific heat capacity in kJ/kgK, and $\dot{Q}_c$ is the released convective heat output in kW. For the equations z is the Cartesian coordinate in the vertical plane, and z_0 is the distance from the source to the virtual origin, both in m.

For a line source, Skåret suggests Equation 8 and 9 for the centerline velocity and plan symmetrical volume flow, respectively [6]. For Equation 9, l is the length of the line source in m. These formulas are as for the point source applicable in an environment with no thermal stratification.

$$U_0 = \frac{1.37}{C_b^{1/3}} \cdot (\frac{g\beta}{\rho c_p})^{1/3} \cdot \dot{Q}_c^{1/3} \tag{8}$$

$$q_z = 1.23 \cdot C_b^{2/3} \cdot (\frac{g\beta}{\rho c_p})^{1/3} \cdot \dot{Q}_c^{1/3}(z + z_0) \cdot l \tag{9}$$

Note that for Equation 8 the centerline velocity is constant after the acceleration phase. A sketch of the plume generated by a line source is shown in Figure 5.
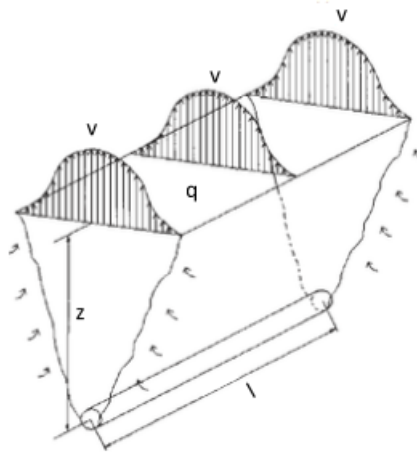
Figure 5: Sketch of thermal plume generated by a line heat source [4]

3.2   Method for empirical model

A general formula for the plume developed by a human body is hard to suggest, as it is strongly dependent on the body's geometrical shape, posture, the heat output of the human and the temperature of the surroundings. The human body has a complex shape, which is

difficult to standardise. The heat source itself is assumed to emit an unsteady flow, which can not necessarily be assumed to be Gaussian distributed. And changes of conditions in the plume surroundings are also a factor which influence the plume development. All of these challenges, and assumptions made for the development of my model will be presented in this chapter. The chapter is divided into three different parts. The first will focus on calculating the right amount of convective heat output for a patient, and the second and third will focus on a way to model the centerline velocity and volume flow by using the equations presented in Chapter 3.1. In the second part the plumes boundary is found by a correlation used in earlier studies, and in the last part of this sub-chapter the boundary is approximated by a formula for a Gaussian distributed velocity profile.

Convective heat output, $\dot{Q}_c$: Besides the proportionality constant, C_b, the convective heat output, $\dot{Q}_c$, and virtual origin, z_0, the rest of the factors in Equation 6, 7 and Equation 8 and 9 are constants that can easily be found. The values for these constant are given in Table 1. A way to estimate the proportionality constant is given in the next part of this chapter, but first the convective heat output will be studied.

Table 1: Constant properties for air at T=25 °C [6]

Parameter	Value	
g	9.81	m/s^2
β	$\frac{1}{298}$	$\frac{1}{K}$
ρ	1.20	kg/m^3
c_p	1.00	kJ/kgK

A real human emits heat by both latent and sensible heat, and several authors suggest that the convective heat output for a human is around 40% of the total heat output [10, 38]. But as seen from Equation 10, the convective heat output, $\dot{Q}_k$ [W], is strongly dependent on for instance the temperature difference of the surface temperature and surroundings, which is dependent on an given situation. The convective heat output for the heat source should therefore be calculated for the specific situation.

$$\dot{Q}_k = h_c \cdot A_c \cdot (T_a - T_o) \tag{10}$$

In Equation 10, h_c is the heat transfer coefficient in $W/(m^2K)$, A_c is the surface area in m^2 and $(T_a - T_o)$ is the temperature difference between the surface and the surroundings [K] [39].

An experiment conducted by Kurazumi et al. showed that the heat transfer coefficient, h_c, is dependent by body posture in natural convection [40]. The suggested value for calculating the convective heat transfer coefficient for a supine body in floor contact in presented by Equation 11. In the formula, ΔT is the difference between the mean skin temperature (corrected using convective heat transfer area) and air temperature, in K. Unfortunately this were the only equation for the convective heat transfer coefficient for a body in lying posture found in articles, so it was decided to use this formula for my calculations.

$$h_c = 0.881\Delta T^{0.368} \tag{11}$$

Generally, most experiments use the total body surface area as the heat transfer area involved in convective heat exchange. This does not cause great inaccuracy for postures where the body surface is actively exposed to airflow, as in standing position [41]. However, this assumption would not be reasonable for postures in sedentary and supine position, where greater parts

of the body's surface area is not exposed to air and hence not involved in convective heat exchange. Kurazumi et al. therefore performed several experiments to find the effective thermal convection area factor for a human body in different body postures [41]. Table 2 gives an overview of suggested values for convective heat transfer area for a body in supine position found in previous studies.

Table 2: Comparison of the effective thermal convection factors suggested in previous studies [7]

Investigator	Factor
Büttner (1934)	0.800
Kurazumi et al. (2003)	0.860
Kurazumi et al. (2004)	0.844
Kurazumi et al. (2008)	0.811

As seen from Table 2, the effective convective area factor for a person in supine position were studied by Büttner in 1934 and suggested to be equal to 0.8 [41]. However, this factor was only estimated and not measured and will therefore not be used in this thesis. Kurazami has researched on the convective area for several years, and suggested in 2003 first a value of 0.860. Five years later he suggests a value of 0.811, which is the chosen value for the empirical model [7]. An expression of Kurazumi et al's. convective area of a human in supine posture is given by Equation 12, where A is the body surface area in m^2.

$$A_c = 0.811 \cdot A \tag{12}$$

The DuBois and DuBois body surface area equation is the most widely used equation to calculate A, and is therefore used in this master's thesis. Even though the equation is derived from only 9 persons, their formula appears to be a valid predictor for body surface area [42]. The DuBois and DuBois formula is given by equation 13 [42, 43].

$$A = 0.007184 \cdot W^{0.425} \cdot H^{0.725} \tag{13}$$

In Equation 13, W and H is the body's weight in kg and height in cm respectively.

By using these formulas the obtained convective heat output for a person with surface area and temperature equal to 1.98 m^2 and 32°C respectively, with surrounding air temperature of 25°C, is 20.27 W.

Method 1: Finding the proportionality constant, C_b: In Chapter 3.1 equations for a point- and line sources are presented. In reality, a supine body is neither a line nor a point source, but more similar to a horizontal surface, thus z_0 in Equation 9, 6 and 7 can not be assumed equal to zero. Convective flows from horizontal surfaces are difficult to determine due to the flows unstable behaviour which leave the flat surface from different positions at different times [44]. Convective horizontal flows are mostly treated as plumes from extended surfaces, and Figure 6 is an illustration of the flow from an extended source with width w [m].
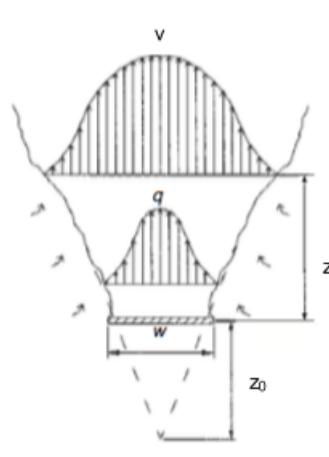
Figure 6: Sketch of thermal plume generated by a horizontal surface [4]

For extended sources, the distance between the heat source and a virtual source must be calculated, and the formula used by researchers to calculate z_0 varies. Some authors suggests to use Pythagoras' theorem, as for jets [45, 44]. Skåret suggests to use a z_0 which is 0-0.5 the times of the diameter or width of the horizontal plate [6]. In "Industrial ventilation" by Goodfellow it is suggested that the position of the virtual source is given by z_0=1.7 - 2.1 · d for a real source and z_0=1.47 - 2.25 · d for a flat plate, where d is the diameter of the heat source [44]. Heskestad claims z_0 is dependent of the convective heat output for the source [46]. Awbi suggests the following formula to calculate z_0 [4].

$$z_0 = C(\frac{d}{2} + \delta)$$ (14)

In Equation 14 C is a constant equal to 4.18 for a point source and 3.8 for a line source. d is the heat source diameter in m and δ is the boundary layer thickness in m, which is equal to 0 for a horizontal source. The value of z_0 is strongly influencing the spread angle α and should therefore be considered carefully. Since Awbi uses the same approach for a point- and a line source for Equation 14, it was chosen to use this equation with different constant C for this master's thesis.

In Skåret's equations for centerline velocity and volume flow, referring to Equation 6, 8, 7 and 9, an empirical proportionality constant C_b is introduced. The C_b is dependent on the spread angle, α, of the plume, which can be found in an empirical way. As shown in Figure 3a, b is the boundary of the plume, which is among others dependent of the height above the heat source and the amount of entraining air. For each height z, a new b can be found from the velocity profile above the heat source, which can be developed after conducting measurements. From Figure 3a it is apparent that b will increase for increasing z.

A plumes boundary, b, at height z is dependent of its maximum velocity at the same height. Both Bjørn et al. and Zukowska present in their work that the boundary at a certain height is where the velocity is given by Equation 15 [47, 2].

$$U_b = \frac{U_m}{e}$$ (15)

After finding the boundary for the convective flow, linear regression can be used to develop a fitted line for the calculated boundaries. This line will have an expression of the sort

$f(x) = ax + b$, where

$$\alpha = \arctan \frac{1}{a} \tag{16}$$

C_b is found by $C_b = \tan \alpha$, which can be used to suggest a formula for the centerline velocity and airflow above a body in supine position. Skåret suggest a C_b equal to 0.235, which was estimated based on a spread angle α equal to 13.4°.

This method is based on a lot of assumptions and should therefore be validated by using the experimental measurements in another way. Because of limitations for the experiment, for instance that velocities below 0.05 m/s were not observed by the measuring equipment (explained in Chapter 4.2.3 and the flows boundary were out of the measuring range, made it challenging to validate the model. Therefore another way to approximate the velocity profile above the thermal plume is suggested. The following method was suggested in collaboration with my supervisor, and is also based on many assumptions, for instance a Gaussian distributed velocity profile.

Method 2: Finding the plume boundary by using a Gaussian approximated velocity profile: Zukowska et al. suggests Equation 17 and 18 for respectively calculating air velocity and temperature excess when plume axis wandering is taken into account, when a Gaussian distribution is assumed [5]. Plume axis wandering is a term used in situations where deviations and movements of the plumes axis differs from the vertical position above the heat source. The phenomenon is caused by the heat source itself due to unsteady flow in the convective boundary layer or changes in the conditions of the plume surroundings [5]. Kofoed suggested in his phD-thesis from 1991 a method to correct the plume axis position [48]. This method requires multipoint measurements in two axes perpendicular to each other (in x- and y-direction) above the whole heat source. Multipoint measurements above the whole manikin were not performed in y-direction for my experiment, so this method were not applied.

$$v_z(r) = v_{zm} \cdot exp[-(\frac{r}{R_v})^2] \tag{17}$$

$$\Delta t(r) = \Delta t_m \cdot exp[-(\frac{r}{R_t})^2] \tag{18}$$

In Equation 17 and 18, v_{zm} and Δt_m is respectively the maximum vertical air velocity component and the maximum air temperature excess. R_v and R_t are the distances from the position of the maximum value to the point where the parameter is e ($e = 2.71828$) times lower than the maximum value, for velocity and temperature excess respectively, see Figure 7a.

After discussions with my supervisor it was decided to use Equation 17 for approximating the plume boundary in this master's thesis. In reality the assumption of Gaussian distribution would be incorrect for an asymmetrical thermal plume, such as generated by human bodies. But this was a chosen simplification. In Equation 17 the velocity distribution must be given. The used omnidirectional anemometers gives values for speed, which according to Zukowska differs from the velocity, meaning that the measured values should be converted into velocity [5]. Zukowska again suggests a formula for converting speed to velocity which is dependent of the turbulence intensity of the flow [5]. As it was not possible to obtain the turbulence intensity due to limitations of the used measuring equipment (explained in Chapter 4.2.3), this method was naturally not possible to use for my measurements, hence speed measurements are used.

(a) Symmetrical thermal plume   **(b)** Asymmetrical thermal plume
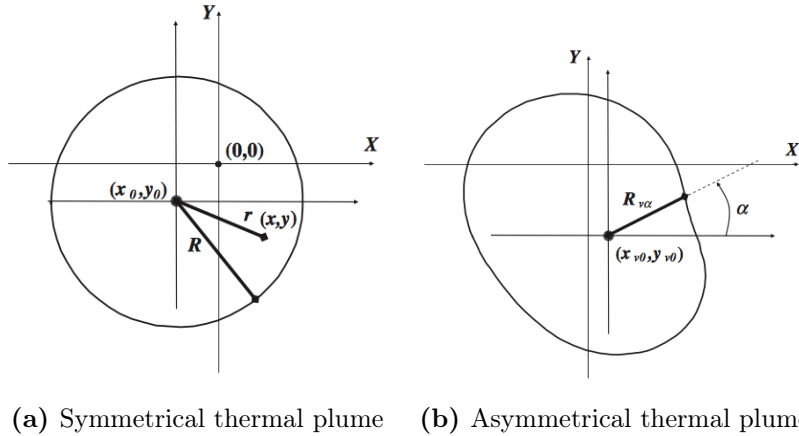
Figure 7: Illustration of profile widths [5]

Based on the measurement results and boundary conditions, Equation 17 was used to describe the velocity profile for the plume generated by the thermal manikin. The formula was also used to find the plume boundary by using its maximum velocity. When obtaining the boundary, b, for each measuring height the spread angle can be found and a formula for the centerline velocity and volume flow rate can be presented.

3.3   Plume modelling from previous studies

In this chapter equations for modelling plumes from previous studies will be presented. The objective with this is to compare the results that will be compiled by an empirical model, and then test the credibility (validate or reject) of the developed mathematical equation. Both equations for line- and point heat source will be given, as there will be performed measurements to cover both types of equations.

Point source: Skåret suggests the following formula for calculating the centerline velocity for a point source [6]. In the formula, C_b is equal to 0.235. The same equation was proposed by Mierzwiski and Popioloek [4].

$$U_0 = 4.27 \cdot (\frac{g\beta}{\rho c_p})^{1/3} \cdot (\frac{\dot{Q}_c}{z + z_0})^{1/3} \tag{19}$$

Heskestad suggests that the centerline velocity generated by a fire plume "point source" is given by Equation 20 [46].

$$U_0 = 3.4 \cdot (\frac{g}{\rho c_p T_0})^{1/3} \dot{Q}_c^{1/3} \cdot (z - z_0)^{-1/3} \tag{20}$$

Line source:

Skåret suggests the following formula for calculating the centerline velocity for a line source with C_b equal to 0.235.

$$U_0 = 2.22 \cdot (\frac{g\beta}{\rho c_p})^{1/3} \cdot \dot{Q}_c^{1/3} \tag{21}$$

For the line source, the volume flow rate generated above the line source is studied. Skåret suggests Equation 22 to describe the volume flow rate above a line source [6].

$$q_z = 0.47 \cdot (\frac{g\beta}{\rho c_p})^{1/3} \cdot \dot{Q}_c^{1/3} \cdot l \cdot (z + z_0) \tag{22}$$

Nielsen suggests an equation for the two-dimensional flow generated by a line source, given by Equation 23 [49].

$$q_z = 0.014 \cdot \dot{Q}_k^{1/3} \cdot l^{2/3} \cdot (z + z_0) \tag{23}$$

Awbi suggests almost the same equation, the only difference is the height for z and z_0 [4]. The result is presented in Equation 24. Note that in Equation 23 and 24 the convective heat loss $\dot{Q}_k$ is in W, and not in kW as for $\dot{Q}_c$ in Equation 22.

$$q_z = 0.014 \cdot \dot{Q}_k^{1/3} \cdot l^{2/3} \cdot (z + z_0)^{5/3} \tag{24}$$

Unfortunately there were a lot of difficulties to find previous literature about on plume modelling of a human thermal plume, and especially from a human in lying position. One study were found, were Suzuki et al. suggested to model the human body in supine posture as a line source [50]. This was done with the assumptions that the plume is generated by a persons entire surface. The same study suggests a length of the line heat source equal to 0.5 m, located at 0.8 m below the human. It is important to have in mind that this is a Japanese study, hence the size of the human body is probably much smaller than for the used 1.9 m tall thermal manikin. Figure 8 shows the idea behind modelling the plume generated by a patient as a line heat source, with a virtual line source placed below the manikin. This sketch is made with the assumption of a Gaussian distributed velocity profile above the human.
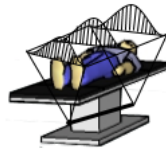
Figure 8: Human plume line source

The suggested formula for by Suzuki et al. is given by Equation 25, where Q_l is the airflow rate in m^3/h and l is the length of the line source in m. Q_k is the convective heat loss in W.

$$Q_l = 0.014 \cdot \dot{Q}_k^{1/3} \cdot (z - z_0) \cdot l \tag{25}$$

4 Method

In this chapter the method for experiments at both St. Olavs Hospital and at a climate chamber at NTNU will be explained in detail. The experimental setup for each case will be presented, as will the build up of the thermal manikin. The used measuring equipment will also be evaluated.

4.1 Scenario 1: Experiment at St. Olavs Hospital with a real human being

The first experiment for this master's thesis was conducted at "Stue 8" at "Bevegelsessenteret" at St. Olavs Hospital. The used operating theatre has a 4 m × 4 m area LAF zone which is surrounded by 110 cm long partial walls. In the operating room there are two exhaust ducts, each consisting of two 27 cm × 71 cm wall mounted low level exhaust outlets. The operating table is placed in the middle of the LAF zone.

During an open surgery the ventilation system is turned on fully. The temperature in the room is controlled by a temperature sensor for the exhaust air, which is set to be 22 °C. For this system it was anticipated that the room air temperature will be heated by the surgical staff, electrical equipment and other factors in the room, saying that the supply temperature is kept lower than 22°C. The supply temperature was measured to be 20 ± 1°C. A screen in the operating room also shows a value for the relative humidity in the room, which is varying around 28.1%.

Scenario 1 was conducted to establish some background knowledge about the condition of the ventilation system at St. Olavs Hospital, and to study the plumes influence of the air flow distribution above the operating table. At this first scenario the airflow in 5 different cases were studied to analyse the effect of thermal plumes on the airflow distribution in an operating room. An overview of the different cases is presented in Table 3. First the background case were studied, where the laminar airflow from the roof is not disrupted by anything. In the second case, the air flow distribution is studied above a patient, which is later used as a reference case. It is expedient to study how the airflow is influenced by a patient with no other disruption sources present, as this is the main focus of this thesis. In Case 3 to 5, one after one disruption source designed to represent typical sources found in a general surgical environment is included. As the main heat gains inside the ultra-clean zone comes from surgical staff and lighting, these heat loads were chosen for the different cases [51]. The different cases presented in Table 3 will be explained in detail in the next subchapter.

Table 3: 5 different cases were studied for Scenario 1 at St. Olavs Hospital

Cases	Description
Case 1	Empty operating table
Case 2	With a patient
Case 3	With a patient, 3 cylinders and no lamps
Case 4	With a patient, 3 cylinders and two lamps in horizontal position
Case 5	With a patient, 3 cylinders and two lamps in 45°

4.1.1   Experimental setup

Before performing the experiment, the room were prepared as for a real operation. The operating table were placed in the ultra-clean LAF zone, and the height of the table is 77 cm. The length and width of the used operating table is 210 cm and 55 cm respectively. For all the cases that contains a patient, i.e. case 2-5, the patient is placed with his heels 40 cm from the edge of the table.

A 175 cm tall, 75 kg heavy male were used to represent a patient for the experiments in Scenario 1. This male is dressed in thin, blue clothing during every experiment, but during real operations a fabric should have been covering the parts of the body that are not exposed to an operation. For all the experiments the occupant is wearing thin clothes, which have a clothing insulation capacity of approximately 0.50 clo [38].

In previous research it is common to use different geometrical shapes, as cylinders, to imitate the human body. This was also done in this master's thesis. In Case 3-5, three cylinders are used to illustrate the surgical staff (two surgeons and one nurse) in the ultra-clean zone during an operation. The cylinders have a diameter of 40 cm and a height of 140 cm, and a heating load of 100 W each, which will resemble the convective heat loss from a standing person. This is a simplification, as the convective heat load for a standing person in the reality would be varying with respect to convective heat area, skin temperature, temperature of the surrounding air among others. But a heat load of 100 W has been used by other researchers, and were available at the laboratory [52, 32].

In Case 4 and 5, two surgical lamps are placed above the operating table, and both has a value of 4300K. The lamps are not equally sized, so the biggest and smallest lamp will therefore be referred to as lamp 1 and 2 respectively. Lamp 1 is placed above the lower, while Lamp 2 is placed above the upper part of the patients body. In Case 4, both lamps were placed horizontally 190 cm above the floor. In the last case, lamp 1 and 2 has their lowest point respectively at 175 cm and 180 cm above the floor.

Explanation of each case: The experimental setup was planned to keep the patient as the main focus. Therefore one disruption source is included in each case. The five different cases that were briefly presented in Table 3 will be explained next.

Case 1:   First the airflow above an empty operating table were studied. The objective of Case 1 is to characterise the airflow from the LAF ventilation system without any disruptions in the operating box. Case 1 will be used as a background case for the other cases and in relation to the experiment with a thermal manikin in Scenario 3. The setup for Case 1 is shown in Figure 9.
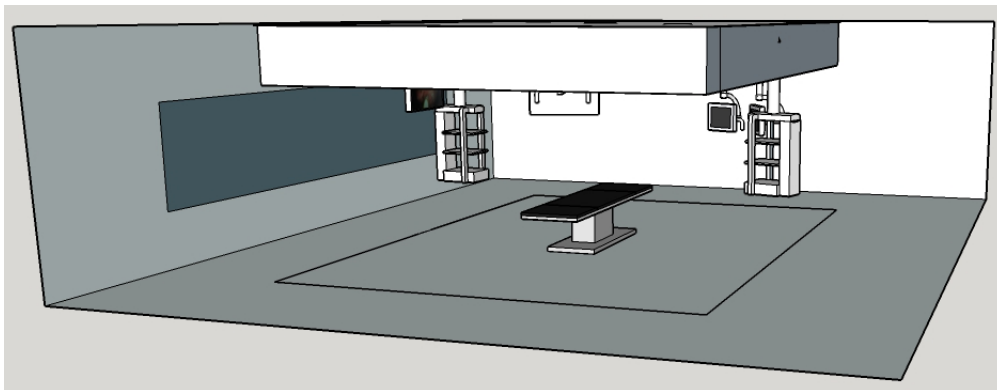
Figure 9: Sketch of the setup for Case 1

Case 2:   In Case 2, a patient is included in the experiment as shown in Figure 10. As the patient is the main focus in this master's thesis, the patient is the first factor that is included in the experiment. In this way, the interaction between the thermal plume raising from the patient and the airflow from the ventilation system can be studied further. The patient is placed on the table with its heel 40 cm from the edge of the bed. This case is the reference case for the experiment with thermal manikin in Scenario 3, Case 1, as a real situation is compared to an experimental. This case could also be used to calibrate the thermal manikin.
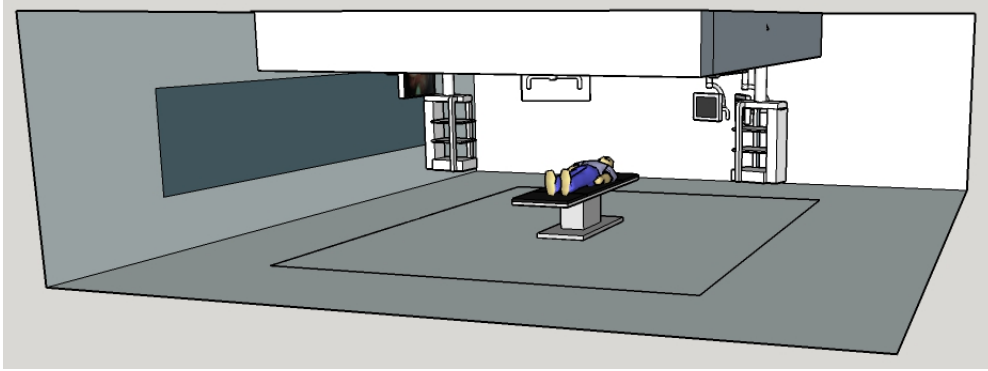
Figure 10: Sketch of the setup for Case 2

Case 3:   In the third case, three cylinders are included in the experiment as shown in Figure 11. The three cylinders are placed to picture the surgical staff; two surgeons and one nurse placed on the edge of the bed like in real operations. The lamps are still not included, so the only lighting is still coming from the roof.
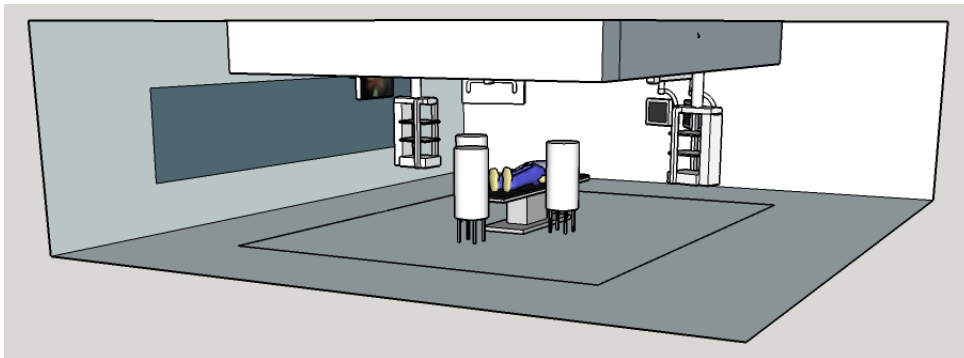
Figure 11: Sketch of the setup for Case 3

Case 4: In the fourth case the surgical lamps are positioned horizontally above the operating table. In this case, both of the lamps are placed 190 cm above the floor. The objective with placing the surgical lamps above the operating table is to study how much these two surfaces will disrupt the laminar air flow distribution from the roof, as they naturally will hinder the airflow to reach the surgical site.

Case 5: Case 5 is similar to Case 4, but the difference is the angle of both of the lamps. In Case 5, the angle of the lamps are changed to 45°. Figure 12 is a sketch of the experimental setup for Case 5.
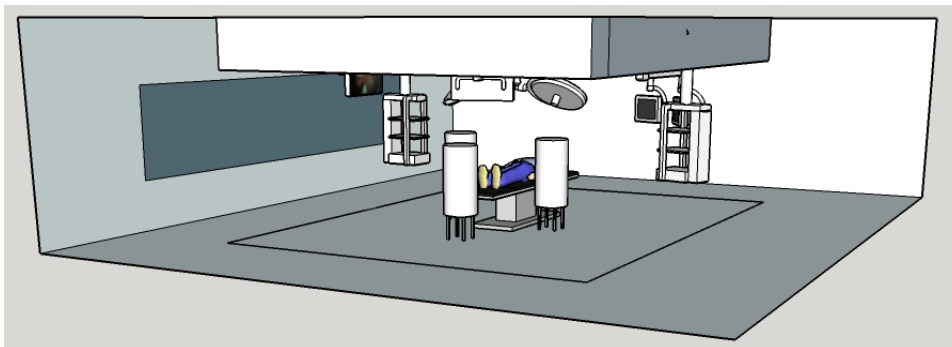
Figure 12: Sketch of the setup with two surgical lamps, here shown for Case 5 (ie. in 45°)

A picture of the actual setup for each case is presented in Figure 13.

(a) Case 1

(b) Case 2
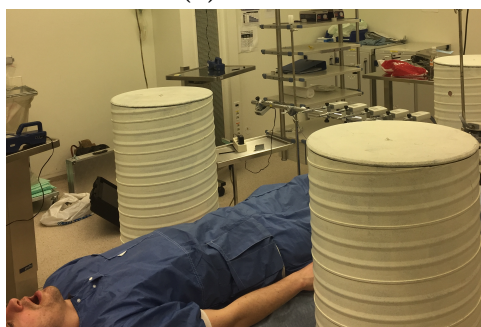
(c) Case 3

(d) Case 4

(e) Case 5

Figure 13: The experimental setup for Scenario 1 at St. Olavs Hospital

4.1.2   Measuring points

The measured points performed for each case in Scenario 1 is presented in Figure 14. An adjustable stand was used for the experiments, where 5 anemometers were aligned with a distance of 10 cm in between each other. The third anemometer is placed in the middle of the table in each experiment. The stand is placed in 5 different positions above the operating table in y-direction (40 cm in between each position), and for three different heights, shown in Figure 14a and 14b respectively. This gives a total of 75 measured points for each case.

(a) Sketch of the 25 different measuring points for one height above the operating table (horizontal plane)

(b) Sketch of the three different measuring heights for the experiment (vertical plane)
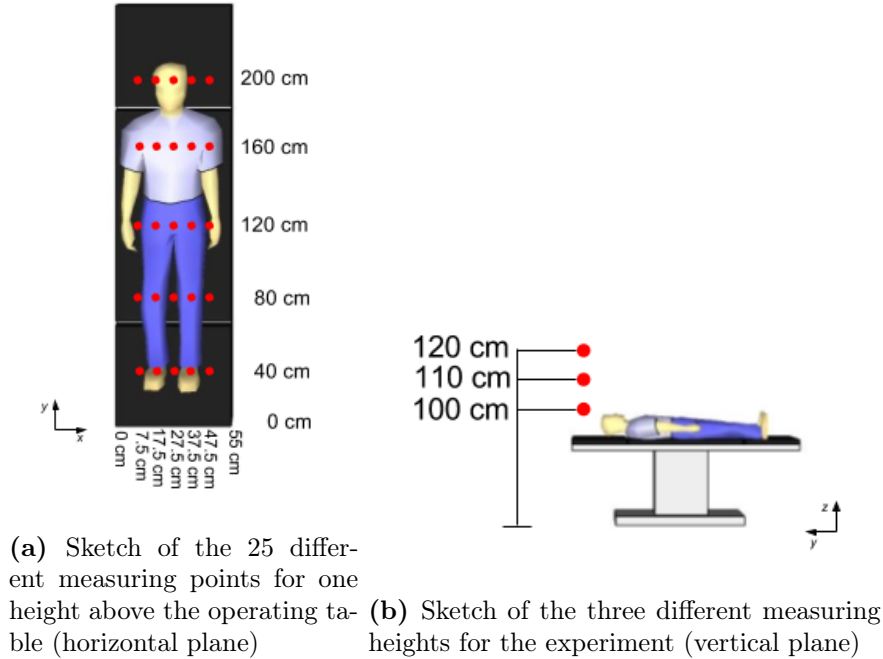
Figure 14: Sketch of measured points in Scenario 1

As shown in Figure 14b, the anemometers have been placed in three different heights above the floor in every case. The heights are chosen to give as exact values as possible for the air distribution above the patient. The first height is therefore chosen to be 100 cm above the floor, which is right above the used patient in this experiment. The next measured heights are 110 cm and 120 cm above the floor, i.e. 10 cm and 20 cm above the patient. The heights of the experiments are chosen to be presented relative to the floor since the humans body does not have an equally height at its whole surface. Both Figure 14a and 14b are only made to give an overview of the placement of the measured points, and the distances on the sketch are therefore not necessarily correct.

4.1.3   Items of measurements

The air distribution measuring system that were used at Scenario 1 was AirDistSys 5000, delivered by Sensor Electronic. The measuring equipment were calibrated beforehand, to ensure accurate measurements during the experiment. The measuring system consists of five omnidirectional anemometer probes, a pressure sensor, a wireless transmitter and a power supply. The pressure sensor is connected to correct the anemometer readings according to the barometric pressure and the transmitter transmits the readings to an USB stick that is connected to a computer. To read and log the recorded data on a computer, a software from

Sensor Electric must be downloaded. The connection between the different components in the measuring system is shown in Figure 15.
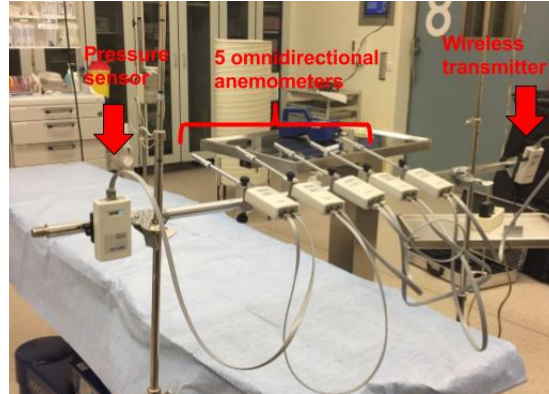
Figure 15: Measuring system connection setup used at St. Olavs Hospital

Table 4 sums up the most relevant technical data for the range and accuracy for the omnidirectional anemometer probes (SensoAnemo5100LSF Transducer) and pressure sensor (SensoBar 5301 Transduces) of AirDistSys 5000. A complete description of the technical data of the anemometers can be found in Appendix B.1.

Table 4: Technical data for AirDistSys 5000

	Measurement	Value
Anemometer probes	Speed range	0.05 to 5.00 m/s
	Accuracy of speed	± 0.02 m/s ± 1.50 % of readings
	Temperature range	-10 to +50 $°C$
	Accuracy of temperature	0.20 $°C$
Pressure sensor	Pressure range	500 to 1500 hPa
	Accuracy of pressure	± 3 hPa

Each anemometer probe is set to log for one minute continuously before being moved on to a new measurement point. The Sensor Electric software was set to record values every two seconds. At each probe the velocity, temperature, pressure, standard deviation and turbulent intensity is logged, and the average value during the total logging period is used for each measurement point. In reality, the omnidirectional anemometers measure the magnitude of the velocity, and it is therefore important to notice that all of the results are presented as speed and not velocity plots.

4.2   Scenario 2: Thermal plume measurements above a thermal manikin

A climate chamber at NTNU with possibility to turn of the ventilation system was used in order to measure the thermal plume generated by a thermal manikin. The dimensions of the room is 4.00 m × 2.30 m floor area and 3.15 m height as shown in Figure 16. The boundary conditions in the room were measured by hanhold anemometer TSI 962, which gave a room temperature equal to 25.1°C and background velocity from 0.01 to 0.02 m/s. Since heat will be emitted by the thermal manikin, the temperature in the climate chamber is

measured to increase by around 1°C during the experiment, as it was not possible to control the temperature in the climate chamber.
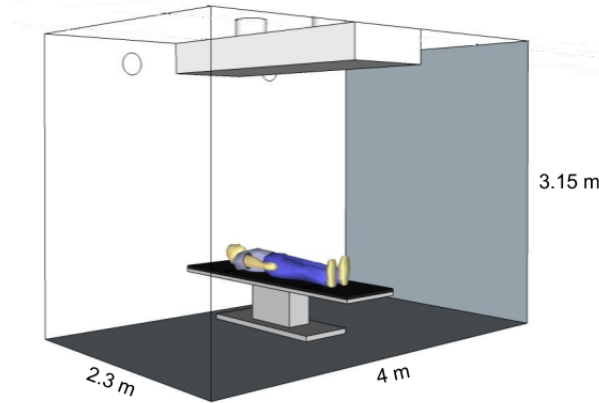
Figure 16: Sketch of the setup at the climate chamber at NTNU

Scenario 2 is the experiment with an objective to study the development of thermal plume generated by a thermal manikin in supine position, due to natural convection. In this way, information of the plumes potential to influence the air distribution in rooms can be studied. The experimental setup in this chapter is also developed to measure the necessary values to suggest a mathematical formula for thermal plume presented in Chapter 3. First, the construction of the heating system of the thermal manikin will be presented.

4.2.1   Heating system of the thermal manikin

A male manikin of the version used for exhibiting clothes in clothing stores was purchased for this experiment. The 1.90 m tall manikin in standing posture is made of fiber glass, meaning it has a hard exterior. As the manikin is designed as a exhibition model, the left knee is in a posing position leading to an outstick formation. The thermal manikin was dressed in light clothing with insulation capacity of about 0.5 clo, which is equal to 0.08 $m^2 \cdot K/W$ [38]. This was the same type of clothes as used in Scenario 1.

The manikin was assumed to have a metabolic rate equal to 0.8 MET, which is based on the activity level for a reclining person [38]. The metabolic rate of 1.0 MET is defined equal to a power production of 58 W/m^2 [38]. The total heat output is therefore calculated to be 0.8 MET $\cdot$58W/m^2 $\cdot$1.98m^2 = 91.87 W, where 1.98 m^2 is the surface are of the thermal manikin. The body surface are can be found by using DuBois and DuBois formula, presented in Equation 13. But since it is difficult to assume a weight for thermal manikin, the surface area was estimated by measurements. The manikin was divided into 16 different body parts when estimating the surface area, as Tanabe et al. did for their experiment in 1994 [37]. The result of the measured surface areas are presented in Table 5.

To achieve the calculated heat output of the manikin, heating cable with the capacity of 20 W/m were wrapped around inside the space of the manikin as shown in Figure 17. The amount of cable at each body part was calculated based on the share of area at the given part from Table 5. In reality the same manikin was also used for an experiment which demanded a heat output of roughly 230 W. The heat load were therefore oversized for my experiment, which made it challenging to get the right heat output and surface temperature for my experiment. The control strategy for my experiments will be explained later on. Because of the way the manikin was constructed it was not possible to lead the cable through his hands

Table 5: Name and surface area of each body part

	Name of part	Area [m^2]
1	Left foot	0.05
2	Right foot	0.05
3	Left leg	0.15
4	Right leg	0.15
5	Left thigh	0.23
6	Right thigh	0.23
7	Crotch	0.18
8	Head	0.11
9	Left hand	0.045
10	Right hand	0.045
11	Left arm	0.07
12	Right arm	0.07
13	Left shoulder	0.08
14	Right shoulder	0.08
15	Chest	0.22
16	Back	0.22
Total		1.98

and feet, which resulted in areas with surface temperature equal to the temperature of the surroundings. The specifications for the heating wire is given in Appendix D.2.1
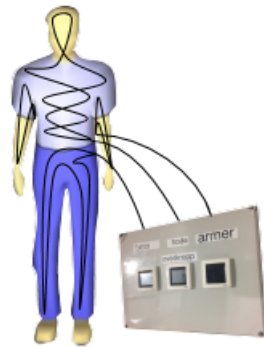
Figure 17: Placement of the heating wire inside the manikin in three different circuits

A correct surface temperature for the manikin is crucial for development of thermal plume and must therefore be controlled carefully. The skin surface temperature of a real human usually varies around 32 to 34°C, so a constant surface temperature kept at that level is desired [38]. McNeill et al. suggests to use a surface temperature of 27.4°C for a patient [51]. This value is much lower than the one earlier suggested, but as this is just a value used for their specific experiment it was chosen to aim for a value between 32 to 34°C. The surface temperature during the experiments was checked regularly.

The control strategy of the thermal manikin is a mix of the two different strategies presented in Chapter 2.4.1, i.e. control of both power supply and surface temperature. The surface temperature is controlled by three different sensors, which measure the temperature in the head and upper body, the arms and the legs. The system is set to heat until it reaches the desired value given by a control panel. If the current value falls below the set value,

the system starts to reheat the manikin. As the sensors measure the air temperature on the inside of the manikin, and not directly the surface temperature, a thermo detector from Bosch PTD 1 were used to assure a correct outer surface temperature in the range of 32 to 34°C. But a non-uniform distribution of the heating cable caused variations in surface temperature for the manikin. This was especially noticed in the head, which showed a clearly lower temperature than the rest of the manikin. But the measured values by the thermo detector was 33.8±0.5°C in the upper body, 28.6±0.2°C in the head, 32.4±0.5°C in the arms and 33±0.8°C in the legs. It was noticed that the manikins left leg was warmer than the right leg, hence a wide measured temperature interval of 0.8°C. These values were measured at the manikins' surface, ie. below the clothing. The technical specification of the thermo detector is given in Appendix D.2.1. Note from the technical data that the accuracy is ± 1°C for the interval 10-30°C, and not given for values above 30°C. But this method was still the most accurate way to control the surface temperature of the thermal manikin.

In addition to surface temperature control a variable transformer unit (variAC) was used to adjust the voltage and hence control the power supply to the manikin. An energy meter were attached the connections to the wall, and made it possible to read the supply power. The variAC was adjusted so that the value of the supply power was at maximum 110 W. Due to how the heating wires were placed it was difficult to reach stable values for a surface temperature of around 32°C for a lower power supply.

4.2.2   Experimental setup

Figure 53 shows the measured points above the manikin at the climate chamber at NTNU. In y-direction, six different cross sections above the manikin were chosen, with objective of study the velocity profile above different parts of the manikin. One of them is above its head- to model plume as a point source. A 190 cm long, old operating table were used for these measurements. The operating table were not entirely complete, but long enough to be covered by the approximately 190 cm tall thermal manikin.

The measured points at each height are shown in Figure 18a. The measuring points in x-direction are placed 5 cm apart, while the distance between the measuring points in y-direction is 30 cm. The points in x-direction are also measured on the outside of the table, to get a proper view of the plume development at the upper heights. The reason for why the first measured height is 110 cm above the floor is because of the posing left knee of the thermal manikin, which is actually right below 110 cm when the thermal manikin is laying at the operating table. 110 cm above the floor is therefore considered as close proximity to the manikin. Eight heights above the manikin is measured, from 110 cm to 180 cm above floor as shown in Figure 18b.

The velocity profile above the manikin for different y's are presented in the results. To make it easier to understand which part is studied, the measuring points in y-direction are named. As seen from Figure 18a, the first measured point in y-direction is above the manikins legs, the second is above its knees, the third is referred to as its upper thigh, the fourth is above its stomach, the fifth at his chest and lastly as above its head.

4.2.3   Items of measurements

Thermoanemometer TSI 962 were used to check the boundary conditions in the climate chamber. The technical data for Thermoanemometer TSI 962 is presented in Table 6, and a
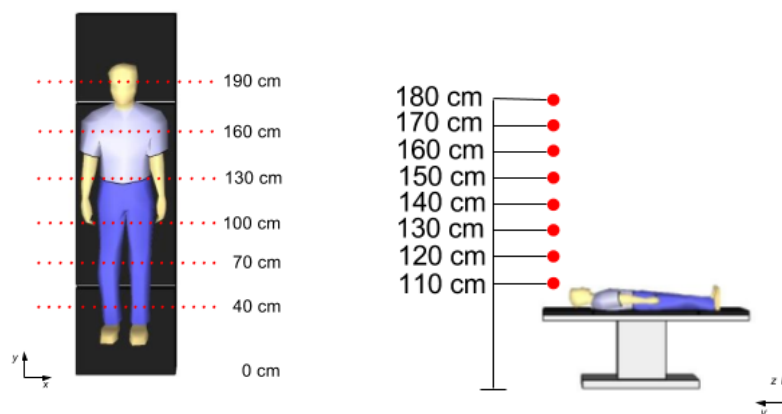
(a) 108 measured points at each height

(b) Eight measured heights

Figure 18: Sketch of measuring points for thermal plume measurements

picture of the handhold anemometer is shown in Figure 19. The complete technical data for TSI 962 is given in Appendix B.2

Figure 19: TSI 962 handheld thermoanemometer

Table 6: Technical data for Thermoanemometer probe TSI 962

Measurement	Value
Speed range	0 to 50 m/s
Accuracy of speed	$\pm$ 0.015 m/s or $\pm$ 3 % of readings, whichever is greater
Temperature range	-18 to +93 $^\circ C$
Accuracy of temperature	$\pm$ 0.30 $^\circ C$

As three of the five AirDistSys 5000 omnidirectional anemometer probes were damaged during the semester, a new type of omnidirectional hot-wire anemometers were used in Scenario 2 and 3. Six TSI 8475 were therefore used and the connection of the anemometers is shown in the Figure 20.
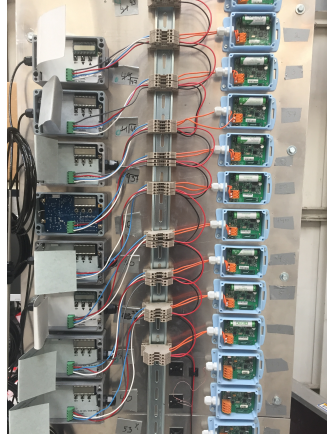
Figure 20: Connection of TSI 8475 omnidirectional anemometers

The onmidirectional anemometers were new and was already calibrated by the factory. Table 7 shows the main technical data for the anemometers. Notice that the speed range goes from 0.05 m/s to 2.54 m/s. For the complete technical data, see Appendix B.3.

Table 7: Technical data for TSI 8475

Measurement	Value
Speed range	0.05 to 2.54 m/s
Accuracy of speed	$\pm$ 3% of readings at 20 to 26°C
Response time	5.0 seconds

The chosen values for each of the omnidirectional anemometer is given i Table 8. The anemometers are set to measure each 0.25 second, but does only give mean values per each 20 seconds to the software. This cause limitations for calculating turbulence intensity and standard deviation. The output value is also given in milliampere (mA) which must be recalculated into velocity. The formula for calculating the velocity is given by Equation 26.

$$V = \frac{E_{out} - E_0}{E_{FS} - E_0} \cdot V_{FS} \tag{26}$$

In Equation 26 V is the velocity output in m/s, E_{out} is the measured output current signal in mA, E_0 is the zero flow output current in mA, E_{FS} is the full scale current output in mA and the V_{FS} is the full scale velocity setting in m/s.

Table 8: Used values for TSI 8475

Variable	Chosen value
Units	m
Full scale velocity	0 to 2.5 m/s
Output	4 to 20 mA
t_c	5 sec
Zero	4
Span	1

In Table 7 it is shown that the range of the measuring equipment begins as 0.05 m/s. For the plume measurements it is expected to get values below 0.05 m/s, which should have been used for analysing the results. But since measured values below 0.05 m/s do not have any accuracy at all, the average speed plots in Chapter 5.2 are based on values greater than 0.05 m/s. This means that only selected values from the logging period are used, and not values from the whole interval, meaning that calculating standard deviation and turbulence intensity will not give a meaningful results. And since the recorded values in the data program is given each 20 seconds, the purpose of calculating SD and Tu will disappear as the instantaneous fluctuations can neither be observed. Error bars is therefore not included in the speed plots, and an analysis of the turbulence intensity will not be conducted. The results are also only presented as mean values, as it was not possible to obtain the instantaneous flow field of the plume.

4.3 Scenario 3: Experiment at St. Olavs Hospital with thermal manikin

The objective of Scenario 3 is to study the interaction between the thermal plume generated by a thermal manikin and the airflow from a LAF ventilation system. As for the plume measurements, it was intended to perform the experiment at the climate chamber at NTNU. But as the were spent almost a month on constructing the 0.80 m × 2.10 m LAF-ceiling ventilation system, without having any luck with an evenly distributed air supply along the ceiling, it was determined to perform the experiment at an operating theatre at St. Olavs Hospital (the same "Stue 8" as used in Scenario 1). This would of course cause some limitations, but as the preconditions and lack of time, this was a necessary decision to complete the master's thesis on time.

4.3.1 Items of measurements

TSI 962 handheld thermoanemometer were used to measure the outlet velocities for the 0.80 m × 2.10 m LAF-ceiling at the climate chamber at NTNU. To measure outlet velocities at plenty of points underneath the LAF-ceiling was necessary in order to calibrate the unidirectional flow later on. The velocity at each point is given by measuring for 10 seconds per point, or until the instrument reads a stable velocity. As the velocity under the 0.80 m × 2.10 m LAF-zone at NTNU were measured to vary between 0.02 and 0.4 for a set value of 0.3, the LAF was clearly not laminar nor kept close to the set point value. Using the ventilation at the climate chamber would therefore not give reasonable results nor could be compared to a real laminar ventilation system, and the experiment was therefore moved to a real operating room at St. Olavs Hospital.

As for the plume measurements in Scenario 2, six omnidirectional anemometers TSI 8475 were used for Scenario 3. For information of their performance see Chapter 4.2.3.

4.3.2 Experimental setup

Figure 16 is a sketch of the planned experimental setup at the climate chamber at NTNU. The operating table were placed in the middle of the room with a height of 77 cm, as used in Scenario 1. This height is chosen for the results to be more comparable, as the distance from the diffuser outlet is the same. As the experiment had to be conducted at St. Olavs Hospital, the real experimental setup is as for Scenario 1, Case 2 in Figure 10. The same

thermal manikin as used for the plume measurements explained in Chapter 4.2.1 is used for this experiment at St. Olavs Hospital.

Two different ventilation modes were possible to chose at the hospital, so the interaction between a thermal plume and a ventilation system could be studied in two different modes. The first mode is with ventilation in resting mode, meaning a minimum airflow is coming from the LAF ventilation. The second mode is normal mode, which is used during open surgery. As the use of ventilation mode in resting condition was with mainly mixing ventilation, and not controlled laminar airflow, the method and following results are chosen to be presented in Appendix D.3. This is because of the content is not directly linked to the main objective of this master's thesis. Scenario 3 is therefore now consisting of two cases. The first case will focus on the interaction between the thermal plume generated by a thermal manikin and laminar airflow while the second case will present the airflow distribution above a thermal manikin surrounded by warm objects as for real operations. The used experimental setup for each of the two cases are presented in the following.

Case 1: Interaction between the human thermal plume and laminar airflow: For each measuring height the velocity is measured at 36 points as shown in Figure 24a. In x-direction the distance between each measuring point is 5 cm, while the distance is 30 cm in y-direction. The experiment was conducted for seven different heights as shown in Figure 24b. These were chosen based on the first height, which is right above the knee of the thermal manikin. The multiple heights were chosen so that a horizontal plot of the interaction between the thermal plume and the laminar ventilation could be pictured. Notice that the measured points are from 15 to 40 cm in x-direction, so the experiment has a focus on the centre of the table.

(a) Measuring points at each height

(b) Seven measured heights
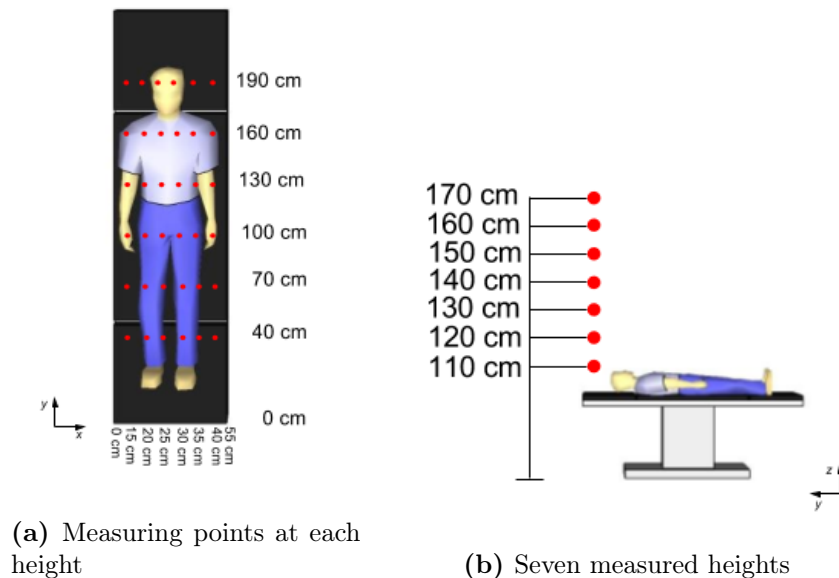
Figure 21: Measuring points for Scenario 3, Case 1

Pictures of the actual experimental setup is shown in the Figure 22.

Case 2: Plume interaction with laminar airflow: To dig further into the relation between the surgical staff related to air movement below the LAF system I was invited to observe a real operation in "Stue 8" at Bevegelsessenteret at St. Olavs Hospital. The surgery was a knee replacement, which is one of the operations with greater risk for infection. During the operation, two surgeons and one nurse were in the ultra-clean zone. The surgical staff consisted of 5 persons in total, but the last two nurses kept distance from the operating zone.
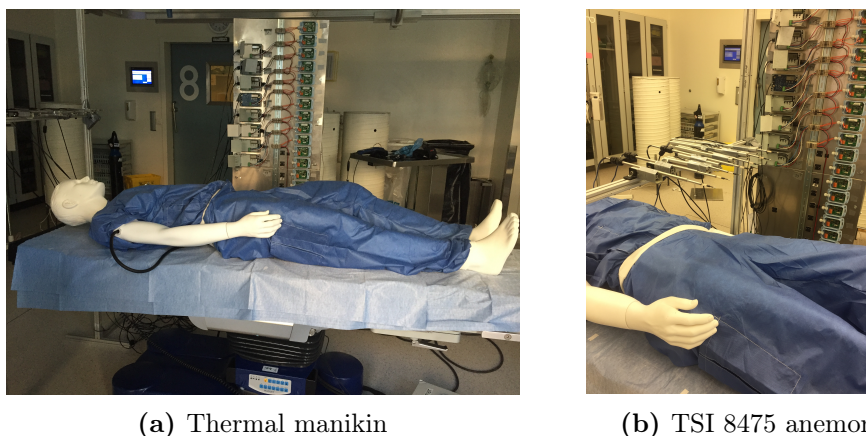
(a) Thermal manikin

(b) TSI 8475 anemometers

Figure 22: Experimental setup for Scenario 3, Case 1

The two surgical lamps were placed in 45°and the patient was covered by a a green fabric. The surgeons and nurses were dressed in green and blue clothing, facemasks, glowes and hair protection. In this way particles from the surgeons skin are prevented to reach the surgical site. But the instrument table were placed in the transition zone between the ultraclean LAF zone and regular ventilated zone, which can cause bacteria dispersion on the instruments. A picture from the real operation is shown in Figure 23a, which is censored due to privacy policy.

(a) Picture from a real operation at "Stue 8"

(b) Experimental setup

Figure 23: Pictures from Scenario 3, Case 2

The experimental setup for this case is similar to Case 5 in Scenario 1. The main difference is the placement of the lamps, which are placed above the right corner of the table lengths, and not right above the table as in Scenario 1. A picture of the actual setup is given by Figure 23b, where the placement of the lamps are clearly shown.

For this case, the speed in total 108 different points, divided on three different heights, were measured above the thermal manikin. A sketch of the actual measuring points for this case is shown in Figure 24.
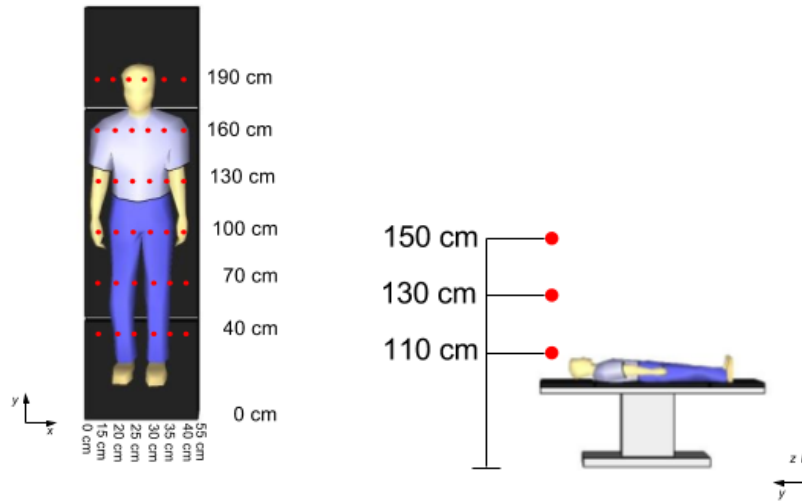
(a) Measured points at each height

(b) Three measured heights

Figure 24: Measured points for Scenario 3, Case 2

5 Results

In this chapter the results from the experiments will be presented. This chapter is divided in three subchapters as for Chapter 4, where the results of each scenario will be presented in one subchapter. The objective with this is to give a systematic layout for this master's thesis. This chapter will therefore first present the results of the measurements at St. Olavs Hospital with a real human being, then focus on the thermal plume from a thermal manikin and lastly the interaction between the thermal plume and the LAF ventilation system.

5.1 Scenario 1: Experiment at St. Olavs Hospital with a real human being

This subchapter will present the results of measurements performed for the five different cases in the operating theatre "Stue 8" at St. Olavs Hospital. The setup of each experiment is conducted as explained in Chapter 4.1. This chapter is divided into several sub-chapters that each will focus on the analysis of one particular measuring variable in relation to every case. The objective with this is to make a clear analysis of the effect of thermal plumes in the LAF ventilated zone. The first part of the chapter will focus on the speed measurements, second the temperature profile will be analysed and lastly the turbulent intensity will be studied. The subfigures in the following chapters are arranged as for Figure 13 in subchapter 4.1.1, where Case 1 to 5 is represented by (a) to (e) respectively. All of the following results are presented as contour plots that are made from 25 different anemometer probe measuring points. In this way it is easy to compare the results from the different cases and evaluate the effects of the thermal plumes in close proximity to the patient. Contour plots for the draft rate was also developed, but as the analysis of draft rate is not completely relevant for the scope of this master's thesis the contours are placed in Appendix D.1.1.

5.1.1 Speed measurements

As one of the main focus of this thesis is to characterise the effect of thermal plumes on the airflow distribution in an operating room, this subchapter will focus on presenting the speed distribution above the table for the five different cases, at three different heights. Figure 25 shows the speed contour 100 cm above the floor, i.e. 23 cm above the operating table and in close proximity to the human patient.

As seen from Figure 25 the velocity contour is clearly varying at each case, meaning that the velocity is disrupted by the addition of thermal plumes and other surfaces. Figure 25a is the background case, and shows the variation in velocity 23 cm above an empty operating table. From the figure it is clear that the speed is not evenly distributed above an empty operating table, but presents a clear stratification from $0.12\,\text{m/s}$ to $0.3\,\text{m/s}$. Figure 25b shows the velocity above a patient, and compared to Figure 25a it is clear that a lower velocity is reached above a greater part of the table in the case with a patient. Since a human thermal plume will be created by the lying patient a velocity will raise from the patient in opposite direction than the LAF from the ventilation system, leading to a lower total velocity in general.

(a) Case 1   **(b)** Case 2   **(c)** Case 3

(d) Case 4   **(e)** Case 5
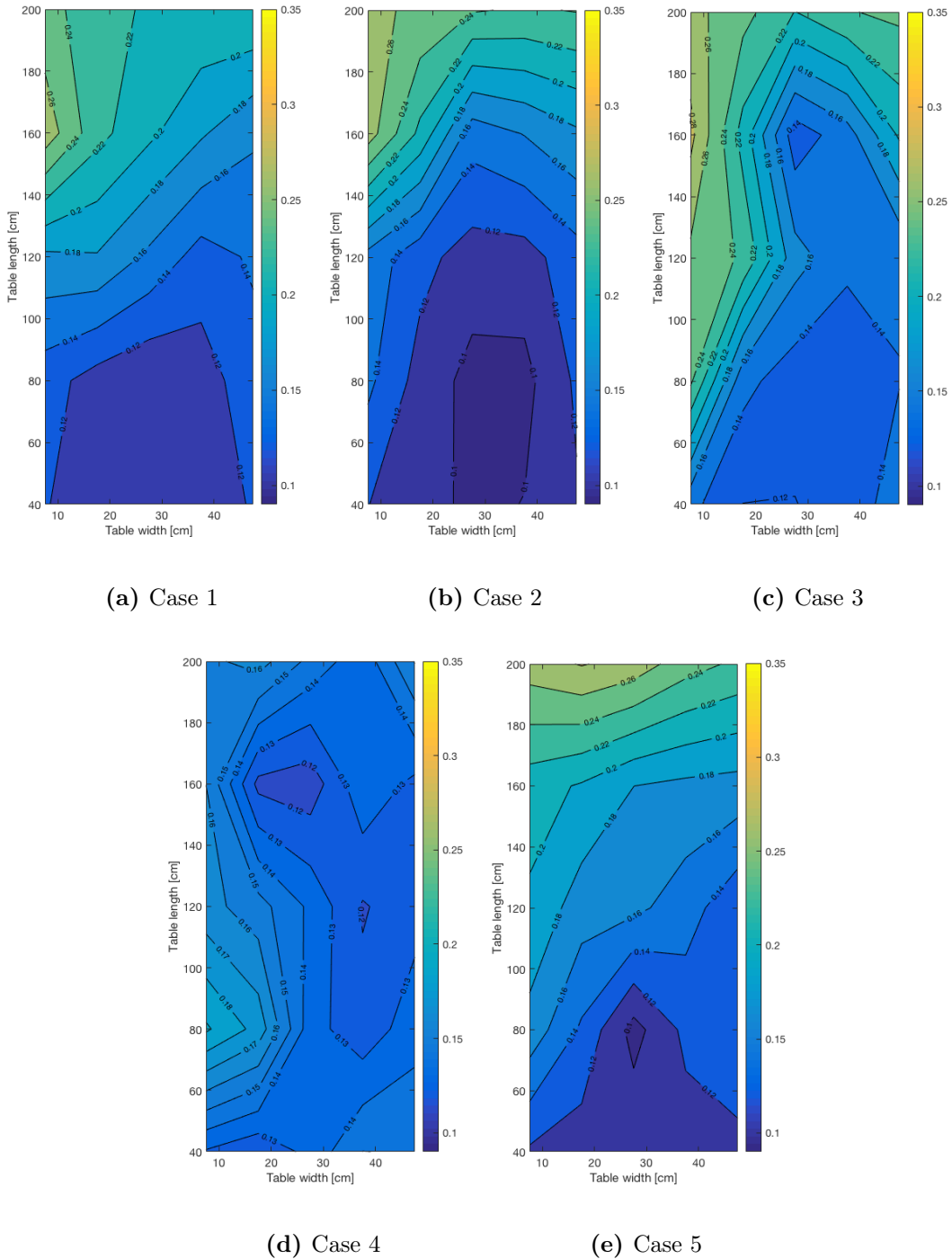
Figure 25: Speed contours at 100 cm above the floor

When the three cylinders are included, i.e. in Case 3, the speed contour at the middle of the table changes pattern compared to the two previous cases. Figure 25c shows the disruption at least at the left side of the table, where the velocity is increased. The velocity is also in general higher than for the previous two cases. Since there is not any knowledge on the direction on the airflow it is challenging to discuss exactly how the three cylinders affects the airflow, but it is evident that they do affect the air distribution above the table.

When surgical lamps are included in the experiment, i.e. Case 4 and 5, the velocity contours are again changed. When the surgical lamps are placed in horizontal position, the speed is

reduced above the whole operating table, see Figure 25d. This is logical, as the surface of the lamps are preventing the airflow to reach the operating table. Figure 25e shows a clearly lower velocity at the lower part of the operating table, where the biggest lamp is placed. The velocity pattern for Case 5 is more similar Case 1 and 2, compared to Case 4 where the lamps are placed in horizontal position. This indicates that the airflow from the ventilation system get less disrupted when the lamps are placed in 45°compared to in horizontal position. This observation may be logical, as the surface of the lamp in 45°will hinder the airflow above a smaller part of the table, and is not necessarily due to the presence of a convective airflow.

Figure 26 gives an overview on the change in airflow distribution for the five cases at 110 cm above the floor, i.e 33 cm above the operating table. Compared to Figure 25, the velocity levels at 110 cm are in general higher, except for Case 4 which gives three areas with velocity level below 0.12 m/s.

The velocity distribution for Figure 26a is similar to Figure 25a, but are in general 0.02 m/s to 0.04 m/s higher at each point. This may be logical as Figure 26a is closer to the LAF diffuser supply outlet. For Case 2 at 110 cm above the floor, the velocity level is also higher than at 100 cm. The velocities in Figure 26b varies from 0.14 to 0.26 m/s.

Figure 26c shows the airflow distribution in which three cylinders are included. The figure shows a clear disruption in the airflow after the cylinders are placed close to the operating table, and shows that convective flows can cause higher local air speeds. The highest speed level is reached at the left side of the table with a value of 0.30 m/s.

When the surgical lamps are placed above the operating table, the speed distribution are changed once again. Figure 26d shows a significant lower speed level above the whole table with three areas of velocities lower than 0.12 m/s, compared to Case 4 100 cm above the floor. For Case 5, the velocity level at 110 cm differs a lot from 100 cm above the floor. The effect of adding lamps in 45°is changing the placement of the local air speed spot at the middle of the table from left to right, ref Figure 26c and 26e. The effect of including surgical lamps in 45°does also increase the velocity at the left corner of the table.

(a) Case 1   (b) Case 2   (c) Case 3

(d) Case 4   (e) Case 5
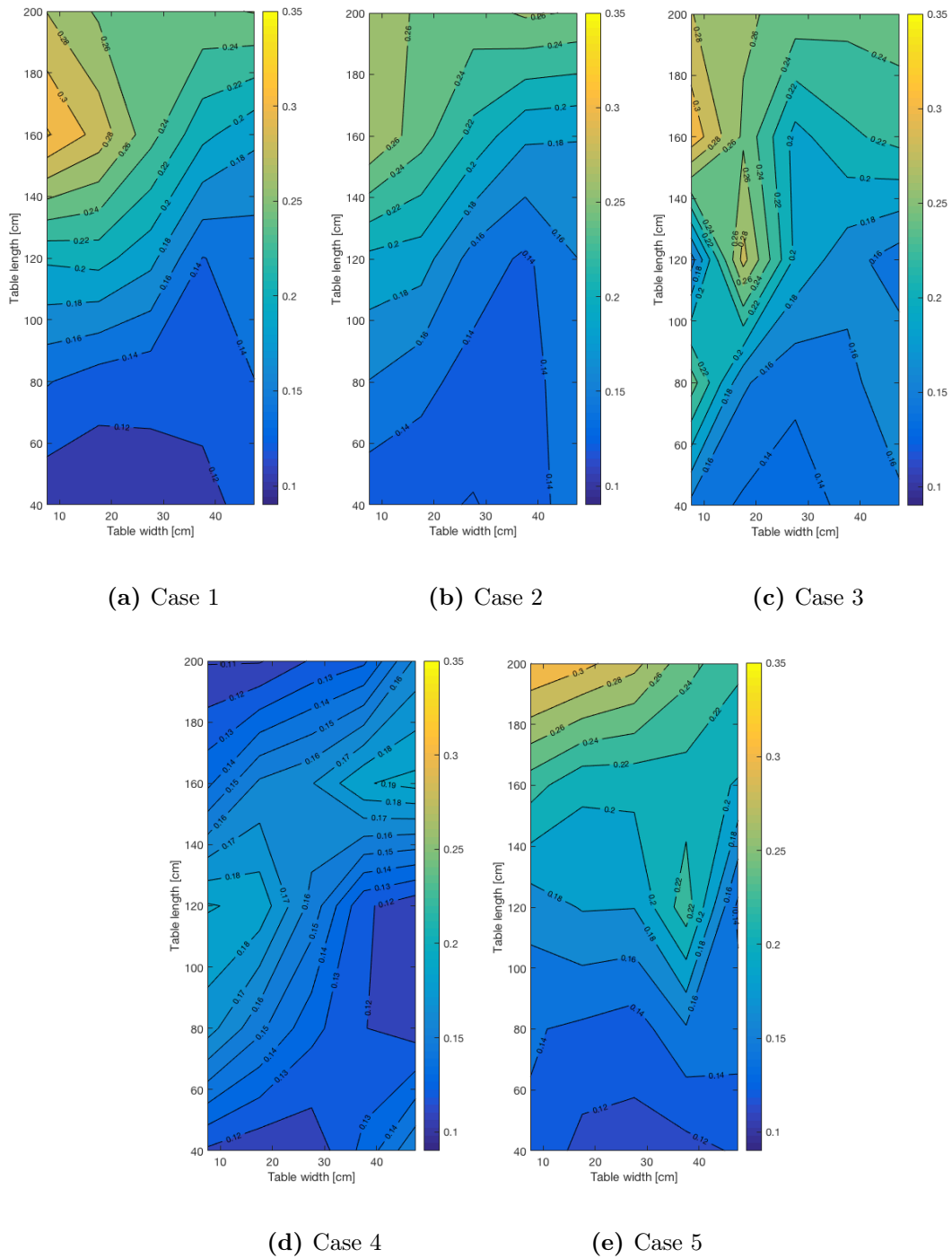
Figure 26: Speed contours at 110 cm above the floor

For the last height, i.e. 120 cm above the floor and 43 cm above operating table, the speed contours are presented in Figure 27. As for Figure 26, the speed levels seem to be higher for each case, except for Figure 27d where the speed is lower than 0.17 m/s above the whole table.

Figure 27a shows the airflow distribution 43 cm above the operating table for Case 1. The figure shows a general higher speed above the lower part of the table with a value of 0.02 m/s, compared to the same case at 100 and 110 cm above the floor. But notice that at the upper part of the table, the speed is actually lower than for Figure 26a.

When a patient is included in the experiment, ref Case 2, the speed distribution above the table is changed. The airflow pattern is similar than before, with the lowest speed at the lower part of the table and the highest speed at the upper, left side of the table. Case 2 does also reach a higher maximum velocity than Case 1, see Figure 27b and Figure 27a respectively.

Figure 27c shows the effect of placing three cylinders next to the operating table. The figure shows a clearly increased speed at the upper, left side of the table, and a general higher speed above the whole table.

As for the two previous presented heights, the speed distribution for Case 4 shows low speed above the entire table surface. As seen from Figure 27d, the speed is reaching a maximum value of 0.17 m/s, which is much lower than for the other cases. The horizontal lamps are again blocking the clean airflow from the ventilation system. Including surgical lamps in 45°will stabilise the speed at the lower part of the table and cause a speed stratification at the upper, left part of the table. Note that the maximum speed in Figure 27e is above 0.4 m/s, which is out of the range of the colorbar for the contour plots.

For an optimal laminar ventilation system, the velocity profile at the entire surface should be the same for Case 1. Figure 25a, 26a and 27a shows that this is clearly not the case at St. Olavs Hospital, where the speed is varying in big intervals at each height, even with no disrupting sources placed around the table. From Figure 25a it is clear that the speed at a height 100 cm above the floor varies from 0.10 m/s to 0.26 m/s, thus is not equal at the whole surface. Figure 26a gives a speed difference from 0.10 m/s to 0.32 m/s, while Figure 27a gives speeds from 0.12 m/s to 0.29 m/s. It may be most logical that the highest values would be closest to the LAF ceiling, as it will be closest to the discharge velocity. This was not the case here, which makes one wonder what may be the explanation for that. But for every height in Case 1, the figures shows that there is a trend for higher speeds at the upper edge of the table, i.e. where the head is placed in Figure 14a.

(a) Case 1   **(b)** Case 2   **(c)** Case 3

(d) Case 4   **(e)** Case 5
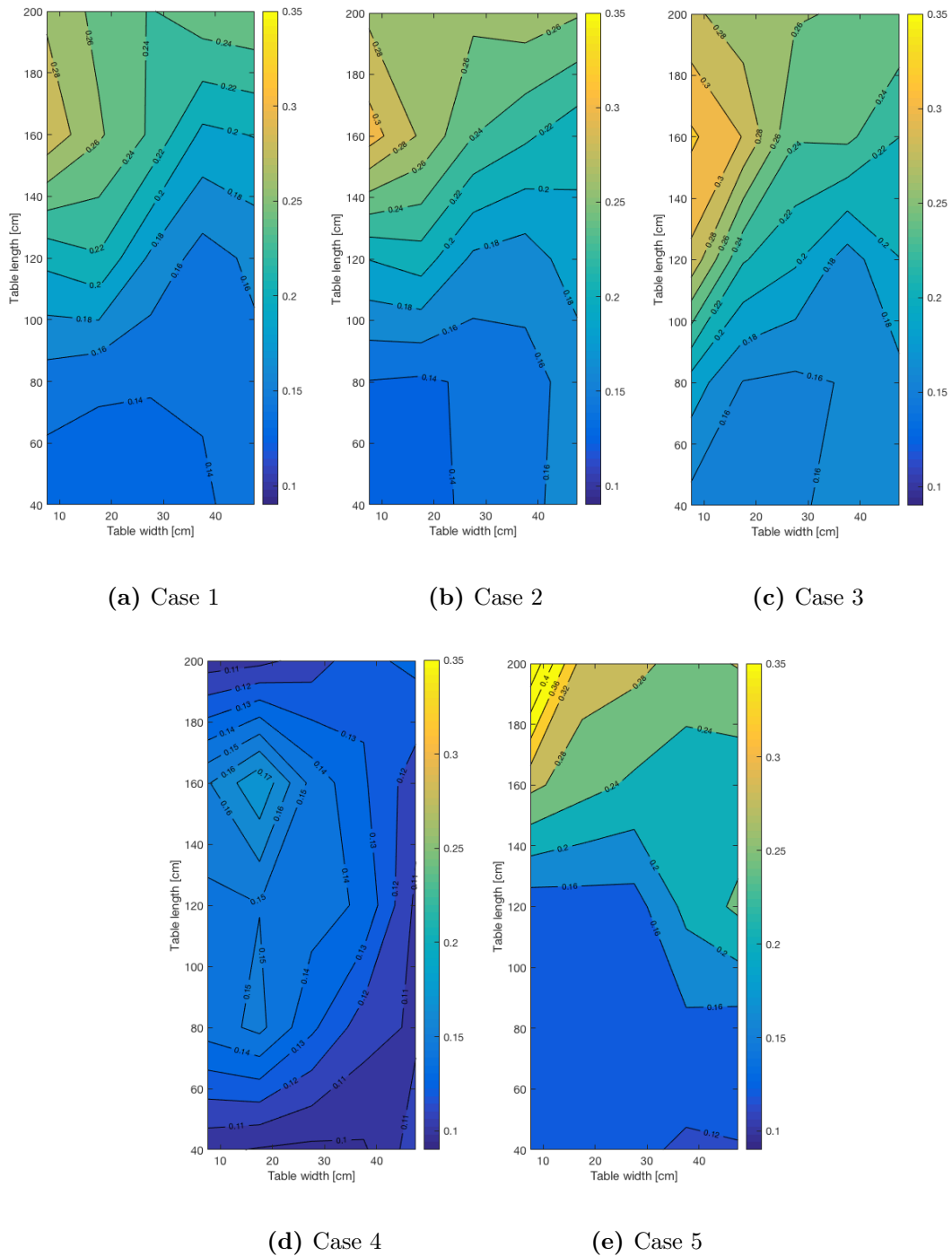
Figure 27: Speed contours at 120 cm above the floor

5.1.2   Temperature measurements

This chapter includes the analysis of the temperature measurements for three different heights above the operating table for five different experimental setups. Figure 28 shows the temperature contours for the five different cases at 100 cm above the floor.

(a) Case 1   **(b)** Case 2   **(c)** Case 3

(d) Case 4   **(e)** Case 5
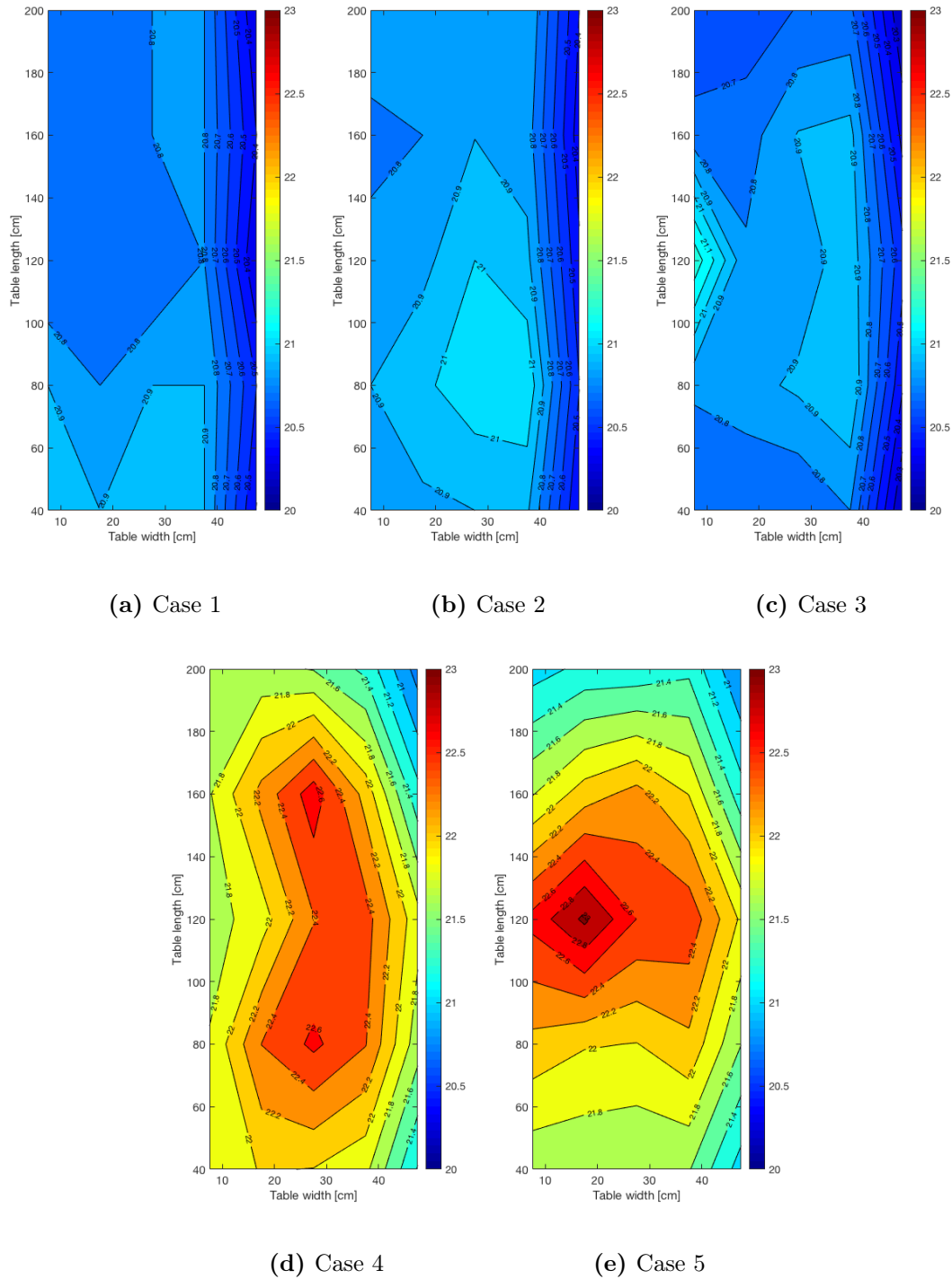
Figure 28: Temperature contours 100 cm above the floor

Figure 28a shows the temperature for the background case, i.e. above an empty operating table. The temperature above the table is varying in an interval of 0.5 °C, between 20.4 and 20.9 °C. The temperature reaches its maximum value in the lower part of the table, in where the speed has its lowest value (see Figure 25a). When a patient is included in Figure 28b, the temperature distribution above the patient is increased. The highest temperatures are in the area where the speeds are lowest, see Figure 25b. As mentioned before, this indicates a convective buoyancy effect created by a human thermal plume, because the warm surface of the human will heat the surrounding air and raise, which will counteract the airflow from

the ventilation system.

For Case 3 the heated cylinders are changing the temperature distribution above the table. As seen from Figure 28c the temperature at the left side of the operating table is increasing in Case 3. This is because of the heated cylinder which is placed 120 cm on the table length (in y-direction). Figure 25c also shows higher speeds at the exact same area. But two equally heated cylinders were also placed at the lower edge of the table and 120 cm in y-direction on the tables right side. As seen from Figure 28c these two cylinders does not affect the temperature distribution as the cylinder on the left side. The fact that the first measuring point in y-direction is 40 cm from the table edge might explain the lack of evidenced influence from one of the cylinders, but not the other. There is no explanation for why the third cylinder does not affect the temperature distribution above the table. It might be due to an old light bulb or measurement faults, as it did not seem to affect the speed distribution above the table too much either.

When the surgical lamps are included, i.e. for Case 4 and 5, the temperature profile changes drastically. From Figure 28d it is clearly shown where the surgical lamps are placed. The lamp with biggest diameter is placed above the lower part of the table, as seen from the figure. Since they are set to light straight down on the operating table, the air at that exact area is heated. For Case 5 the surgical lamps are set to shine in 45°to the middle of the table at the exact same spot, and this is the red spot shown in Figure 28e. The temperature at this point is 23 °C. The figure also shows a clear temperature stratification from 21°C to 23°C.

Figure 29 shows the temperature contours at 110 cm above the floor. The figures shows in general lower temperatures, except for Case 1. The peak temperature for Case 3 is also higher at 110 cm compared to 100 cm above the floor.

Figure 29a gives the temperature contour 33 cm above an empty operating table. The temperature is varying more at this height compared to for 23 cm above the operating table. For Case 2, the temperature above the table decrease, see Figure 29b. As the distance from the patient is bigger, the thermal plume is cooled by the entrainment of the surrounding "cold" air, hence reducing the temperature of the plume. For Case 3 the temperature at the left, middle side of the table reach a value of 21.5 °C. As for 100 cm above the floor, the two other cylinders does not seem to affect the temperature distribution at this height.

Figure 29d and 29e shows the temperature distribution with lamps in horizontal- and in 45°position respectively. At this height, the temperature rise caused by the lamps is not as big as for 100 cm above the floor. For Case 4 the temperature is higher on the upper part of the operating table, which is illuminated by the smallest lamp. For Case 5 the maximum temperature reach 22.4 °C, which is 0.6 °C lower than for the same point 10 cm below.

(a) Case 1   **(b)** Case 2   **(c)** Case 3

(d) Case 4   **(e)** Case 5
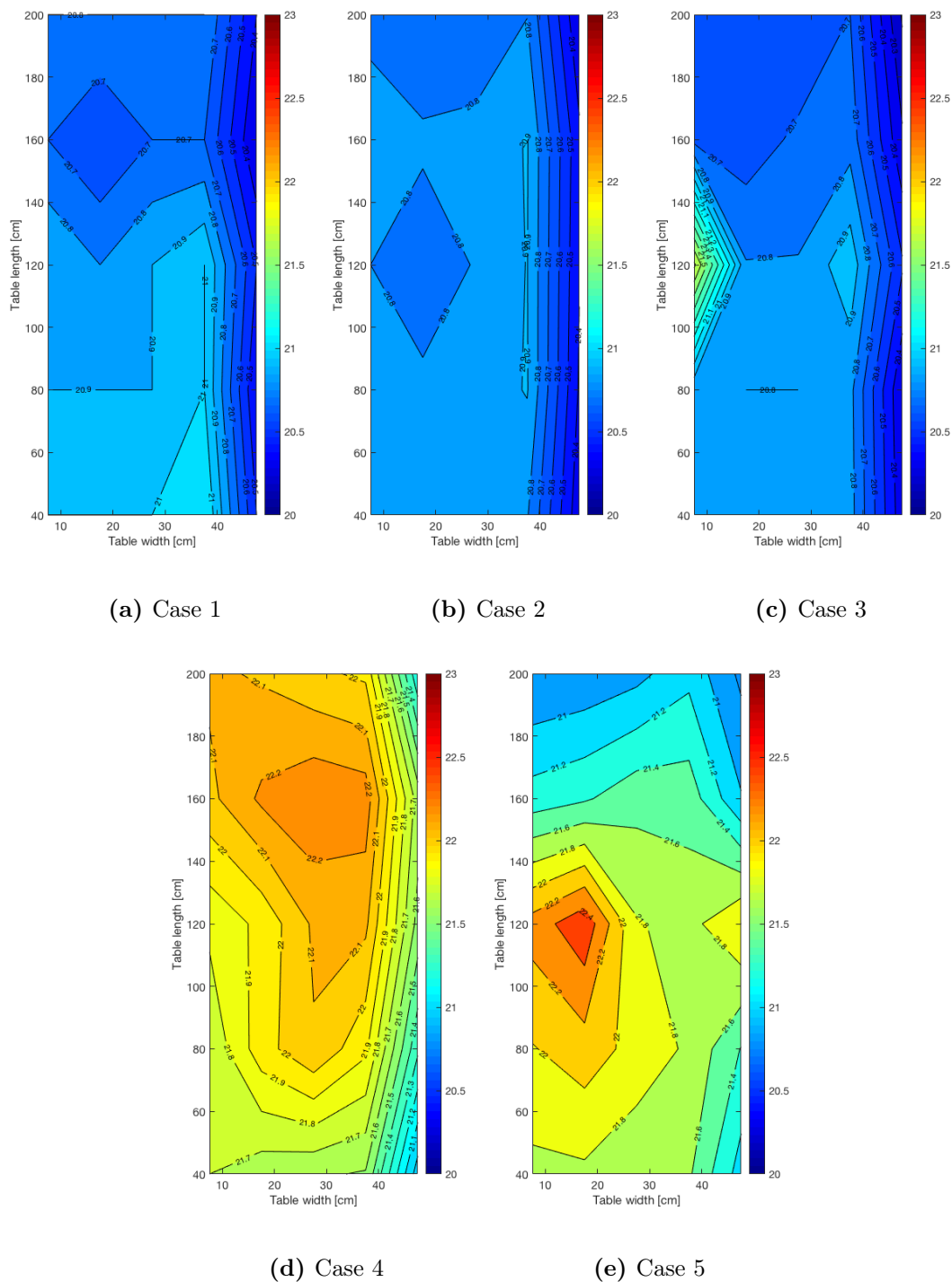
Figure 29: Temperature contours at 110 cm above the floor

Figure 30 shows the temperature distribution 120 cm above the floor, i.e. 43 cm above the operating table. At this height the temperature is more stable than for the two previous heights for the first three cases.

For the first case the temperature at the majority of the table is 20.9 °C. For Case 2, this temperature is decreased to 20.8 °C. In Case 3 the effect of the three cylinders are not creating a peak on the temperature distribution, as the left one did 100 and 110 cm above the floor.

When surgical lamps are included, the temperature level differs a lot from the three previous

cases. As for 100 cm, it is clear from Figure 30d where the two horizontal lamps are placed. At this level the temperatures are measured closer to the lamps, leading to higher temperatures compared to Figure 29d. For Case 5, the temperatures are general lower compared to the two previous heights. The temperature at the target spot is 22.2°C, which is 0.2°C lower than at 110 cm and 0.8°C lower than at 100 cm above the floor.

(a) Case 1   (b) Case 2   (c) Case 3

(d) Case 4   (e) Case 5
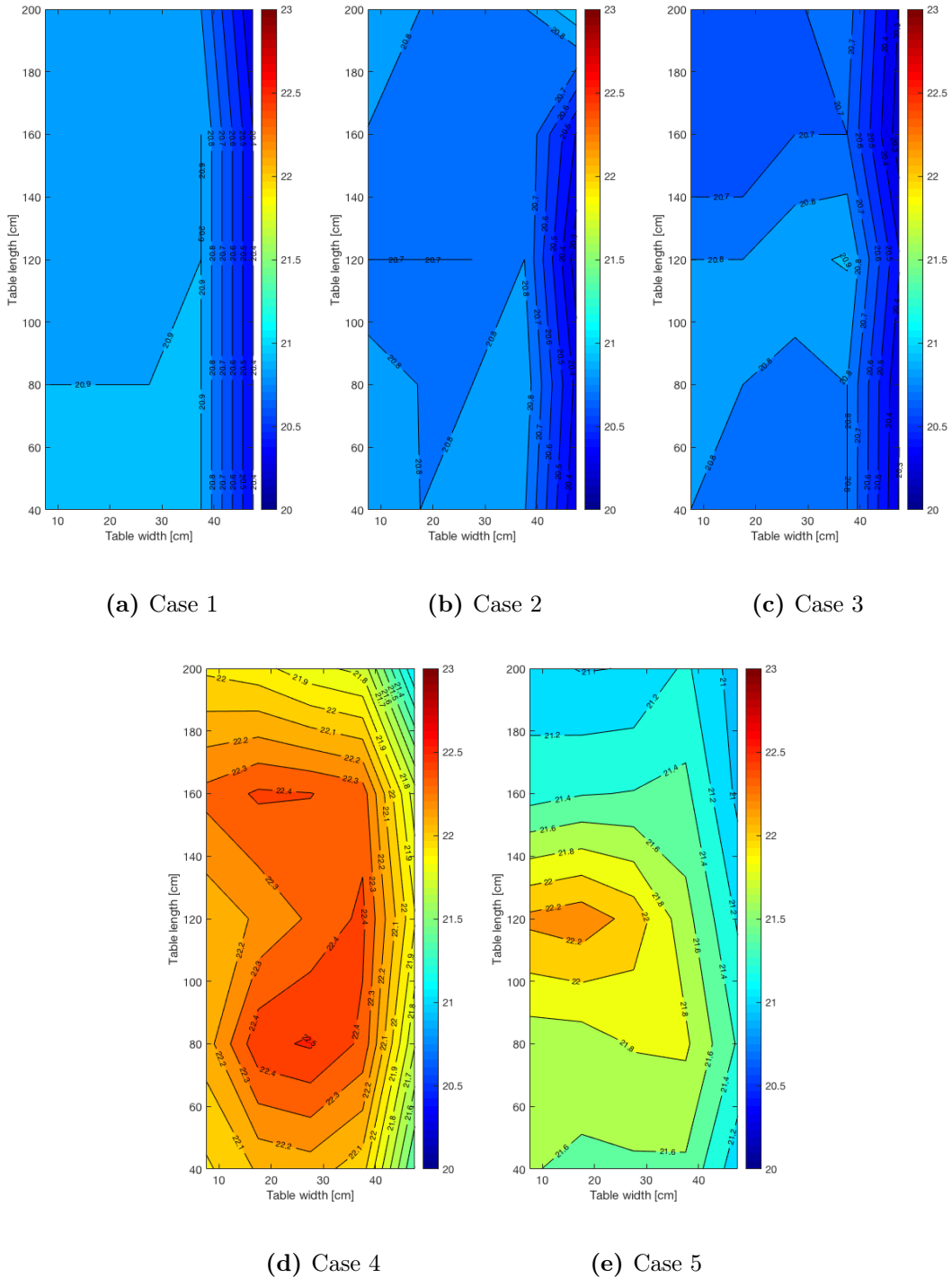
Figure 30: Temperature contours 120 cm above the floor

5.1.3   Turbulence intensity

In this chapter, turbulence intensity contours for the five different cases will be presented. It was not found any particular standard that described what level of turbulence is considered as low, medium or high for LAF ventilation. This chapter will therefore just present the results briefly. As seen from Figure 31 the TU above the operating table is quite steady for the first case but increase drastically when surgical lamps are included. According to Karthikeyan et al. a turbulence intensity of 12.5% is high level of turbulence, meaning there is a high TU in the middle of the empty operating table [27].

From Figure 31b the effect of the human patient on the turbulence intensity is shown. The figure shows an increased turbulence level above the patient, compared to Case 1 given by Figure 31a. By including a human patient the turbulence level at the middle of the table increase with 10%. Figure 31c shows a lower maximum turbulence level compared to Figure 31b, but also a higher minimum TU above the table. The effect of the cylinder placed on the left side of the table is again affecting the contour plot.

The surgical lamps are increasing the turbulence level above the whole surface to a high turbulence level. The turbulence intensity is more stable when the lamps are placed in horizontal position compared to in 45°, with variance between 18 to 28% compared to from 12 to 32%. So even though the speed at the same altitude, ref Figure 25d, is the most disrupted airflow of all of the cases, the turbulence level is still not highest for Case 4.
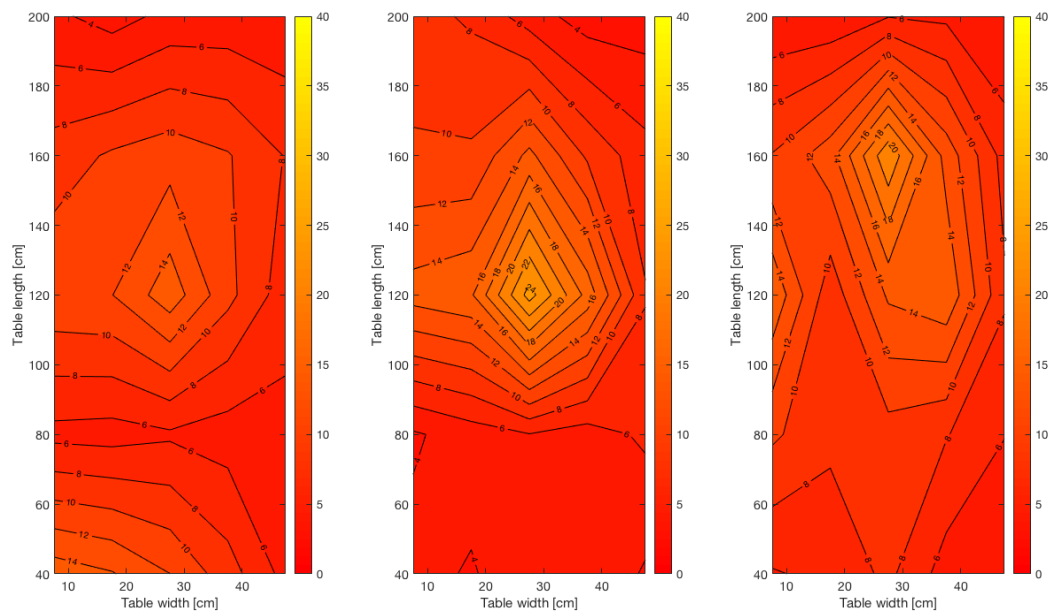
(a) Case 1   **(b)** Case 2   **(c)** Case 3
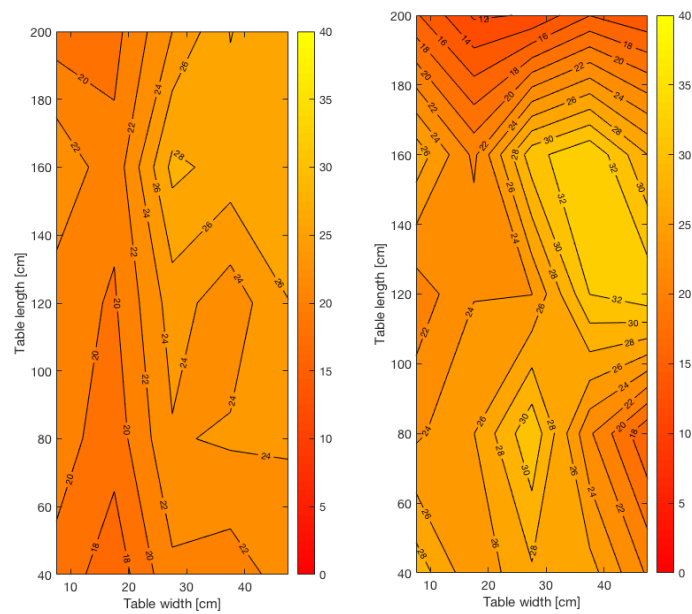
(d) Case 4   **(e)** Case 5

Figure 31: Turbulence intensity at 100 cm above the floor

The turbulence intensity for every case at 110 cm above the floor, i.e. 33 cm above the table is presented in Figure 32. For the background case, i.e. Case 1, the turbulence level above the table is lower at an altitude of 110 cm compared to at 100 cm. The maximum TU above the empty operating table is as shown in Figure 32a 12%. The turbulence level for Case 2 is also decreasing at this height, and moving to the left side of the table as seen from Figure 32b. Figure 32c shows how the cylinder placed on the left side of the operating table affects the turbulence intensity, where the turbulence level is increased to roughly 22%, which is the highest level in the figure.

For Case 4 and 5 the turbulence level contours are again changed. Figure 32d shows a clearly higher turbulence intensity below the lamps, and a lower level in between them. For Case 4 the turbulence level in increased, while the level in decreased for Case 5 at 110 cm compared to 100 cm above the floor.

(a) Case 1   **(b)** Case 2   **(c)** Case 3

(d) Case 4   **(e)** Case 5
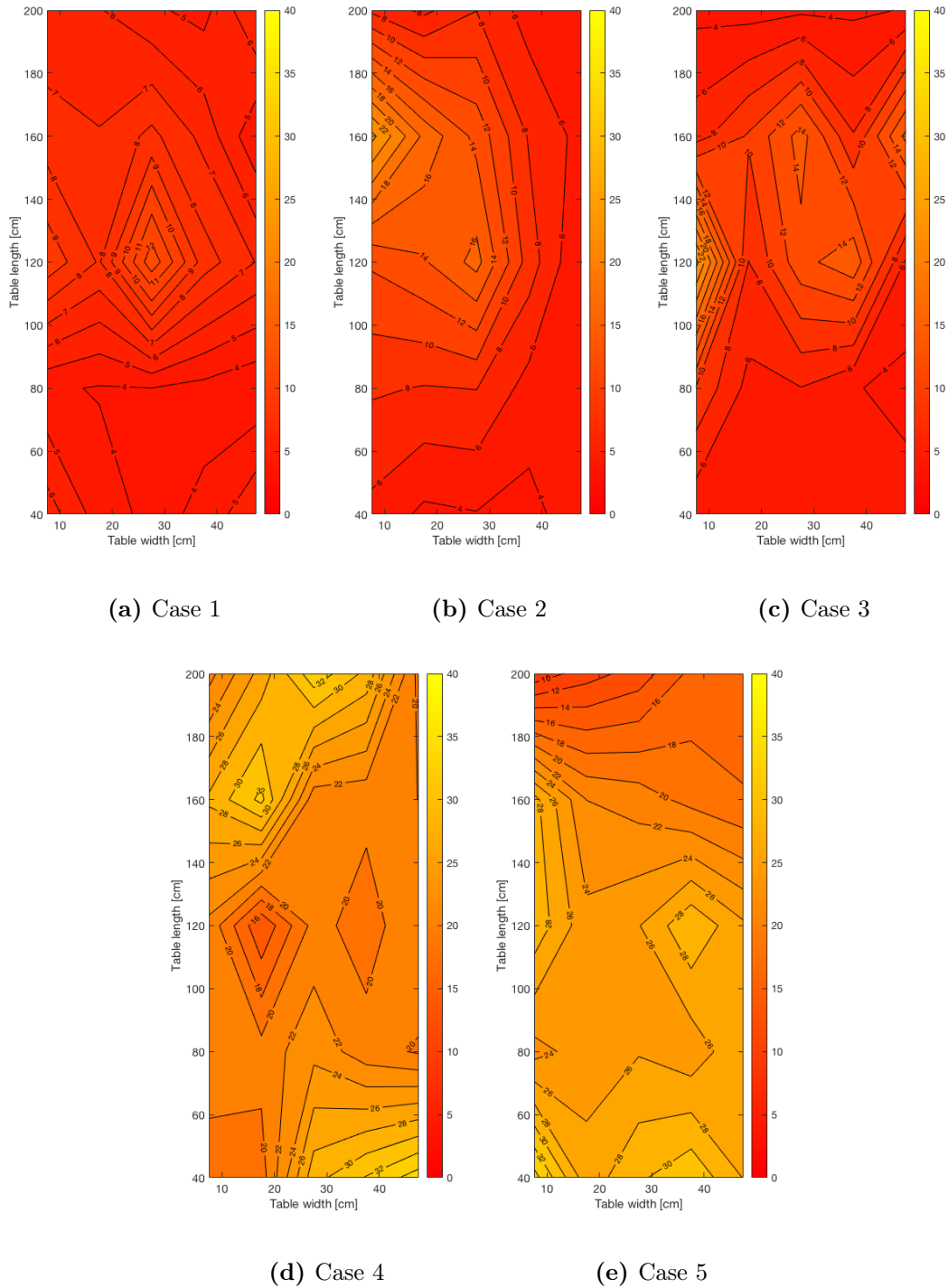
Figure 32: Turbulence intensity at an altitude 110 cm above the floor

Figure 33 shows the turbulence level at an altitude of 120 cm above the floor. The turbulence level for Case 1 is varying in an interval of 6%, from 4 to 10%. This is the contour with the lowest turbulence level reached for Case 1. For Case 2, Figure 33b shows the highest turbulence level at the left, upper part of the table. In Figure 33c it is shown that the majority of the table has a turbulence intensity below 10% for Case 3, which is quite low. When the lamps are included in Case 4 and 5, the turbulence level is at its highest. For Case 4 the turbulence intensity reaches 36%, which is much higher than for its two previous presented heights. For Case 5 the highest turbulence level is 34%, see Figure 33e.

(a) Case 1   **(b)** Case 2   **(c)** Case 3

(d) Case 4   **(e)** Case 5
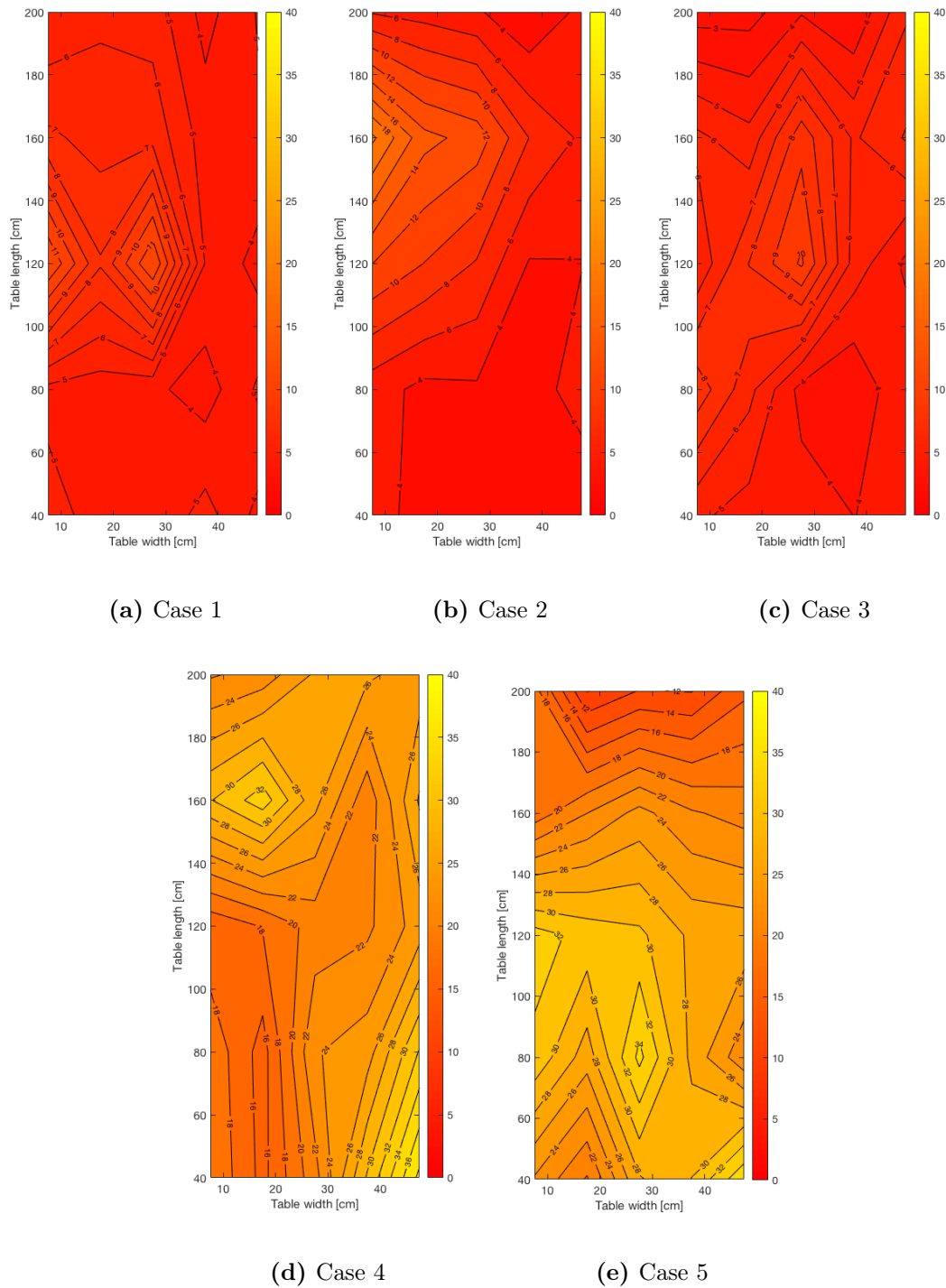
Figure 33: Turbulence intensity at 120 cm above the floor

5.2   Scenario 2: Thermal plume measurements above a thermal manikin

In this chapter the results from the plume development caused by natural convection is presented. First, the results will be presented as speed contours and speed plots. Then the two different methods explained in section 3.2 will later be used to suggest a formula for the plume development.

Figure 34 shows the speed contour at six different places above the thermal manikin: above the legs, knees, upper thighs, stomach, chest and head. The convective flow is clearly pictured in all of the figures, and it is evident that the greatest plume development is happening above the manikins stomach. From all of the contours it can be seen that there is generated swirling right outside of the boundary of the convective flow, which may be due to instabilities because of entrainment of the surrounding air. All of the figures shows the potential the convective flow generated by a manikin in supine position can have on the air distribution in a room. In Figure 34, the operating table is placed in the interval for a width from 15 cm to 70 cm. During the experiment it was measured that the manikins legs were not equally heated, which is probably the reason for the stronger convective flow against one side in Figure 34a to 34c.

Figure 34a shows the plume above the manikins legs. The maximum speed for the convective airflow above the legs are 0.08 m/s, which is reached at 120 cm above the floor, i.e. about 10 cm above the legs. From the figure it can be seen that the coherent plume stops at 30 cm above the legs.

Above the knees, a considerably stronger convective flow is developed as pictured in Figure 34b compared to Figure 34a. The highest speed above the knees are 0.12 m/s, which occurs roughly 10 cm above the manikin. Figure 34b shows that the convective flow keeps affecting the room air at 180 cm above the floor, meaning that the range of the plume cannot be determined by analysing the figure. As already mentioned the manikins legs were not equally heated and the most asymmetric plume has developed above the knees.

The convective flow above the upper thighs are noticeably stronger than above the rest of the manikins legs. The plumes maximum speed is 0.11 m/s, which is reached 30 cm above the heat source.

Figure 34d shows that the convective flow above the manikins stomach is significantly stronger than above the rest of the manikins surface. Even though it can't be seen from the figure, the maximum speed above the stomach 0.139 m/s, which also is the maximum speed above the whole manikin. From the figure it is clearly pictured how the boundary of the plume increase with height, which is consistent with plume theory. Figure 34d does also show that the plumes intensity has a potential to affect the room airflow with 0.12 m/s 70 cm above the manikin, which can have a significantly impacts on the room airflow distribution. And as it is uncertain what happens above 180 cm, the plume can potentially have even greater impacts than initially considered.

The convective speed presents a quasi-symmetric distribution above the manikins chest area in Figure 34e. The highest speed on the figure is 0.07 m/s. Figure 34f shows the plume generated above the manikins head. The shape of the plume is more narrow and weak than above other parts of the body, and only raise about 35 cm above the head. The maximum speed is 0.08 m/s, which only occurs in tiny regions of the plume. Notice how the airflow swirls around the thermal plume, indicating the the plumes create turbulence in the surrounding air. The plume above the head is quite axis-symmetric, as above the chest.

(a) Legs

(b) Knees

(c) Upper thighs

(d) Stomach

(e) Chest

(f) Head
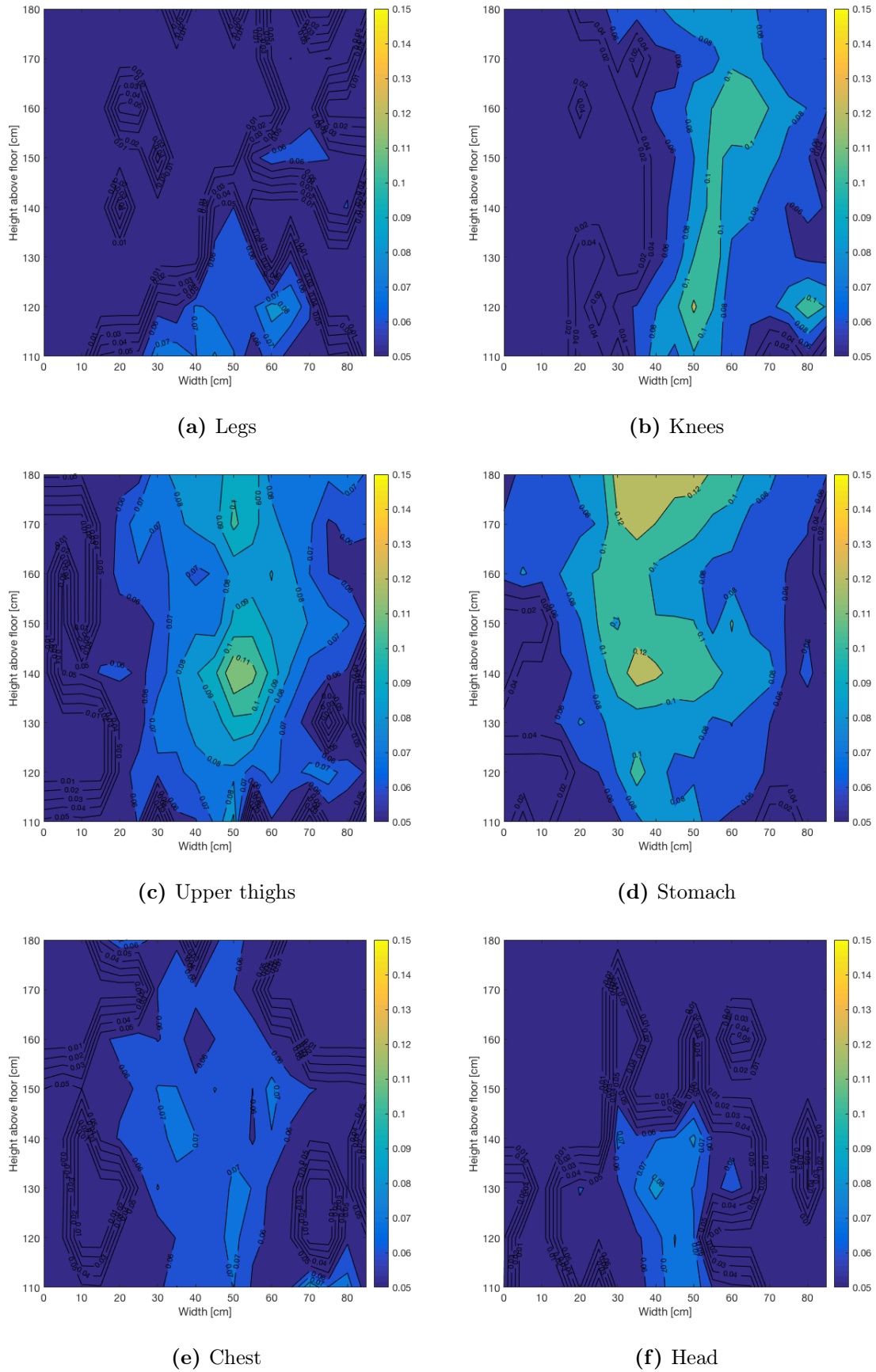
Figure 34: Speed contour for six different cross sections above the thermal manikin

Figure 35 shows the velocity profile at 6 different places across the thermal manikin, as explained in Chapter 4.2.2. Even though omnidirectional anemometers are used for the measurements, there is only a convective air flows in the climate chamber, and the direction of the measured speed can therefore be assumed to be upwards. The measured speed is therefore denoted as velocity for Figure 35. Each of the graphs in each figure represent the velocity profile at a certain height above the thermal manikin, but the heights are named relative to the floor as for the rest of the figures. All of the six different sub-figures in Figure 35 are made from the exact same measuring results as for Figure 34, leading to similar observations from the figures. For example is the velocities geared to the right side of the figure in Figure 35b as for Figure 34b, making them non-axis-symmetric.

Equal for most of the graphs, especially in Figure 35b, 35c, 35d and 35f, is a greater velocity in the middle of the plume. A maximum velocity at the centerline of the plume is consistent with plume theory of a Gaussian distributed velocity profile. From plume theory the centerline velocity is also decreased with height since more ambient air is entrained. This is observed for most of the cases, but especially not above the stomach, ref Figure 35d. The velocity profile furthest away from the stomach is actually representing the highest velocity profile for the plume above the stomach, which is not consistent with theory. Figure 35d also shows really unstable pattern for the developed velocity profiles, where they increase and decrease interchangeably. For instance does the velocity profile closest to the stomach have one of the lowest maximum velocities. This velocity development is also seen in Figure 3b from theory, and may indicate a plume developments in the region close to the manikin.

The maximum velocity reached above the thermal manikin 0.139 m/s, which occurs above the stomach, 180 cm above the floor.

(a) Legs

(b) Knees

(c) Upper thighs

(d) Stomach

(e) Chest

(f) Head
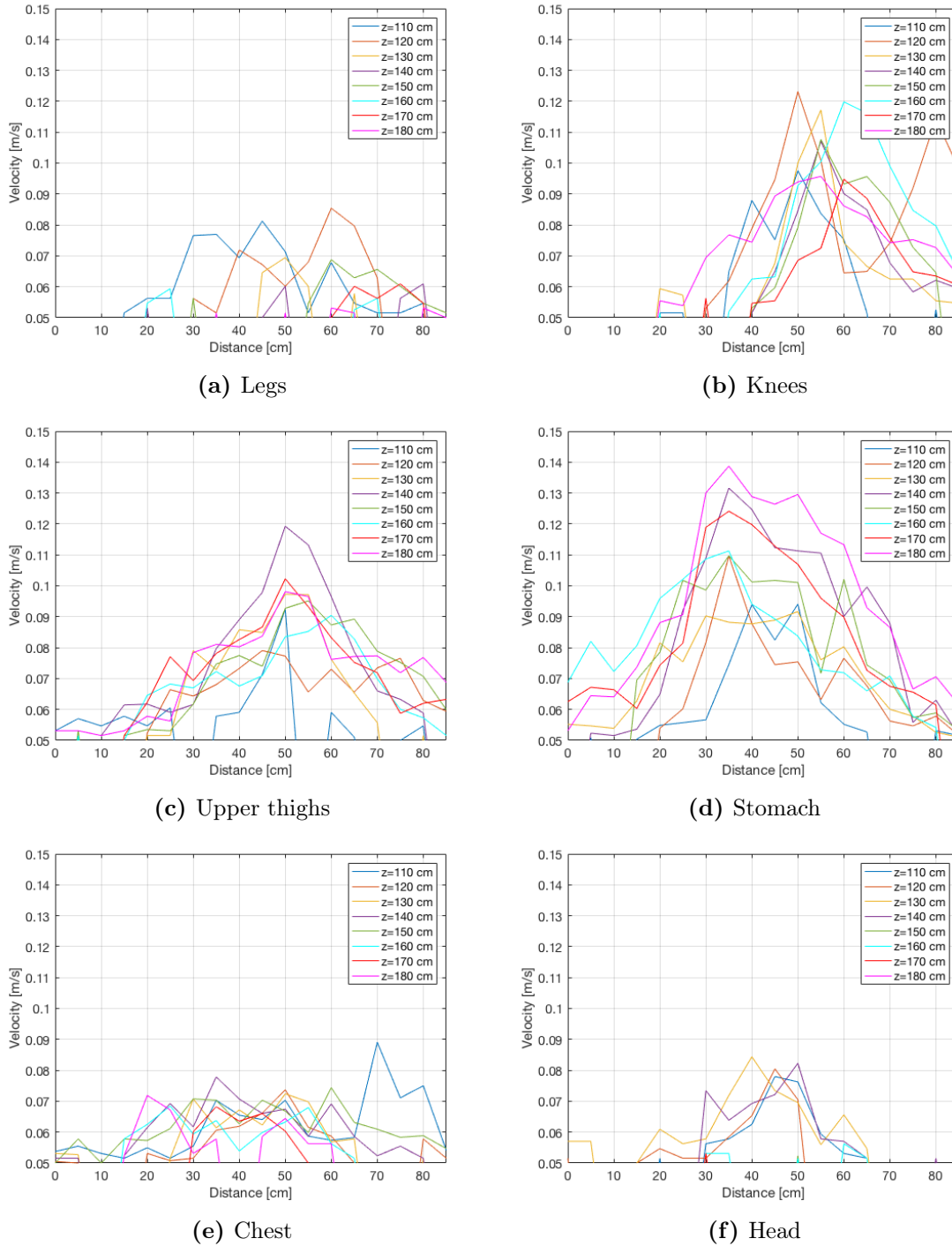
Figure 35: Speed plots for six different places above the thermal manikin

5.2.1   Method 1: Finding the proportionality constant, C_b

As the heat output for the thermal manikin is not constant throughout the source, see Figure 35, it can not be considered as a line source directly. It is therefore assumed as a quantity of point sources placed in line, which each has a different heat output. In reality the development of plumes generated by point sources close to each other will collide and disrupt each others development, but in this study it will be focused on different parts of the body separately. But first, the plume generated by the whole body is presented as a line source.

The convective heat generated by the thermal manikin was first modelled as a line source. As the airflow above the thermal manikin was clearly dependent on the manikin's cross section, it was chosen to calculate the mean velocity profile for each height above the manikin. The result is presented in Figure 36a. The figure shows the plume development above the manikin, independently of the cross section of the manikin. The average diameter for the cross sections for the manikin was about 0.4 m, which gave a z_0=0.76 and a virtual centre at 0.34 m above the floor. By using Method 1 from Chapter 3.2 the plume boundary were found at each height, which resulted in Figure 36b. From the figure it is clear that the boundaries are not increasing linearly with height, which make it difficult to suggest a fitted line. But the spread angle of the current fitted line is approximately 15.9°, which gave a C_b=0.286.
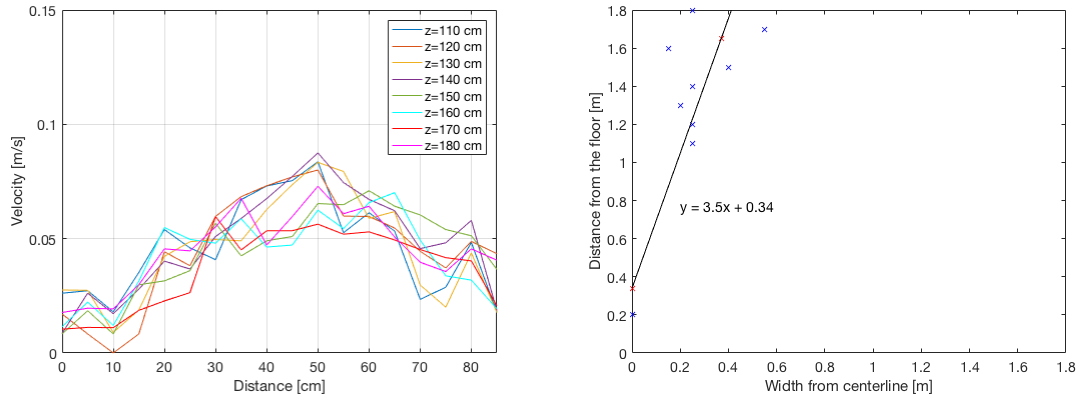
(a) Averaged velocity profiles to modify as a line source   **(b)** Spread angle for the manikin modelled as a line source

Figure 36: Line source averaged velocities and corresponding spread angle

The corresponding formula for the line source is given by the centerline velocity in Equation 27 and by volume flow rate in Equation 28.

$$U_0 = 2.08 \cdot (\frac{g\beta}{\rho c_p})^{1/3} \cdot \dot{Q}_c^{1/3} \tag{27}$$

$$q_z = 0.53 \cdot (\frac{g\beta}{\rho c_p})^{1/3} \cdot \dot{Q}_c^{1/3} \cdot l \cdot (z + z_0) \tag{28}$$

From Equation 27 it is given that the velocity is constant after the acceleration phase. To investigate if that was the case for the performed measurements, the averaged maximum velocities above the line source was found. The result is presented in Figure 37, which shows that the centerline velocity is not constant but varies from 0.0596 m/s to 0.0875 m/s.
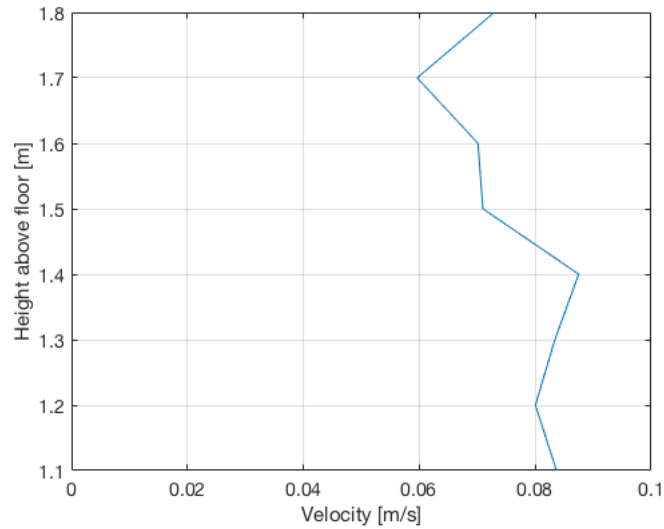
Figure 37: Centerline velocity for line source

As a persons head is not covered by clothes, and normally has a high temperature, it was planned to model the head as a point source. But as the thermal manikin did not get heated properly this idea did not give any proper results. The results are therefore placed in Appendix D.2.2, and it is instead focused on the plume generated above the stomach.

The velocity profile above the stomach was chosen to be modelled as a point source. The velocities presented in Figure 35d were therefore used to find the spread angle α and consequentially C_b. The diameter above the stomach of the manikin was approximately 0.50 m, which gave a z_0 equal to 1.045 m by using Equation 14 for a point source. This again gave the virtual point centre at 0.055 m above the floor, which is represented by a red cross in Figure 38. The plume boundary layer is then calculated to develop as shown in Figure 38, and based on linear regression for a fitted line a spread angle of α=17.9°was found. This leads to an empirical C_b equal to 0.323.
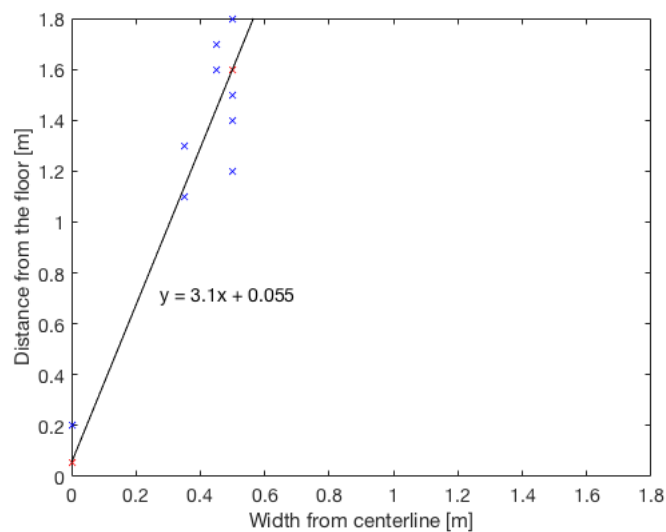
Figure 38: Spread angle for velocities above the stomach, modelled as a point source

This gives the development of centerline velocity above the stomach given by Formula 29 and

volume flow rate given by Formula 30.

$$U_0 = 3.31 \cdot \left(\frac{g\beta}{\rho c_p}\right)^{1/3} \cdot \left(\frac{\dot{Q}_c}{z + z_0}\right)^{1/3} \tag{29}$$

$$q_z = 0.29 \cdot \left(\frac{g\beta}{\rho c_p}\right)^{1/3} \cdot \dot{Q}_c^{1/3} (z + z_0)^{5/3} \tag{30}$$

5.2.2 Method 2: Finding the plume boundary by using a Gaussian approximated velocity profile

Because it was questioned whether the plume boundary could be approximated by the correlation $U_b = \frac{U_m}{e}$, the boundary was also found by Equation 17. As the measuring range for TSI 8475 omnidirectional anemometers are from 0.05 to 2.54 m/s, the plume speed is unknown outside that range. To check if $U_b = \frac{U_m}{e}$ can be applied for this specific plume, the measured values should include this point. From Figure 35 the only maximum velocity divided on e which results in a value above 0.05 m/s is the measured above the stomach, 180 cm above the floor. The maximum speed, U_m at this heights is 0.139 m/s, which results in an U_b equal to 0.051 m/s. This results in a boundary outside the measuring range, but approximately above 42.5 cm. After discussion with my supervisor the value for the boundary were set to 42.5 cm. Based on Formula 17 and the measurement results given in Figure 35d the boundary of the plume were calculated and the velocity distribution were approximated as a Gaussian distributed curve. The boundaries were found based on the actual measured maximum velocity at each height z. The results from the approximation are presented in Table 9 and the corresponding plot is shown in Figure 39. Figure 39 is an axis-symmetric plot and should be comparable with Figure 35d.

Table 9: Results by using the Gaussian approximation

Height above floor	U_0	Boundary
110 cm	0.094 m/s	0.516 cm
120 cm	0.110 m/s	0.461 cm
130 cm	0.092 m/s	0.523 cm
140 cm	0.132 m/s	0.413 cm
150 cm	0.110 m/s	0.470 cm
160 cm	0.111 m/s	0.412 cm
170 cm	0.124 m/s	0.511 cm
180 cm	0.139 m/s	0.425 cm
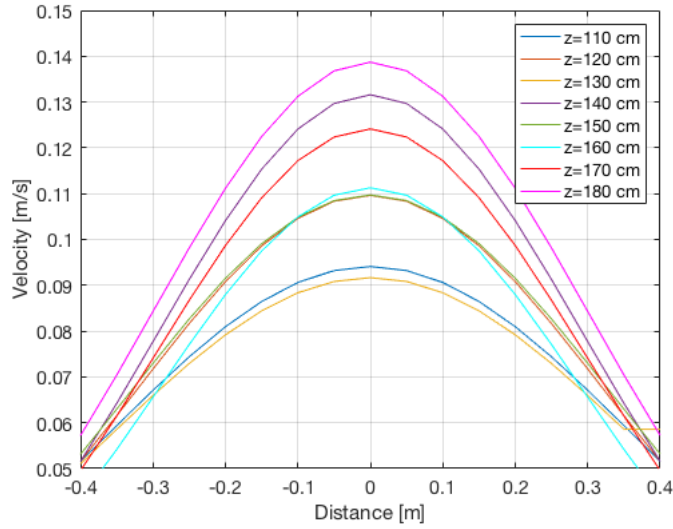
Figure 39: Calculated velocity profiles above the stomach

Even though Figure 35d, and hence Figure 39, is not fully consistent with the plume theory, by the fact that the maximum velocities for each height does not develop in any particular pattern, indicate an unstable flow emitted by the heat source. By utilising the calculated plume boundaries presented in Table 9, the spread angle α can be found. A plot of the boundaries and corresponding spread angle is presented in Figure 40. As seen from the figure the boundaries are not increasing with height, which make it challenging to suggest a fitting, linear line. However, a line is suggested which lead to an α equal to 18.4°, and C_b equal to 0.333. The virtual centre of the plume is logically the same as used for Figure 38.
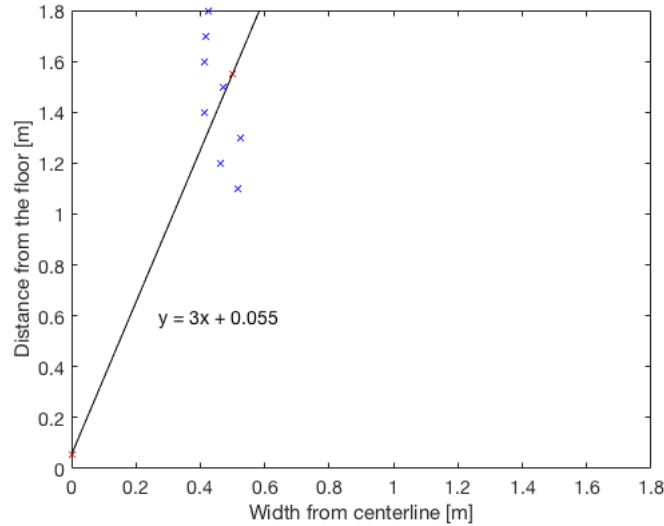
Figure 40: Spread angle above the stomach modelled as a point source with Gaussian distribution

The suggested formula for the centerline velocity is presented in Equation 31 when the stomach is suggested to be modelled as a point source.

$$U_0 = 3.39 \cdot \left(\frac{g\beta}{\rho c_p}\right)^{1/3} \cdot \left(\frac{\dot{Q}_c}{z + z_0}\right)^{1/3} \qquad (31)$$

Equation 32 is the suggested formula for the developed volume flow rate above the stomach.

$$q_z = 0.30 \cdot (\frac{g\beta}{\rho c_p})^{1/3} \cdot \dot{Q}_c^{1/3} (z + z_0)^{5/3} \tag{32}$$

5.3 Scenario 3: Experiment at St. Olavs Hospital with thermal manikin

Scenario 3 will focus on the interaction between convective airflow generated by a thermal manikin and LAF supplied from a ceiling diffuser, and is divided into two sub-chapters as for the experimental setup explained in sub-chapter 4.3. For both of the experiments the thermal manikin was heated as explained in Chapter 4.2.1, and TSI 962 handheld anemometer was used to measure the outlet velocity from the the ceiling supply diffuser. The outlet velocities was measured to be 0.27±0.4 m/s.

5.3.1 Case 1: Interaction between the human thermal plume and laminar airflow

As for Scenario 1, the speed above the operating table is presented as speed contours. The results from the measurements in Scenario 3, Case 1 for seven different heights is presented in Figure 41. In this case the development of thermal plume generated by a manikin by forced convection is studied. It can not be assumed that the plume developed by forced convection is equally formed as for natural convection (studied in Scenario 2), meaning that the two scenarios are not completely comparable. For the two different experiments, the boundary conditions in climate chamber vs. hospital are not the same and should therefore not be compared. This is because a lower temperature difference between the manikins surface and ambient air will cause less convective flow, and vice versa. The temperature at the operating theatre was roughly 5°C lower than at the climate chamber, saying that a more powerful plume is expected to be developed at the operating theatre.

Figure 41 shows the airflow distribution above an operating table containing a thermal manikin. Seen from the different sub-figures the airflow distribution changes with height, and is clearly lowest closest to the manikin. The airflow in close proximity to the manikin varies from 0.1 m/s to 0.26 m/s. From Figure 41 it is evident that the speed contours furthest away from the operating table are most similar, see Figure 41e to 41g. From this it can seem like the speed is stabilised and not affected by the plume. From Figure 41 it is actually only in close proximity to the patient that the airflow is seemed to be noticeably affected by a buoyancy, convective flow.

(a) 110 cm   **(b)** 120 cm   **(c)** 130 cm

(d) 140 cm   **(e)** 150 cm   **(f)** 160 cm

(g) 170 cm
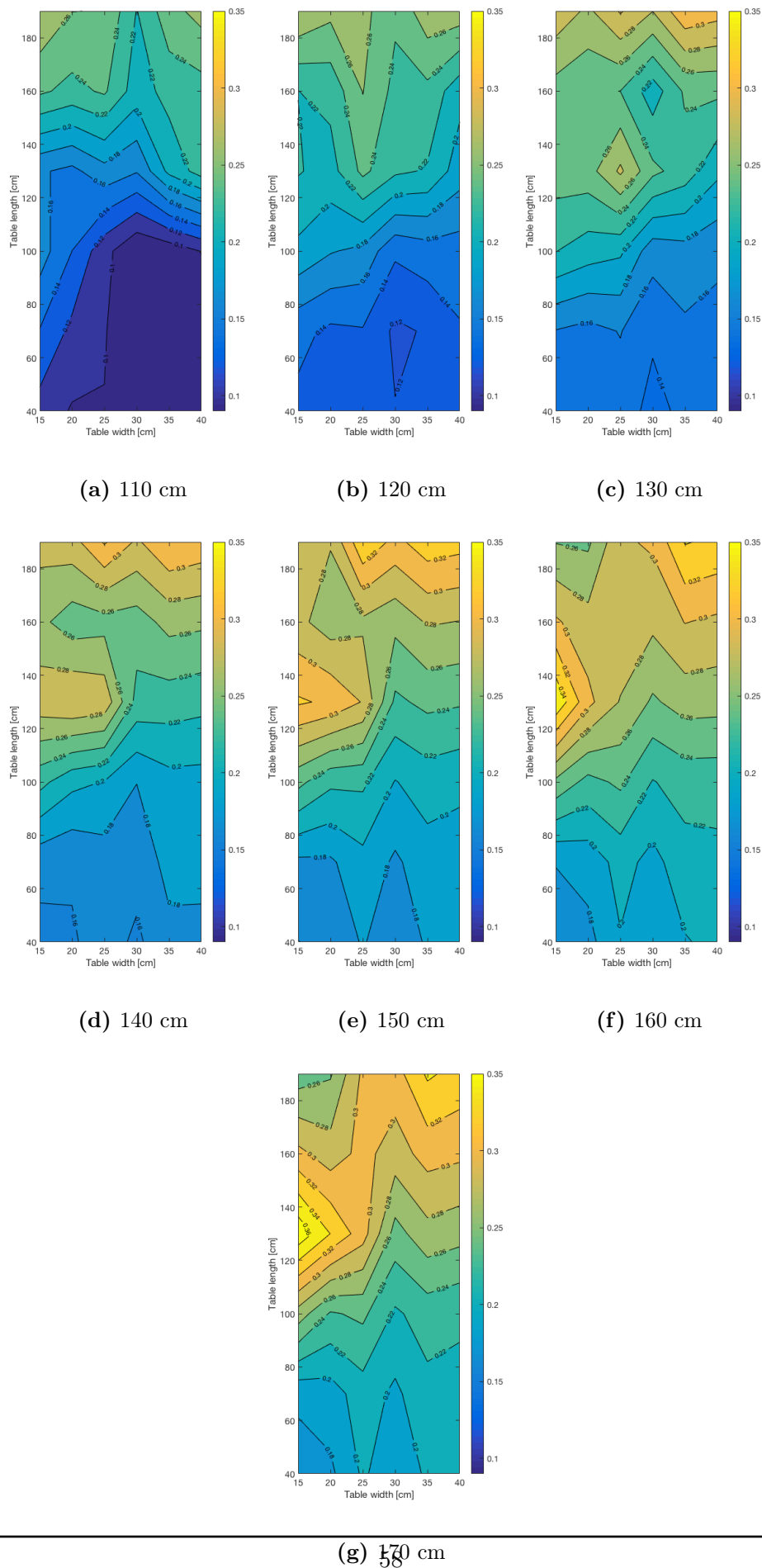
Figure 41: Horizontal speed contours for seven different heights above the floor

As this experiment is performed at the same operating room as for Scenario 1, Case 1 and 2 can be used respectively as a background- and reference case. The comparison with Scenario 1, Case 1 is necessary to analyse the influence of the thermal plume generated by the manikin, and is therefore examined in this chapter. The comparison of the air distribution above a real human being and a thermal manikin is discussed in Chapter 6.1.

The results from this chapter is compared to the speed contours from Scenario 1, Case 1, which is the background case. The airflow distribution above the empty operating table has a clearly lower speed at the lower part of the table and higher speeds on the upper parts. Figure 41a shows the same pattern, a lower speed at the lower part and a higher speed at the upper part of the table. This observations may therefore just be due to the ventilation system and not necessarily because of a convective plume generated by the thermal manikin. But the air flow speed above the lower part of the table is mostly 0.02 m/s lower in Figure 41a compared to Figure 25a, which again may be due to convective flow from above the patient. On the upper part of the table, the air distribution is disrupted on Figure 41a compared to Figure 25a. This may also be because of the unstable heat source.

As the direction of the speed is unknown, vertical contours were developed to spot the interaction between the plume and LAF ventilation. Figure 42 shows the plume developed in forced convection for six different cross sections above the thermal manikin. The convective flow in Figure 42 is not as distinct as flow caused by natural convection presented in Figure 34. In Figure 42 what seems like supply air jets from the ceiling is actually better pictured than a convective plume. However, some of the sub-figures can indicate the development of a plume. As earlier stated, the low speeds at the lower part of the body may be due to how the ventilation system at "Stue 8" operates. This hypothesis is substantiated by the lower supply velocity from the ceiling in Figure 42a to 42c than for Figure 42d to 42f. Still, the speeds close to the operating table in Figure 42a to 42c may resemble a buoyant plume, as the velocity is slightly lower close to the manikin. From Figure 42d it may look like the plume generated above the stomach is minimal, i.e. ventilated by the supply air. And above the chest it is difficult to analyse the effect of the plumes, as the direction of the airflow is unknown. But from Figure 42e it is pictured two local speed spots which are developed either by disruption from the plume or by the ventilation system itself. The plume generated above the head seems to be the most developed plume, as it is clearly pictured some interaction above the head in Figure 42f, even for the high velocities from the ceiling supply diffuser. The measured speed 15 cm above the manikins head is roughly 0.28 m/s, which is decreased to 0.24 m/s right above the manikins head. This can indicate that the head has a potential to develop a convective airflow with capacity of 0.04 m/s 10 cm away from the heat source.

(a) Legs

(b) Knees

(c) Upper thigh

(d) Stomach

(e) Chest

60

(f) Head
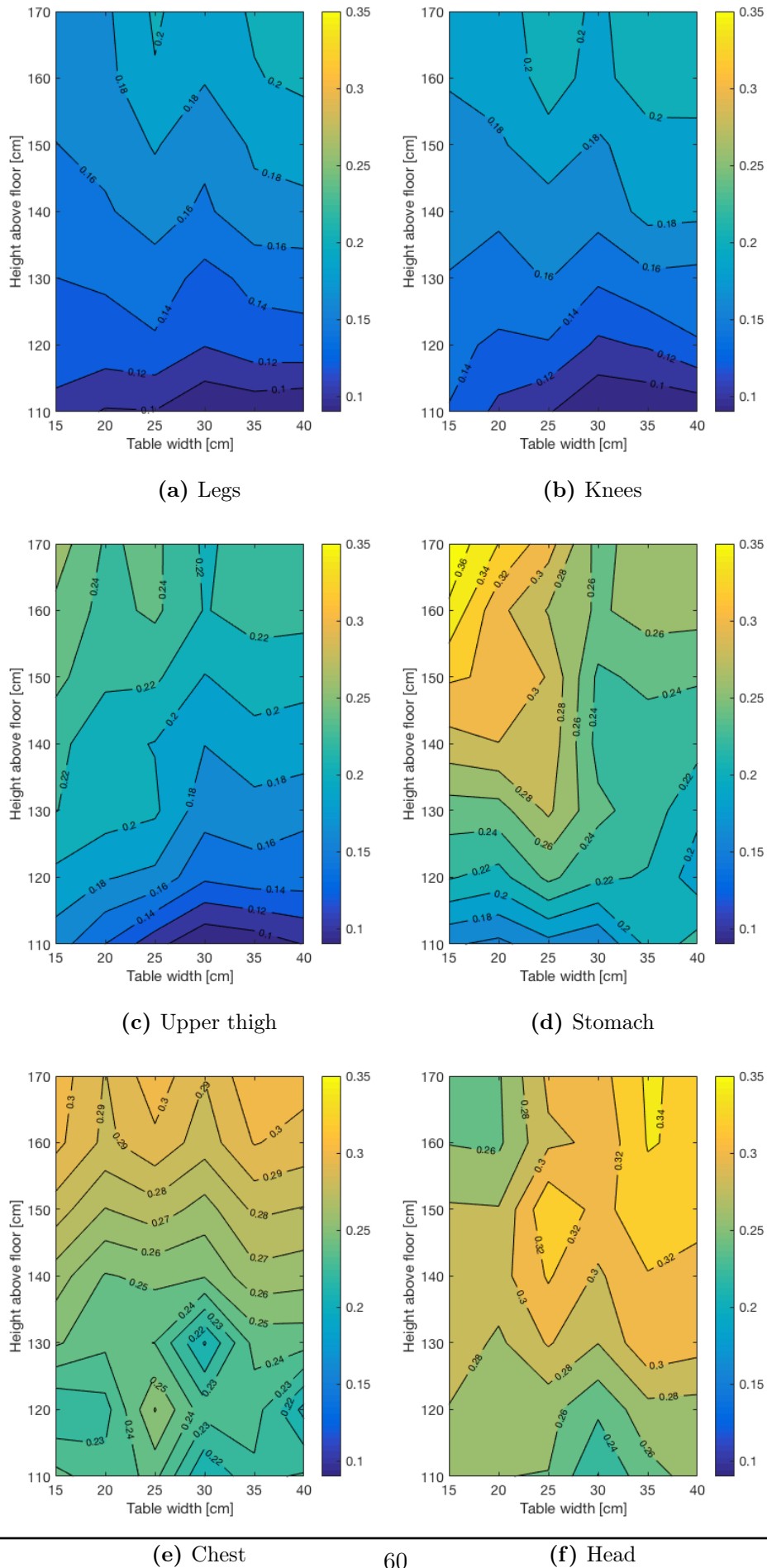
Figure 42: Vertical speed contour for six cross sections above the manikin

A plot of vertical speeds for six different lengths above the operating table were also made. The result is presented in Figure 43. From the figure it looks like a plume is developed along the manikins legs up to its chest. Around 160 cm for the table length, which is above the manikins chest, there is some flow which may resemble a developed plume. But this can not be confirmed due to the lack of knowledge of the air flow direction. From Figure 43 it also looks like the laminar flow panels are mixed with perforated ceiling diffusers that produce conventional air jet supplies, as a vertical jet-similar airflow is supplied from the ceiling and is especially pictured in Figure 43a.
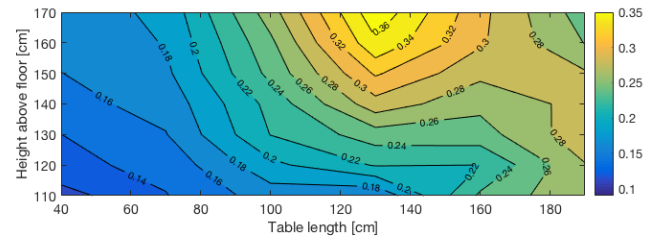
(a) 15 cm in x-direction
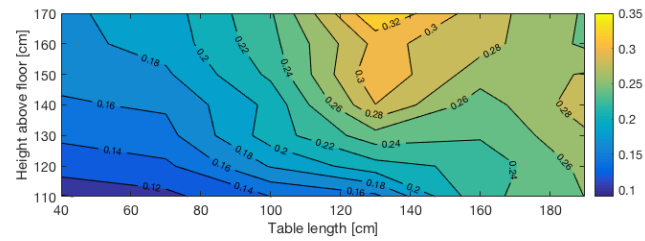
(b) 20 cm in x-direction
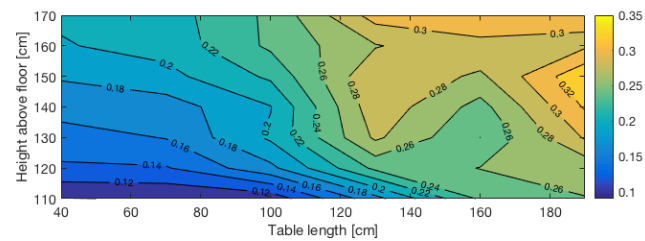
(c) 25 cm in x-direction
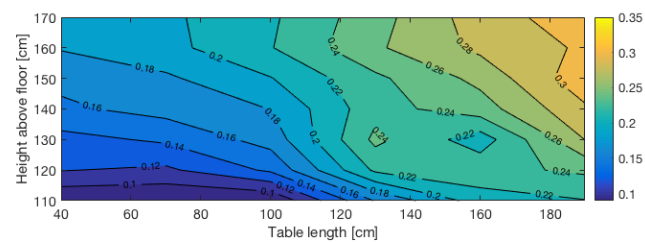
(d) 30 cm in x-direction
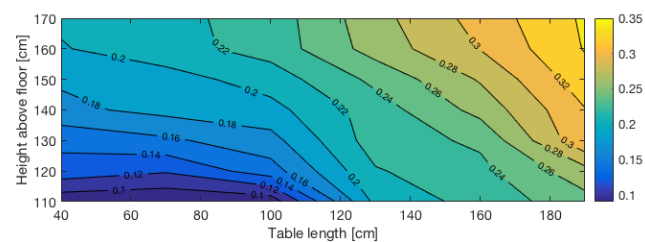
(e) 35 cm in x-direction
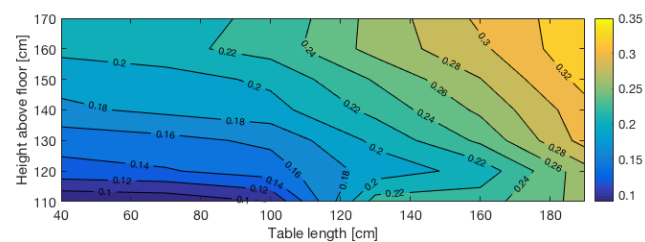
(f) 40 cm in x-direction

Figure 43: Vertical speed contours for six different cross sections of widths

5.3.2   Case 2: Plume interaction with laminar airflow

The results of the measured speed distribution above the thermal manikin is presented as speed contours for three different in Figure 44. The figures shows some similar speed distribution above the table, compared to Case 4 and Case 5 from Scenario 1, where the airflow from the supply diffuser is clearly disrupted by the lamps. The airflow below the lamp at the upper edge of the table is clearly decreased, see Figure 44c. From Case 1 in Scenario 1, it was concluded that the ventilation system operates with lower velocities at the lower part of the table, and higher velocities at the upper part of the table. Since the speeds at the upper part of the table is decreased to the lowest speeds at 150 cm, it looks like the upper lamp hinders the air flow the most.
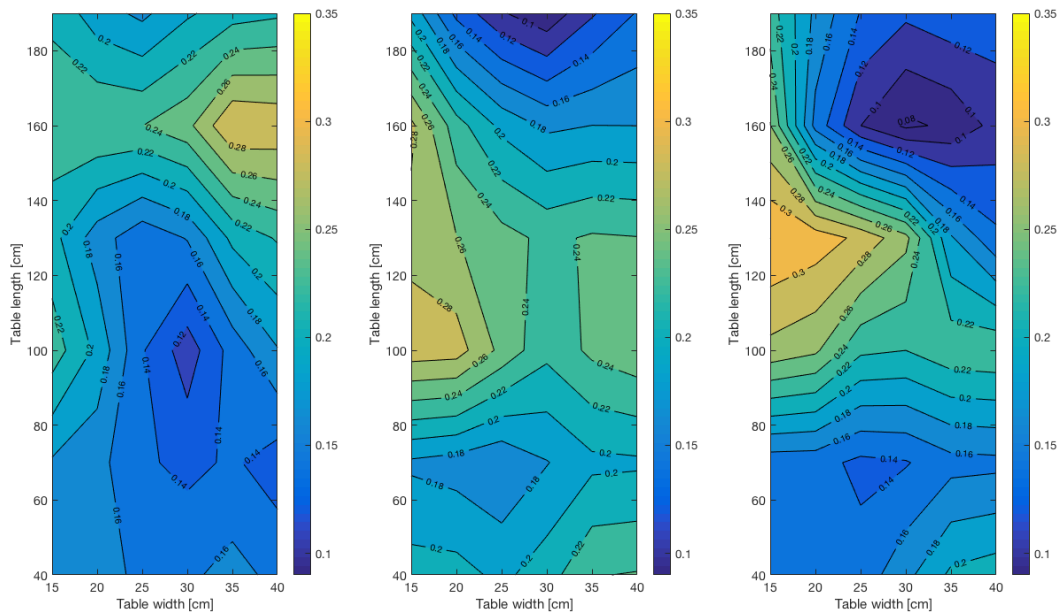
(a) 110 cm above the floor   (b) 130 cm above the floor   (c) 150 cm above the floor

Figure 44: Horizontal speed contours for Case 2, Scenario 3

Figure 44a shows the speed right above the manikin. Compared to Figure 41a, it is clear that the experimental setup for this case is hindering the air to reach the thermal manikin, and hence the surgical site. The air speed above the manikin is varying between 0.12 m/s and 0.28 m/s. The air distribution at 130 cm above the floor is also clearly influenced by the placement of the lamps, which is most visible at the upper part of the table. This is also apparent in Figure 44c, which also shows a clear speed gradient at the left, middle side of the table.

6   Discussion

This chapter contains a throughout comparison of the experiment and the mathematical models. Questionable aspects of scientific methods is discussed. The chapter does also include limitations and recommendations of aspects that should be considered if the topic of this master's thesis is to be investigated further. Task 5 from the assignment text will also be answered.

6.1   Comparison of results

As there is strongly restricted scientific articles which study the LAF distribution influenced by a patient by performing experiments, it was difficult to compare the scenarios with previous studies. In this chapter findings in Scenario 1 and 3 will therefore be compared to each other, to see if they correspond. Scenario 2 will be compared to previous studies, but since there also were strongly restricted previous studies on modelling the thermal plume generated by a person in supine position, it was naturally difficult to make comparisons.

Scenario 1 and 3:   Both Scenario 1 and 3 studied the air distribution above a patient in a LAF ventilated operating theatre. In both of the scenarios it was shown that the airflow was strongly influenced by the different setups, and especially the ones that included surgical lamps. In Scenario 1 it was shown that the additions of surgical lamps also increased the turbulence intensity drastically, and that the placement in horizontal position affected the airflow the most. The different scenarios showed that plume generated by warm surfaces actually have a great impact on the LAF in a ceiling ventilated operating room. The addition of surgical lamps were observed to block the airflow, and is therefore not considered to affect the airflow pattern necessarily by convective flows. But one of the three cylinders did definitely affect the airflow distribution above the operating table both for Scenario 1 and 3, and the addition of warm surfaces did increase the turbulence intensity above the patient in Scenario 1. Scenario 1 did also show that thermal plumes can cause larger local temperature gradients and higher local air velocities above the table.

This study has measured the buoyancy driven flow above a real human and a thermal manikin below a laminar supply diffuser. Case 2 from Scenario 1 should be a reference case for Case 1, Scenario 3, since the manikin is constructed to be approximated as a human. In other words the contour plots presented in Figure 41 in Chapter 5.3.1 can be compared to Figure 25b, 26b and 27b from Chapter 5.1.1. As the only difference of the cases is the use of a thermal manikin instead of a real human being, the speed contours in Figure 41 should not differ too much from the figures in Chapter 5.1.1. If they do, the calibration of the thermal manikin is not performed good enough to be comparable to a real person. Nevertheless the contour plots are expected to differ due to a few inequalities. Firstly, the size of the thermal manikin is bigger than the human used in Scenario 1, hence a plume generated from a greater surface area is expected. Secondly, the position of the measured points above the operating table are not equal for the two experiments, and lastly the measured heights above the operating table are not the same due to the larger manikin, but the distance from person/manikin to anemometers are almost equal.

Figure 41 was compared to the speed contours from Scenario 1, Case 2 in Chapter 5.1.1. The speeds in Figure 41a and Figure 25b are observed to vary in the same interval, from 0.10 m/s to 0.26 m/s. The contours in Figure 41 are nevertheless observed to fluctuate more than for Scenario 1, Case 2, especially at the upper part of the table, which can be caused by a larger convective flow. This can again indicate that the surface temperature for the upper part of

the manikin was overheated. Figure 41a also shows a non-axis-symmetric distribution above the table that may be caused by an uneven heat distribution of the manikin, as observed in Scenario 2.

The study showed that the buoyancy driven flow above the manikin has some similarities to what obtained from a real human being, but differs slightly for the upper part of the body. This predict that manikins can be used as persons for these kind of studies, but also indicate that the construction and calibration of the used manikin has room for improvement. The two different cases also showed that the airflow in close proximity to the patient was reduced, compared to the airflow above an empty operating table. Scenario 3, Case 1 focused on the interaction between the plume and the LAF from the ventilation system. The case showed that the plume was difficult to observe, as the used anemometers were omnidirectional. But it was shown that there were slightly lower velocities in close proximity to the manikin, meaning that the plume influenced the airflow from the ventilation system. This was also observed in Scenario 1, Case 2, which contained measurements above a real human being. This shows that the plume from the patient has an effect on the airflow distribution in the ultra-clean zone, which must be considered when designing the ventilation system.

Scenario 3 also showed that the airflow at "Stue 8" at St. Olavs Hospital may be with conventional jet suppliers, as the vertical contour plots showed air flows from the ceiling that looked like air jets. This is like written in Chapter 2.2 used for less demanding applications.

Scenario 2:   In Scenario 2 the plume generated by a thermal manikin was studied, and equations for both centerline velocity and volume flow rate above separate parts of the body were suggested. The velocity profiles for the six different cross sections above the manikin were also averaged to model the whole body as a line source, which will be presented next.

Figure 45 shows the correlation between the height and volume flow rate when the lying manikin is modelled as a line source. The length of the line source was set equal to 1.85 m. The figure shows that the volume flow rate increase with height for all of the graphs, which is reasonable as air is entraining the plume from the surroundings. The proposed formula is given by Equation 28, which has the highest airflow rate for heights lower than 1.4 m. The three other equations, suggested by Skåret, Nielsen and Awbi, is given by Equation 22, 23 and 24 respectively.
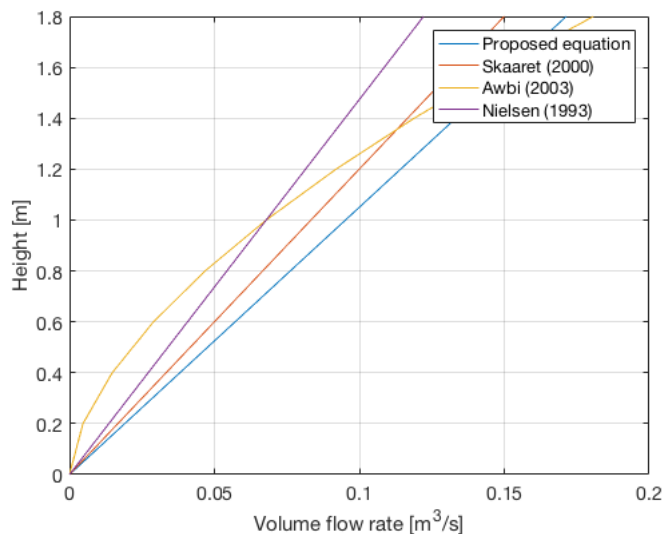
Figure 45: Comparison of formulas for volume flow rate development

As all of the formulas in Equation 45 are describing the volume flow rate above a line source, and not a human in supine position, it is difficult to consider whether the suggested formula is representative or not. It is therefore suggested that this should be looked further into in future work.

In Scenario 2, two different approaches were used to model the centerline velocity above the manikins stomach. A plot of centerline velocity for the two different methods are presented in Figure 46, where "Method 1" and "Method 2" is given by Equation 29 and 31 respectively. The figure also includes the actual measured maximum velocities above the stomach, where the development is highlighted by a fitted line.
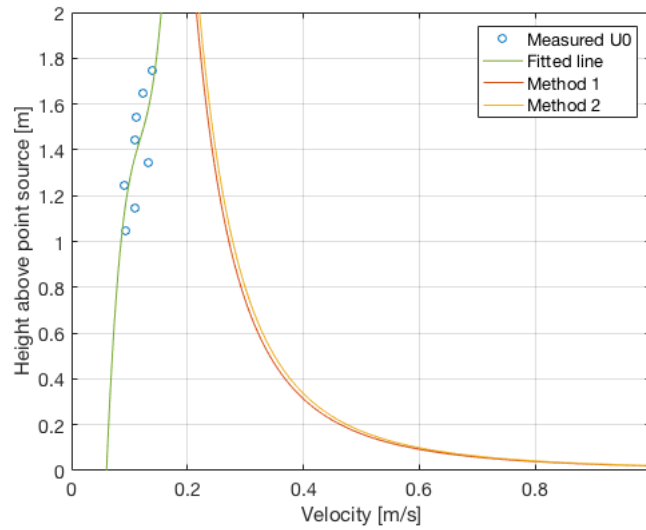
Figure 46: Centerline velocity development above the stomach

Figure 46 shows that the centerline velocity profile obtained by the two different methods give almost the exact same velocity, but that Method 1 gives a slightly lower velocity than Method 2. The figure also shows that both of the methods gives centerline velocities which are higher than the actual measured velocities. One reason for this could be that the spread angles found from Figure 38 and 40 are incorrect, which is reasonable since it was challenging to make a fitted line for the plume boundaries on the figures. It was the instability of the heat source that affected the velocity distribution above the stomach, and hence the plume boundary, which made it difficult to suggest a fitted line for the boundaries. The fact that the anemometers did not measure speed below 0.05 m/s did also affect given boundaries. When the set of data values were arranged it was observed that the values close to the plume boundary was only averaged by a few measured values, as the speed was mostly below 0.05 m/s at the edge of the plume.

But another factor that make the modelled centerline velocity profiles above the stomach too high is the convective heat release. As it was difficult to assume a value for the amount of heat released only by the stomach, the graphs in Figure 46 is made for total $\dot{Q}_c$, which is much higher than $\dot{Q}_c$ for the stomach (and the actual measured values). This is a natural explanation for the higher velocities. From Figure 46 it may seem that the measured centerline velocity, U_0, is increasing with height. This does not conform with the suggested equations, which may indicate that the suggested equations are not a good approach.

In Figure 47 the obtained equations for centerline velocity is compared to suggested formulas from previous studies. The used convective heat output is the same in all of the formulas. In the figure, the formula suggested by Heskestad is Equation 20 and the formula suggested by

Skåret is Equation 19.
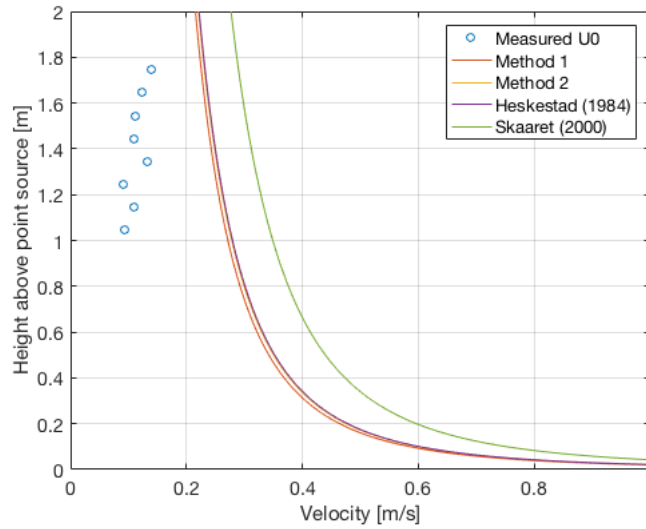
Figure 47: Comparison of formulas for centerline velocity development suggested by authors

As showed in Figure 47 the velocity suggested by literature is even higher than the ones found by Method 1 and 2, but the formula suggested by Heskestad is only slightly higher than Method 2, which make it look like the same graph on the figure. Heskestad does therefore has the closest approximation. However, the centerline velocity for all of the suggested equations were based on plume from a point source, and not generated by a human, which is a reason for why the centerline development in the suggested equations differs from the actual measured values.

Another inaccuracy by the suggested formulas is the plumes calculated virtual centre. Authors suggest different formulas for calculating z_0, which all of them gives different values for the virtual centre. This has the potential to affect the spread angle α, and hence C_b dramatically.

Even though the two methods gave similar formulas, there are many questionable aspect in the two proposed methods for obtaining C_b, and a formula for plume modelling should be carefully considered again. Restricted literature about these subjects from previous studies made it challenging to improve the scientific methods. From Method 1 the main uncertainty is the correlation between the boundary and the centerline velocity. This correlation should therefore be examined furthered. The use of Method 2 does already have a lot of room for improvements, and will most likely give different results if plume axis wandering is taking into account and velocity is being used. But the fact that the convective flow is unsteady make it questionable if a suggested formula should even be done through finding the plume boundary.

Other findings from Scenario 2 is as written in Chapter 3.2 that the heat source is emitting an unsteady flow, which make it challenging to make a standardised model of the plume. This is clearly shown in Figure 35. Due to an uneven heat distribution in the thermal manikin, the velocity profile above certain parts of the body were not axis-symmetric. But in the figure the maximum velocities is often observed at the middle of the table, which may indicate that the curves are correlating to theory by being Gaussian distributed. From Figure 35 it is evident that the plume development is strongly dependent on the placement above the manikin, which also complicates a standardised formula. It can be concluded that to find

a general plume model is extremely challenging, as there are so many characteristics that are difficult to standardise, as body geometry and unstable heat output. It was therefore suggested to analyse body parts separately, which neither gave any reliable results. This should therefore be looked further into, by doing ever more measurements above the thermal manikin. It is also suggested to use a proper thermal manikin to avoid even more fluctuated heat output than necessary.

From the measurement results it was shown that the convective airflow above the stomach was the strongest, and the maximum velocity was 0.139 m/s, which was contained 180 cm above the floor and about 70 cm above the thermal manikin. As 180 cm above the floor was the highest measured point, it is not possible to describe the velocity development further away from the manikin. Yang et al. stated that an airflow above 0.20 m/s is sufficient to control the thermal plume generated by a lying person [31]. This would also apply in my case, as the plumes maximum velocity is roughly 0.14 m/s.

6.2 Suggestions and guidance to design the airflow distribution in operating rooms

One of the tasks in the assignment text was to provide suggestions and guidance to design the airflow distribution in operating rooms to avoid transmission of the indoor airborne pollutants to operating sites. As the focus in this master's thesis was on the air distribution, and not the bacteria dispersion, in close proximity to the patient there were not performed any measurements of particles in the operating theatre. But some observations done in this thesis can still be used to give some suggestions.

Previous studies has revealed that the human microenvironment has a significantly higher content of microorganisms than ambient air, which is of great importance when studying bacterial transport in for instance operating theatres [10]. The airflow from the ventilation system should therefore supply clean and controlled airflow to the surgical site, with a velocity that is sufficient to swipe away undesired particles. From Scenario 1 and 3 in this master's thesis it was concluded that the plume generated by warm surfaces have a great impact on the LAF from a ceiling supply diffuser in an operating room. It was also shown that the use of surgical lamps hindered the airflow from the ventilation to reach the operating table, and hence the surgical site. The addition of warm surfaces did also increase the turbulence intensity above the patient. These two findings can strongly influence the bacteria dispersion in the critical zone around the surgical site, where a clean airflow is desirable and crucial to prevent SSIs. Chow et al. stated that microbial dispersion increases with turbulent flow [15]. My experiments showed a great increase in turbulence intensity for the cases that included surgical lamps. The placement of the lamps did also affect the airflow distribution the most and should therefore be considered carefully before a surgery.

At the specific operating theatre "Stue 8" at St. Olavs Hospital it was measured lower velocities at the lower, compared to the upper part of the operating table. This is unfavourable, as there is shown a general higher rate of SSIs at hip- and knee-replacements, which is performed at the middle/lower part of the table [12]. HTM recommended a minimum velocity of 0.2 m/s above the operating table, which is higher than the measured speed at the lower part of the operating table at St. Olavs Hospital. This cause some concern on whether the LAF at "Stue 8" works properly. During the observation of the real operation it was observed that the instrument table was placed in the semi-clean zone. As it was stated from a previous study that the critical areas in the operating room are the operating wound and the instrument tables, it is important to place the instrument table completely in the ultra clean zone [13].

The plume measurements in Scenario 2 showed the potential the plume have on the air distribution in a room. This information could be of great importance in for instance personalised ventilation in infirmaries where patients are assumed to be resting throughout the day. The study on plume generated by a lying human body should therefore be analysed further.

6.3   Limitations of the experimental setup

During the semester there were some challenges related to the experimental setup. As already stated in Chapter 1.4, there were some problems with building a laminar supply diffuser at the laboratory at NTNU, which caused some limitations for Scenario 3. The interaction between the thermal manikin and LAF ventilation was supposed to be studied for different discharge velocities, but this was not possible due to a non-existent LAF at the climate chamber. This again made it difficult to draw reasonable statements of plume development by forced convection, and find out experimentally what is a sufficient discharge velocity to ventilate the total human plume.

The wireless omnidirectional anemometers used for Scenario 1 were damaged during the semester, and a new type of anemometers were therefore used in Scenario 2 and 3. This type did not measure temperature, and TU and SD were not possible to obtain. If the temperature were measured, more information about the plume development and interaction with the LAF could be discussed further. The anemometers did neither measure velocities above 0.05 m/s, which especially caused limitations in Scenario 2. The fact that the direction of the speed were not possible to obtain did also cause limitation for the analysis of the results.

Limitations of available equipment made it difficult to measure the velocity higher than 180 cm above the floor, which made it impossible to describe the plume above that level. The heating system of the thermal manikin did also cause some limitations on the reliability of the results, as the heat were not evenly distributed at the surface. Another unfortunate was that the LAF ventilation used in the both Scenario 1 and Scenario 3 did not have evenly distributed, laminar air flow above the whole operating table.

6.4   Further work

This master's thesis is investigating issues in a rather new field, and there still remains work to make more reliable conclusions. The used methods does also have room for improvements. This chapter will present a list of suggestions and recommendations of what should be further investigated for the topic of this master's thesis.

- Find out what is a high-, medium- and low turbulence level for laminar airflow systems

- Build a ceiling supply diffuser with laminar airflow at the climate chamber at NTNU. An evenly distributed airflow throughout the operating table will ease the analyse of the interaction between a thermal plume and the LAF.

- Have an air cooler at the climate chamber at NTNU, to ensure right temperature in the climate chamber throughout the whole experiment.

- The thermal manikin should have a more evenly distributed heating system, that include heat in hands and feet. The calibration of the manikin should be done even more precise, where a control system can regulate heat at even more segments independently. Preferably, use a proper thermal manikin made for these kind of experiments.

- Use a proper traverse stand for the anemometers. Limitations of available equipment made it difficult to measure the velocity higher than 180 cm above the floor. The use of more anemometers would speed up the experiment session and make time to do measurements at even more points.

- As the convective heat flow were so unsteady in Scenario 2, it can be a good idea to log the velocities above the plume for a longer period than 3 minutes.

- Measure velocity distribution above a thermal manikin in a non-ventilated room at even more points above the manikin, for more heights above the stomach, and further away from the manikin to obtain the entire velocity profile. Study the convective airflow at even more points at y-direction, to take plume axis wandering into account.

- Deduce a better correlation between the plume boundary and the centerline velocity, for convective airflow generated by a manikin in supine position.

- Deduce a mathematical model for the generated convective airflow by a manikin in supine position.

- Study the interaction between thermal plume and LAF ventilation by performing experiment "Scenario 3, Case 1" for different discharge velocities from the ventilation system.

- The human thermal plumes interaction with laminar airflow should be investigated further, where thermal stratification in the room should be included for modelling a thermal plume development in a standard room environment. A formula for the acceleration of the airflow from a LAF ceiling in an environment with thermal stratification should be found.

- The use of a more accurate measurement technique that also shows the direction of the airflow, as Particle Image Velocimetry (PIV), should be used. The lack of knowledge of the direction of the measured speed is a continuous uncertainty throughout this master's thesis. The measuring equipment should also include temperature and speed below 0.05 m/s. The logged data should also be given more frequently, so turbulence intensity and standard deviation can be obtained.

7 Conclusion

This master's thesis has experimentally investigated the airflow distribution in close proximity to a lying human body in a LAF ventilated operating theatre. The thesis is divided in three main scenarios, that each is investigating one main tasks of this assignment. The objective of the first scenario is to focus on the analysis of the effect of thermal plumes on the air distribution, the second will focus on the convective airflow generated by a lying body in a non-ventilated room, and lastly the interaction between the LAF and thermal plume from a patient is investigated.

The results from the first scenario clearly showed a difference in the air distribution due to different heat sources in the operating zone, which has the potential to hinder the clean airflow to reach the surgical site. The airflow was most disrupted by the addition of surgical lamps, which is natural as the lamps were placed between the supply diffuser and operating table, and hence hindered the air flow to reach the table. The lamps did also have a great impact on the turbulence intensity above the operating table. It is therefore suggested that the placement of the lamps are carefully considered before an operation, to ensure that the clean supply air reaches the surgical site. The first scenario did also show that the addition of thermal plumes can cause larger local temperature gradients and higher local air speeds above the operating table.

In the second scenario the thermal plume generated above a thermal manikin by natural convection was analysed. The velocity profiles above the manikin was in general unstable, but the highest velocities above the manikin was registered above its stomach with a value of 0.139 m/s. This shows that the plume has a potential to influence the air distribution in a room, which were also observed in the two other scenarios. The manikin was emitting an unsteady flow which was strongly development on the cross section above the manikin. This, and its complex body shape, makes it challenging to suggest a general formula for the airflow development above a supine body. The flow was neither axis-symmetric, but had in general the characteristic of a higher velocity at the middle of the plume, which may indicate Gaussian distribution. Some equations for the centerline velocity and volume flow rate development of the thermal plume is suggested. But as the convective flow were so unsteady it was concluded that even more experiments should be performed to examine the plume development and develop more reliable formulas. From this experiment it was experienced that it is really challenging to suggest a general mathematical model of the human thermal plume, as the body shape is so complex and the emitted heat is so unsteady. This is a well-known aspect that also has been stated in earlier work by several researchers.

The last scenario focused on the interaction between plume generated by the thermal manikin and laminar airflow from a ceiling supply diffuser. The experiment showed that a weak plume could be pictured above the whole manikin, and was most developed above the manikins head. An unsteady flow was also pictured above the manikins chest, but it could not be concluded whether the flow came from the plume or the supply diffuser due to the used measuring equipment. The presence of the human thermal plume indicates that it should be considered when designing laminar airflow ventilation systems.

As there are a lot of uncertainties in the experiments, and the fact that the used omnidirectional anemometers made it impossible to know the direction of the speed, did make the analysis of the results extra challenging. It is therefore recommended to use a more accurate measurement technique to increase the reliability of the results. But the master's thesis still gave some interesting findings, that should be considered when designing a laminar ventilation system. The study on the human thermal plume can also hopefully contribute to the lack of previous studies on the field.

8 Bibliography

[1] B. E. Friberg, S. Friberg, and L. G. Burman, "Zoned vertical ultraclean operating room ventilation: A novel concept making long side walls unnecessary," *Acta Orthopaedica Scandinavica*, vol. 67, no. 6, pp. 578–582, 1996.

[2] D. Zukowska, "Airflow interactions in rooms–convective plumes generated by occupants," Ph.D. dissertation, PhD thesis]. Technical University of Denmark, 2011.

[3] B. Karlsson and J. Quintiere, *Enclosure fire dynamics.* CRC press, 1999.

[4] H. B. Awbi, *VENTILATION OF BUILDINGS. Second edition.* ISBN 0–415–27056–1: Spon Press. Taylor & Francis Group, 2003.

[5] D. Zukowska, Z. Popiolek, and A. Melikov, "Determination of the integral characteristics of an asymmetrical thermal plume from air speed/velocity and temperature measurements," *Experimental Thermal and Fluid Science*, vol. 34, no. 8, pp. 1205–1216, 2010.

[6] E. Skåret, *Ventilasjonsteknisk håndbok. Håndbok 48.* ISBN 82-536-0714-8: Byggforsk, 2000.

[7] Y. Kurazumi, T. Tsuchikawa, N. Matsubara, and T. Horikoshi, "Effect of posture on the heat transfer areas of the human body," *Building and Environment*, vol. 43, no. 10, pp. 1555–1565, 2008.

[8] Folkehelseinstituttet, "Infeksjoner etter kirurgi, rapport nois-posi for 2015," https://www.fhi.no/nyheter/2016/infeksjoner-etter-kirurgi-nois-posi-2015/, 2016, accessed: 20th of July 2017.

[9] S. Sadrizadeh, S. Holmberg, and A. Tammelin, "A numerical investigation of vertical and horizontal laminar airflow ventilation in an operating room," *Building and Environment*, vol. 82, pp. 517–525, 2014.

[10] H. Lewis, A. Foster, B. Mullan, R. Cox, and R. Clark, "Aerodynamics of the human microenvironment," *The Lancet*, vol. 293, no. 7609, pp. 1273–1277, 1969.

[11] T.-T. Chow and X.-Y. Yang, "Performance of ventilation system in a non-standard operating room," *Building and environment*, vol. 38, no. 12, pp. 1401–1411, 2003.

[12] M. A. Melhado, J. Hensen, and M. Loomans, "Review of ventilation systems in operating rooms in view of infection control," in *Proceedings of the 6th Int. Postgraduate Research Conf.. in the Built and Human Environment, Technische Universiteit Delft*, 2006, pp. 478–487.

[13] W. Zoon, M. Loomans, and J. Hensen, "Testing the effectiveness of operating room ventilation with regard to removal of airborne bacteria," *Building and Environment*, vol. 46, no. 12, pp. 2570–2577, 2011.

[14] C. Brandt, U. Hott, D. Sohr, F. Daschner, P. Gastmeier, and H. Rüden, "Operating room ventilation with laminar airflow shows no protective effect on the surgical site infection rate in orthopedic and abdominal surgery," *Annals of surgery*, vol. 248, no. 5, pp. 695–700, 2008.

[15] T.-T. Chow and X.-Y. Yang, "Ventilation performance in operating theatres against airborne infection: review of research activities and practical guidance," *Journal of Hospital Infection*, vol. 56, no. 2, pp. 85–92, 2004.

[16] W. Whyte, "The effect of mechanical ventilation and clothing on airborne microbes and wound sepsis in hospital operating rooms, part 1," *Clean Air and Containment Review*, vol. 22, pp. 4–11, 2015.

[17] G. F. Peters, M. R. McKeon, and W. T. Weiss, "Potential for airborne contamination in turbulent-and unidirectional-airflow compounding aseptic isolators," *American Journal of Health-System Pharmacy*, vol. 64, no. 6, pp. 622–631, 2007.

[18] W. Whyte, *Cleanroom Technology. Fundamentals of Design, Testing and Operation. Second edition.* 978-0-470-74806-0: John Wiley & Sons, 2010.

[19] B. Friberg, "Ultraclean laminar airflow ORs," *AORN journal*, vol. 67, no. 4, pp. 841–851, 1998.

[20] M. L. Pereira and A. Tribess, "A review of air distribution patterns in surgery rooms under infection control focus," *Revista de Engenharia Térmica*, vol. 4, no. 2, 2005.

[21] B. E. Friberg, L. G. Burman, and S. Friberg, "Zoned exponential, vertical and horizontal ultra-clean laminar airflows: No differences in bacteriological efficiency," *Acta Orthopaedica Scandinavica*, vol. 69, no. 2, pp. 169–172, 1998.

[22] Health Technical Memorandum 2025, NHS Estates, "Ventilation in health-care premises- design considerations," https://www.mintie.com/assets/img/education/NHS%20Estates%20-%20HVAC.pdf, 1999, accessed: 27th of July 2017.

[23] Standard Norge, "Norsk Standard NS-EN ISO 7730. Ergonomics of the thermal environment. Analytical determination and interpretation of thermal comfort using calculation of the PMV and PPD indices and local thermal comfort criteria (ISO 7730:2005)."

[24] P. E. Nilsson, *Achieving the Desired Indoor Climate.* ISBN 91-44-03235-8: Studentlitteratur, 2003.

[25] G. Cao, J. Kurnitski, M. Ruponen, and O. Seppänen, "Experimental investigation and modeling of the attached plane jet velocity development characteristics in the transition process in a room," *HVAC&R Research*, vol. 15, no. 3, pp. 489–508, 2009.

[26] P. O. Fanger, A. K. Melikov, H. Hanzawa, and J. Ring, "Air turbulence and sensation of draught," *Energy and buildings*, vol. 12, no. 1, pp. 21–39, 1988.

[27] C. Karthikeyan and A. A. Samuel, "Co 2-dispersion studies in an operation theatre under transient conditions," *Energy and Buildings*, vol. 40, no. 3, pp. 231–239, 2008.

[28] Y. Cho and H. B. Awbi, "Effect of heat source location in a room on the ventilation performance," 2002.

[29] D. Zukowska, A. Melikov, and Z. Popiolek, "Thermal plume above a simulated sitting person with different complexity of body geometry," in *Proceedings of the 10th International Conference on Air Distribution in Rooms—Roomvent*, vol. 3. Technical University of Denmark, 2007, pp. 191–198.

[30] D. Licina, A. Melikov, C. Sekhar, and K. W. Tham, "Human convective boundary layer and its interaction with room ventilation flow," *Indoor air*, vol. 25, no. 1, pp. 21–35, 2015.

[31] C. Yang, X. Yang, and B. Zhao, "The ventilation needed to control thermal plume and particle dispersion from manikins in a unidirectional ventilated protective isolation room," in *Building Simulation*, vol. 8, no. 5. Tsinghua University Press, 2015, pp. 551–565.

[32] R. Clark and R. Cox, "An application of aeronautical techniques to physiology 1. the human microenvironment and convective heat transfer," *Medical and biological engineering*, vol. 12, no. 3, pp. 270–274, 1974.

[33] R. Clark and N. Toy, "Forced convection around the human head." *The Journal of physiology*, vol. 244, no. 2, pp. 295–302, 1975.

[34] G. Cao, J. Kurnitski, and O. Seppänen, *Effect of occupant thermal plume on air flow pattern and temperature distribution in an office room*, 2008, p. 8.

[35] B. A. Craven and G. S. Settles, "A computational and experimental investigation of the human thermal plume," *Journal of Fluids Engineering*, vol. 128, no. 6, pp. 1251–1258, 2006.

[36] I. Holmér, "Thermal manikin history and applications," *European journal of applied physiology*, vol. 92, no. 6, pp. 614–618, 2004.

[37] S. Tanabe, E. A. Arens, F. Bauman, H. Zhang, and T. Madsen, "Evaluating thermal environments by using a thermal manikin with controlled skin surface temperature," *Ashrae Transactions*, vol. 100, 1994.

[38] V. Novakovic, S. O. Hanssen, J. V. Thue, I. Wangensteen, and F. O. Gjerstad, *ENØK I BYGNINGER - Effektiv energibruk.* 978-82-05-37496-6: Gyldendal undervisning, 2014.

[39] F. P. Incropera, D. P. Dewitt, T. L. Bergman, and A. S. Lavine, *Principles of heat and mass transfer.* 978-0-470-64615-1: John Wiley & Sons Inc., 2013.

[40] Y. Kurazumi, T. Tsuchikawa, J. Ishii, K. Fukagawa, Y. Yamato, and N. Matsubara, "Radiative and convective heat transfer coefficients of the human body in natural convection," *Building and Environment*, vol. 43, no. 12, pp. 2142–2153, 2008.

[41] Y. Kurazumi, T. Tsuchikawa, N. Matsubara, and T. Horikoshi, "Convective heat transfer area of the human body," *European journal of applied physiology*, vol. 93, no. 3, pp. 273–285, 2004.

[42] Y. Wang, J. Moss, and R. Thisted, "Predictors of body surface area," *Journal of clinical anesthesia*, vol. 4, no. 1, pp. 4–10, 1992.

[43] D. Du Bois and E. Du Bois, "A formula to estimate the approximate surface area if height and weight be known. 1916." *Nutrition (Burbank, Los Angeles County, Calif.)*, vol. 5, no. 5, p. 303, 1989.

[44] H. D. Goodfellow, *Industrial ventilation design guidebook.* Academic press, 2001.

[45] G. Abramovich, "Theory of turbulent jets,(1963), 586."

[46] G. Heskestad, "Engineering relations for fire plumes," *Fire Safety Journal*, vol. 7, no. 1, pp. 25–32, 1984.

[47] E. Bjørn and P. V. Nielsen, "Merging thermal plumes in the indoor environment," Dept. of Building Technology and Structural Engineering, Tech. Rep., 1995.

[48] P. Kofoed, "Thermal plumes in ventilated rooms," Ph.D. dissertation, Dept. of Building Technology and Structural Engineering, Aalborg University, 1991.

[49] P. V. Nielsen, "Displacement ventilation," Dept. of Building Technology and Structural Engineering, Tech. Rep., 1993.

[50] T. Suzuki, K. Sagara, T. Yamanaka, H. Kotani, and T. Yamashita, "Vertical profile of contaminant concentration in sickroom with lying person ventilated by displacement,"

in *The 6th International Conference on Indoor Air Quality, Ventilation & Energy Conservation in Buildings IAQVEC*, 2007, pp. 28–31.

[51] J. McNeill, J. Hertzberg, and Z. J. Zhai, "Experimental investigation of operating room air distribution in a full-scale laboratory chamber using particle image velocimetry and flow visualization," *Journal of Flow Control, Measurement & Visualization*, vol. 1, no. 01, p. 24, 2013.

[52] F. Memarzadeh and A. P. Manning, "Comparison of operating room ventilation systems in the protection of the surgical site/discussion," *ASHRAE transactions*, vol. 108, p. 3, 2002.

A   Agreement with FOR

Avtale om oppdrag

Mellom

NTNU- Norwegian University of Science and Technology,
Pb 8905
7491 Trondheim, Norway

ORG.NR: 974 767 880

Institutt for energi- og prosessteknikk

ATT: Madeleine Charlotte Aviles Storås

OG

St. Olavs Hospital, Fremtidens Operasjonsrom (FOR)

ORG.NR: 883 974 832

Olav Kyrres gt 17
7006 Trondheim
ATT: Daglig leder, Jan Gunnar Skogås

Om utførelse av oppdrag, nedenfor kalt Oppdraget, med følgende tittel:

Navn på oppdrag
Characterization of the airflow distribution in close proximity to a patient in an operating room with different ventilation systems at St. Olavs Hospital
Karakterisering av luftfordeling i umiddelbar nærhet til en pasient i en operasjonsstue med forskjellige ventilasjonssystemer på St. Olavs Hospital

1. Innhold
The following tasks are to be considered:
- Literature review: state of the art analysis of the airflow distribution close to a patient in an operating room.
- Model the thermal plumes from a patient in an operating room.
- Conduct experimental measurements of airflow distribution close to a patient with different ventilation systems.
- Analyse the effect of thermal plumes on the airflow distribution in an operating room.
- Provide suggestions and guidance to design the airflow distribution close to a patient to avoid the transmission of the room airborne pollutants to operating sites.

Oppgaven gjennomføres av:
Student Madeleine Charlotte Aviles Storås

2. Varighet

Ut fra de forutsetninger som foreligger av kontrakten, er følgende tidsrom fastlagt:

Startdato: 01.03.2017

Sluttdato: 01.08.2017

Avtalen er gyldig fra startdato når den er undertegnet av begge parter. Avtalen prolongeres om partene fortsatt har behov ut over sluttdato.

3. Kontaktpersoner
a) FOR, daglig leder, Jan Gunnar Skogås
b) NTNU, Madeleine Charlotte Aviles Storås
c) NTNU, Professor, Guangyu Cao
d) FOR, forskningskoordinator Liv-Inger Stenstad

4. Rapportering og eierrettigheter til prosjektresultater
NTNU ved department of energy and process engineering og FOR har eierrettighetene til prosjektresultatene.
Madeleine Charlotte Aviles Storås kommer til å nevne «Fremtidens Operasjonsrom, FOR» i sin oppgave, og samtykker til at oppgaven blir omtalt i FOR årsrapport.
St.Olavs Hospital, FOR kan benytte kunnskap ervervet i prosjektet.
Evt. publisering av prosjektresultater skal skje i samtykke mellom partene.

5. Øvrige betingelser
Alle prosjekter som skal utføres ved FOR skal først godkjennes av Fagrådet.
Det skal lages en protokoll for prosjektet og viser til vedlegg "Veiledningen prosjektbeskrivelse til fagrådet for Fremtidens Operasjonsrom".

Kjørereglene som er nedfelt for prosjekter ved FOR gjelder alle samarbeidspartnere som for eksempel NTNU, SINTEF, ulike industriselskaper osv.
PhD grader, Mastergrader, Bachelorgrader og fordypningsoppgaver samt utprøving av utstyr (evt. legemidler), skal innom Fagrådet før prosjektet settes i gang.

Ved gjennomføring av prosjektarbeid ved FOR skal det inngås en gjensidig avtale mellom FOR og den aktuelle institusjon/person som skal gjennomføre prosjektet. Det skal som nevnt legges frem en forskningsprotokoll. Etter møtet i Fagrådet bør det være et oppstartmøte med representant fra prosjektutøver, veileder og FOR. Det bør også være evalueringsmøter underveis. Endelig bør det også arrangeres et sluttrapportmøte der en går igjennom resultatene av prosjektet.

Før et prosjekt starter er det viktig at representanter for FOR kommer sammen med prosjektutøver slik at en får gått igjennom den kliniske hverdag og de rutinene som

ST. OLAVS HOSPITAL
UNIVERSITETSSYKEHUSET I TRONDHEIM

St.Olavs Hospital
Operating Room of the Future, FOR

Managing Director

Telefon: +47 72823244
Telefaks: +47 72823270
Mobil: +47 982 80 585
www.stolav.no

kliniske studier der så vel personal som pasienter er involvert. Fortrinnsvis skal resultatene publiseres i tidsskrifter med peer review.

Hensikten med dette er blant annet at den daglige ledelse ved FOR og den aktuelle klinikk må vite om hvilke prosjekter som utføres. Det kan også være aktuelt i enkelte tilfeller å justere protokollen. Det må også være ressurser nok til å gjennomføre prosjektene. En bør også diskutere realismen i prosjektet når det gjelder omfang og innhold. Når prosjektet er avsluttet og før resultatene offentliggjøres må disse **presenteres først for FOR** og den avdeling, klinikk hvor prosjektet er gjennomført.

Alle forskningsprosjekter der pasienter og pasientdata er involvert skal godkjennes av Regional Etisk Komité (REK).

6. Avtaledokumenter
Avtalen består av to deler:
- Dette dokument - kalt avtale
- Prosjektskisse
- Avtaler om Master med NTNU
- Konfidensialitetsavtale
- Taushetserklæring

7. Avtaleeksemplar og signaturer
Denne avtale er underskrevet i 2 eksemplarer, hvorav ett eksemplar beror hos hver av partene.

Trondheim, / 3 2017
For Leverandør:

Daglig leder, FOR
St. Olavs Hospital

Navn: Jan Gunnar Skogås

Trondheim, 2 / 3 - 2017
For Oppdragsgiver:

Madeleine C. Storås

NTNU, Institutt for energi- og prosessteknikk
Navn: Madeleine Charlotte Aviles Storås

VEDLEGG:
-Konfidensialitetsavtale
-Protokoll
-Avtale NTNU om Master
-Taushetsplikt

HELSE MIDT-NORGE

St. Olavs Hospital HF

Olav Kyrres gate 17
7006 Trondheim
Org.nr: 883 974 832

Bankgiro: 8601.05.10270
Telefon: +47 72823244
Telefaks: +47 72823270
Mobil: +47 982 80 585

.·.· ST. OLAVS HOSPITAL
UNIVERSITETSSYKEHUSET I TRONDHEIM

St.Olavs Hospital
Operating Room of the Future, FOR

Managing Director

Telefon: +47 72823244
Telefaks: +47 72823270
Mobil: +47 982 80 585
www.stolav.no

Agreement on Confidentiality

between

St.Olavs Hospital, Operating Room of the Future

and the

Partner NTNU v/ Madeleine Charlotte Aviles Storås
related to and as long as the parties have research activities at the
Operating Room of the Future at St Olavs Hospital/NTNU

All information which the Parties have received from each other in writing, orally or in any other manner, shall be treated confidentially and may not be used without a written agreement, unless the receiving Party can prove that the information was:

i) publicly known at the time of receipt
ii) known by the recipient at the time of receipt
iii) received legally from a third party without any agreement on confidentiality
iv) developed independently by the recipient

Disputes that may arise in connection with this Agreement or is a result there of, shall be settled by private negotiations between the Parties. If such agreement cannot be obtained within a reasonable time period, the parties shall choose Trondheim District Court as legal venue.

The present Agreement shall be governed by and construed in accordance with the laws of Norway.

For
Partner: Madeleine Charlotte Aviles Storås

Madeleine C. Storås

Date: 2/3 - 2017

For
Operating Room of the Future:

Date: 1/3 - 2017

HELSE ·•·• MIDT-NORGE

St. Olavs Hospital HF

Olav Kyrres gate 17
7006 Trondheim
Org.nr: 883 974 832

Bankgiro: 8601.05.10270
Telefon: +47 72823244
Telefaks: +47 72823270
Mobil: +47 982 80 585

ST. OLAVS HOSPITAL
UNIVERSITETSSYKEHUSET I TRONDHEIM

Taushetserklæring

Jeg er kjent med at jeg gjennom mitt arbeid kan få tilgang til taushetsbelagte opplysninger, og forplikter meg til å overholde bestemmelsene om taushetsplikt slik de framkommer i foretakets prosedyre, med grunnlag i nedenfor stående lovbestemmelser:

Alle som arbeider ved St. Olavs Hospital, studenter, lærere ved høyskole og universitet, partnere/leverandorer plikter å hindre at andre får adgang eller kjennskap til det hun/han i forbindelse med tjenesten eller arbeidet får vite om folks legems- eller sykdomsforhold eller andre personlige forhold som de får vite om i egenskap av å være helsepersonell og/eller i tjeneste for et offentlig forvaltningsorgan.

Taushetsplikten gjelder også:

- pasientens fodested, fodselsdato, personnummer, pseudonym, statsborgerforhold, sivilstand, yrke, bopel og arbeidssted. Opplysning om en pasients oppholdssted kan likevel gis når det er klart at det ikke vil skade tilliten til helseinstitusjonen.

- tekniske innretninger og fremgangsmåter samt drifts- eller forretningsforhold som det vil være av konkurransemessig betydning å hemmeligholde av hensyn til den som opplysningen angår.

Opplysninger til andre forvaltningsorganer kan bare gis når dette er nødvendig for å bidra til løsning av oppgaver etter forvaltningsloven, eller for å forebygge vesentlig fare for liv eller alvorlig skade for noens helse.

"Taushetsplikten gjelder også etter at du har avsluttet tjenesten eller arbeidet. Overforstående opplysninger kan ikke utnyttes i egen virksomhet eller i tjeneste eller arbeid for andre."

Den som forsettelig eller grovt uaktsomt krenker taushetsplikten kan straffes med boter eller med fengsel inntil 6 måneder.

Begås taushetsbrudd i den hensikt å tilvende seg eller andre en uberettiget vinning er stafferammen 3 år. Det samme gjelder når det foreligger andre særdeles skjerpende omstendigheter.

St. Olavs Hospital 2/3-2017
                          dato

MADELEINE CHARLOTTE AVILES STORÅS   _Madeleine C. Storås_
Navn med blokkbokstaver   Signatur

Institutt for energi- og prosessteknikk   NTNU
Avdeling   firmatilhorighet

Følgende lovparagrafer omhandler taushetsplikten og brudd på taushetsplikten:
- **Helsepersonelloven § 21**
- **Lov om spesialisthelsetjenesten § 6.1**
- **Forvaltningsloven § 13**
- **Straffeloven § 121**
- **Lov om folkeregistrering §13**
- **Lov om helseregistre og behandling av helseopplysninger § 15**
- **Lov om personopplysninger kap. II**
- **Forskrift til personopplysningsloven, kap. 2**
- **Pasientrettighetsloven tas med, §3-6 Rett til vern mot spredning av opplysninger**

B Instrumentation

B.1 Air distribution measuring system "AirDistSys5000"

"AirDistSys5000" measuring system consists of five anemometer probes, a pressure sensor, a wireless transmitter and a power supply. The complete technical data is extracted directly from the following link: http://www.sensor-electronic.pl/pdf/MAN_AirDistSys5000. pdf (downloaded May 12th 2017), and is presented in the following subchapters.

B.1.1 Anemometer probes: SensoAnemo series 5100LSF transducer

Technical data:

- type of speed sensor: omnidirectional, spherical

- diameter of speed sensor: 2 mm

- measurement speed range: 0.05... 5 m/s

- accuracy of speed measurement: $\pm 0.02 m/s \pm 1.5\%$ of readings

- directional error above 2m/s: $\pm 2.5\%$

- automatic temperature compensation: $<$ than $\pm 0.1\%/K$

- upper frequency f_{up}: min. 1 Hz, typ. 1.5 Hz

- temperature range: -10...+50 $°C$

- accuracy of temperature: 0.2 $°C$

- sampling rate: 8 Hz

- interface: port RS485

- baud rate: 115000 bps

- optional analog output: current 0...20 mA, voltage 0-2V or 0-5V. Only for velocity, non-linear (set of equations) V [m/s]= f(Iv)

- max analog output resistance: 100 Ohm

- power supply: 3.3...9 VDC

- power consumption: max. 80mA, typ.60mA, peak. 110mA, economy mode 6mA

B.1.2 Barometer: SensoBar 5301 transducer

Technical data:

- measurement range: 500...1500 hPa

- accuracy: ± 3 hPa

- response time: 2s

- humidity measurement range: 0...100 % RH

- humidity accuracy: $\pm$ 2% in range 10...90% RH

- long term stability of humidity: <1% RH/year

- response time of humidity: <4s

- interface: port RS485

- baud rate: 115000 bps

- power supply: 3.3...9 VDC

- power consumption: max. 6mA, typ.60mA, economy mode 1mA

B.1.3   Wireless transmitter: SensoBee wire-less transmitter

Technical data:

- indoor (urban) range: up to 60m

- outdoor line-of-sight range: up to 100m

- transmit power output: 100mW (20dB) EIRP

- operating frequency: 2.4GHz

- RF data rate: 250 kbps

- power supply: 6...9 VDC/1A

B.2   THERMOANEMOMETER ARTICULATED PROBE 962

Technical data for Thermoanemometer probe TSI 962 is directly extracted from the following link: http://www.tsi.com/products/_product-accessories/thermoanemometer-articulated-probe-962.aspx (downloaded May 12th 2017). The product details is the following:

Range:

- 0 to 9,999 ft/min (0 to 50 m/s)

- 0 to 200 °F (-18 to 93°C)

Accuracy:

- ± 3% of reading or ± 3 ft/min

- (± 0.015 m/s), whichever is greater

- ± 0.5°F (±0.3°C)

Resolution:

- 1 ft/min (0.01 m/s)

- 0.1°F (0.1°C)

Probe Dimensions:

- Length 40 in. (101.6 cm)

- Tip dia. 0.28 in. (7.0 mm)

- Base dia. 0.51 in. (13.0 mm)

- Articulating Section Length 6 in. (15.2 cm)

- Articulating Knuckle dia. 0.38 in. (9.5 mm)

B.3   AIR VELOCITY TRANSDUCER TSI 8475

TSI 8475 were used to measure thermal plume above a person in supine position, as well as for the experiment with a thermal manikin at St. Olavs Hospital. The complete technical data for TSI 8475 can be found via http://www.tsi.com/uploadedFiles/_Site_Root/ Products/Literature/Spec_Sheets/8455-65-75-AVT_2980575_USA.pdf (Downloaded 21. of June 2017).

- Accuracy: $\pm$ 3% of readings, $\pm$ 1% of full scale of selected range

- Repeatability: N/A

- Response to flow: 5 sec

- Resolution (minimum): 0.07% of selected full scale

- Input power: 11 to 30 VDC or 18 to 38 VAC, 350 mA max

- Output: Impedance; Voltage mode: less than 1 ohm, 20 mA max source current. Resistance; Current mode: 500 ohms maximum load Field selectable 0 to 5V, 0 to 10V, 0 to 20, 2 to 10V, mA, 4 to 20 mA. Time constant; Field selectable 0.05 to 10 seconds.

- Probe length: 7.5 cm, 15 cm, 22.5 cm, or 30 cm

An explaination of how to chose the set parameters for the TSI 8475 and the method for converting the output signal to velocity is given in the following link: http://docplayer. fr/9109501-Air-velocity-transducer-model-8455-8465-8475.html (downloaded 28. june 2017). The following equations is used to convert the output signal to velocity:

$$V = \frac{E_{out} - E_0}{E_{FS} - E_0} \cdot V_{FS} \tag{33}$$

Where V is the measured velocity in m/s, V_{FS} is the full scale velocity setting in m/s, E_{out} is the measured output voltage or current signal, E_0 is the zero flow output voltage or current and E_{FS} is the full scale voltage or current output.

C   Risk assessment report

NTNU | **SINTEF**

Risk Assessment Report

Diffuser experiment with laminar airflow

Prosjektnavn	Characterization of the airflow distribution in close proximity to a patient in operating rooms with laminar airflow at St. Olavs Hospital
Apparatur	Klimarom VVS-lab
Enhet	NTNU
Apparaturansvarlig	Guangyu Cao
Prosjektleder	Guangyu Cao
HMS-koordinator	Morten Grønli
HMS-ansvarlig (linjeleder)	Olav Bolland
Plassering	Klimarom, Varmetekniske laboratorier
Romnummer	C247C, 2. etg i klimalab, Varmetekniske laboratorier
Risikovurdering utført av	Inge Håvard Rekstad

Approval:

Apparatur kort (UNIT CARD) valid for:	6 måneder
Forsøk pågår kort (EXPERIMENT IN PROGRESS) valid for:	6 måneder

Rolle	Navn	Dato	Signatur
Prosjektleder	Guangyu Cao	15.5.2017	Gru Cao
HMS koordinator	Morten Grønli		
HMS ansvarlig (linjeleder)	Olav Bolland		

TABLE OF CONTENTS

1 INTRODUCTION

The purpose of the experiment is to investigate the interaction between a thermal plume rising from a supine occupant and the laminar airflow from the diffuser. The experiment will therefore be performed below the laminar airflow diffuser in the Klimalab.

The experiment will be performed in several steps:

   i.   Presetting of the laminar airflow diffuser by measuring the velocity at the outlet of the diffuser. This step is to ensure an even outflow throughout the whole surface. Then the fans will be adjusted to get the desired value for the flow velocity.

  ii.   Calibrating the anemometers and the thermal manikin

 iii.   Measurements of the thermal plume above the thermal manikin

 iv.   Measurements of the airflow above the thermal manikin under the laminar airflow diffuser

  v.   Carry out each experiment by positioning anemometers

2 ORGANISATION

Rolle	
Prosjektleder	Guangyu Cao
Apparaturansvarlig	Guangyu Cao
Romansvarlig	Lars Konrad Sørensen
HMS koordinator	Morten Grønli
HMS ansvarlig (linjeleder):	Olav Bolland

3 RISK MANAGEMENT IN THE PROJECT

Hovedaktiviteter risikostyring	Nødvendige tiltak, dokumentasjon	DATE
Prosjekt initiering	Prosjektinitieringmal	27.03.2017
Veiledningsmøte Guidance Meeting	Skjema for Veiledningsmøte med pre-risikovurdering	06.04.2017
Innledende risikovurdering Initial Assessment	Fareidentifikasjon – HAZID Skjema grovanalyse	06.04.2017
Vurdering av teknisk sikkerhet Evaluation of technical security	Prosess-HAZOP Tekniske dokumentasjoner	28.04.2017
Vurdering av operasjonell sikkerhet Evaluation of operational safety	Prosedyre-HAZOP Opplæringsplan for operatører	
Sluttvurdering, kvalitetssikring Final assessment, quality assurance	Uavhengig kontroll Utstedelse av apparaturkort Utstedelse av forsøk pågår kort	

4   DESCRIPTIONS OF EXPERIMENTAL SETUP

The experimental setup of the main experiment is showed in Figure 1. The airflow distribution will be measured underneath the diffuser.
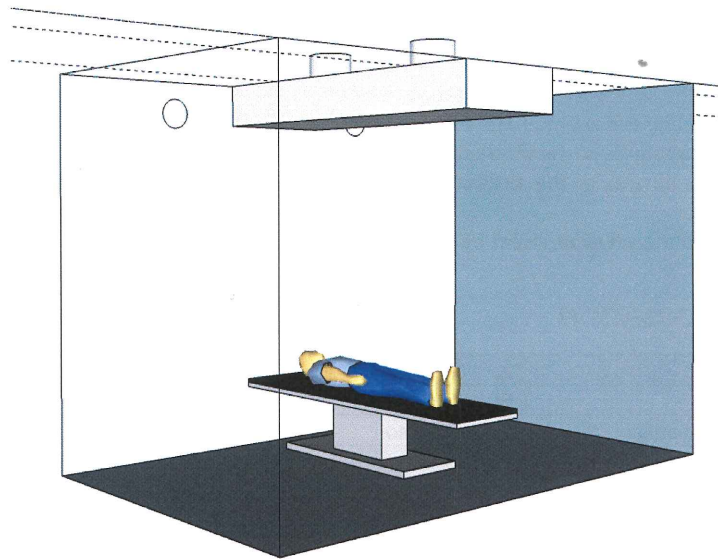
Figure 1: Experimental setup at C247C (KlimaLab, 2nd floor at Varmeteknisk)

There airflow distribution close to the thermal manikin will also be measured, with and without ventilation. The temperature will also be measured. The airflow measurements will be done by omnidirectional anemometers. For experiments with LAF-ventilation, the air will enter the room only by the 0.8m · 2.0m-diffuser, and is extracted by two exhaust fans on the back wall.

The manikin will be fitted by a heating cable to ensure a heating load similar to a supine human body. The heat load can be adjusted by dimmers. The heating cable are using 230V current.

Instrumentation to be used:
- Anemometer
- Thermometer
- Pre-made diffuser
- Fan controlling the volume flow of the diffuser
- Two exhaust fans
- Thermal manikin

5 EVACUATION FROM THE EXPERIMENTAL AREA

Evacuate at signal from the alarm system or local gas alarms with its own local alert with sound and light outside the room in question, see 6.2

Evacuation from the rigging area takes place through the marked emergency exits to the assembly point, (corner of Old Chemistry Kjelhuset or parking 1a-b.)

Action on rig before evacuation:
In case of evacuation, the fans and thermal manikin should be shut down and unplugged.

6 WARNING

6.1 Before experiments

Send an e-mail with information about the planned experiment to:
iept-experiments@ivt.ntnu.no

The e-mail must include the following information:
- Name of responsible person:
- Experimental setup/rig:
- Start Experiments: (date and time)
- Stop Experiments: (date and time)

You must get the approval back from the laboratory management before start up. All running experiments are notified in the activity calendar for the lab to be sure they are coordinated with other activity.

6.2 Abnormal situation

FIRE
If you are NOT able to extinguish the fire, activate the nearest fire alarm and evacuate area. Be then available for fire brigade and building caretaker to detect fire place.
If possible, notify:

NTNU	SINTEF
Morten Grønli, Mob: 918 97 515	Harald Mæhlum, Mob: 930 14 986
Olav Bolland: Mob: 918 97 209	Petter Røkke, Mob: 901 20 221
NTNU – SINTEF Beredskapstelefon	800 80 388

GAS ALARM
If a gas alarm occurs, close gas bottles immediately and ventilate the area. If the level of the gas concentration does not decrease within a reasonable time, activate the fire alarm and evacuate the lab. Designated personnel or fire department checks the leak to determine whether it is possible to seal the leak and ventilate the area in a responsible manner.

Alert Order is in the above paragraph.

PERSONAL INJURY
- First aid kit in the fire / first aid stations

- Shout for help
- Start life-saving first aid
- **CALL 113** if there is any doubt whether there is a serious injury

OTHER ABNORMAL SITUATIONS

NTNU:
You will find the reporting form for non-conformance on:
https://innsida.ntnu.no/wiki/-/wiki/Norsk/Melde+avvik

SINTEF:
Synergi

7   ASSESSMENT OF TECHNICAL SAFETY

7.1   HAZOP

See Chapter 13 "Guide to the report template".
The experiment set up is divided into the following nodes:

Node 1	Test rig in Klimalab
Node 2	

Attachments, Form: Hazop_mal
Conclusion: (Safety taken care of)

7.2   Flammable, reactive and pressurized substances and gas

Are any flammable, reactive and pressurized substances and gases in use?

NO	

Attachments: EX zones?
Conclusion:

7.3   Pressurized equipment

Is any pressurized equipment in use?

NO	

Attachments: Certificate for pressurized equipment (see Attachment to Risk Assessment)
Conclusion:

7.4   Effects on the environment (emissions, noise, temperature, vibration, smell)

Will the experiments generate emission of smoke, gas, odour or unusual waste?
Is there a need for a discharge permit, extraordinary measures?

NO	

Attachments:

Conclusion:

7.5   Radiation

See Chapter 13 "Guide to the report template".

NO	

Attachments:
Conclusion:

7.6   Chemicals

Will any chemicals or other harmful substances be used in the experiments? Describe how the chemicals should be handled (stored, disposed, etc.) Evaluate the risk according to safety datasheets, MSDS. Is there a need for protective actions given in the operational procedure?

NO	

Attachments: MSDS
Conclusion:

7.7   Electricity safety (deviations from the norms/standards)

NO	

Attachments:
Conclusion: The use of electrical equipment in this experiment complies with the standards and regulations in terms of touch danger.

8   ASSESSMENT OF OPERATIONAL SAFETY

Ensure that the procedures cover all identified risk factors that must be taken care of. Ensure that the operators and technical performance have sufficient expertise.

8.1   Procedure HAZOP

See Chapter 13 "Guide to the report template".
The method is a procedure to identify causes and sources of danger to operational problems.

Attachments:: HAZOP_MAL_Prosedyre

8.2   Operation procedure and emergency shutdown procedure

See Chapter 13 "Guide to the report template".
The operating procedure is a checklist that must be filled out for each experiment.
 Emergency procedure should attempt to set the experiment set up in a harmless state by unforeseen events.

Attachments: Procedure for running experiments

Emergency shutdown procedure: In case of emergency, the experiment should be shut down; fans should be switched off and manikin turned off if possible before leaving the rig.

8.3 Training of operators

The operator should know how to use the anemometers, adjust the heating level of the thermal manikin and how to operate both the supply- and exhaust fan. Training must be completed before the actual experiment begin. The operator should also be tidy ad responsible, to prevent accident to occur. In case of evacuation, the operator should turn off the fans and manikin before leaving the building.

8.4 Technical modifications

- *Technical modifications made by the operator (e.g.Replacement of components, equal to equal)*
- *Technical modifications that must be made by Technical staff (for example, modification of pressure equipment).*
- *What technical modifications give a need for a new risk assessment(by changing the risk picture)?*

Conclusion:

8.5 Personal protective equipment

- *Use gloves when there is opportunity for contact with hot/cold surfaces.*

Conclusion:

8.6 General Safety

An operator should always be present to follow the measurements. However, there is no risk involved when leaving the rig for a few moments.

8.7 Safety equipment

Not required.

8.8 Special predations

9 QUANTIFYING OF RISK - RISK MATRIX

See Chapter 13 "Guide to the report template".

The risk matrix will provide visualization and an overview of activity risks so that management and users get the most complete picture of risk factors.

IDnr	Aktivitet-hendelse	Frekv-Sans	Kons	RV
xx	*Rotating shaft, sanger of contact*	1	C1	C1
	Much noise, people without protective gear enter the rig site	1	B1	B1

Conclusion: The *Participants has to make a comprehensive assessment to determine whether the remaining risks of the activity/process is acceptable.*

◻ NTNU   **◎ SINTEF**

10   REGULATIONS AND GUIDELINES

Se http://www.arbeidstilsynet.no/regelverk/index.html
- Lov om tilsyn med elektriske anlegg og elektrisk utstyr (1929)
- Arbeidsmiljøloven
- Forskrift om systematisk helse-, miljø- og sikkerhetsarbeid (HMS Internkontrollforskrift)
- Forskrift om sikkerhet ved arbeid og drift av elektriske anlegg (FSE 2006)
- Forskrift om elektriske forsyningsanlegg (FEF 2006)
- Forskrift om utstyr og sikkerhetssystem til bruk i eksplosjonsfarlig område NEK 420
- Forskrift om håndtering av brannfarlig, reaksjonsfarlig og trykksatt stoff samt utstyr og anlegg som benyttes ved håndteringen
- Forskrift om Håndtering av eksplosjonsfarlig stoff
- Forskrift om bruk av arbeidsutstyr.
- Forskrift om Arbeidsplasser og arbeidslokaler
- Forskrift om Bruk av personlig verneutstyr på arbeidsplassen
- Forskrift om Helse og sikkerhet i eksplosjonsfarlige atmosfærer
- Forskrift om Høytrykksspyling
- Forskrift om Maskiner
- Forskrift om Sikkerhetsskilting og signalgivning på arbeidsplassen
- Forskrift om Stillaser, stiger og arbeid på tak m.m.
- Forskrift om Sveising, termisk skjæring, termisk sprøyting, kullbuemeisling, lodding og sliping (varmt arbeid)
- Forskrift om Tekniske innretninger
- Forskrift om Tungt og ensformig arbeid
- Forskrift om Vern mot eksponering for kjemikalier på arbeidsplassen (Kjemikalieforskriften)
- Forskrift om Vern mot kunstig optisk stråling på arbeidsplassen
- Forskrift om Vern mot mekaniske vibrasjoner
- Forskrift om Vern mot støy på arbeidsplassen

Veiledninger fra arbeidstilsynet
se: http://www.arbeidstilsynet.no/regelverk/veiledninger.html

11   DOCUMENTATION

- Tegninger, foto, beskrivelser av forsøksoppsetningen
- Hazop_mal
- Sertifikat for trykkpåkjent utstyr
- Håndtering avfall i NTNU
- Sikker bruk av LASERE, retningslinje
- HAZOP_MAL_Prosedyre
- Forsøksprosedyre
- Opplæringsplan for operatører
- Skjema for sikker jobb analyse, (SJA)
- Apparaturkortet
- Forsøk pågår kort

12   GUIDANCE TO RISK ASSESSMENT TEMPLATE

Chapter 7 Assessment of technical safety.
Ensure that the design of the experiment set up is optimized in terms of technical safety.
Identifying risk factors related to the selected design, and possibly to initiate re-design to ensure that risk is eliminated as much as possible through technical security.
This should describe what the experimental setup actually are able to manage and acceptance for emission.

7.1 HAZOP
The experimental set up is divided into nodes (eg motor unit, pump unit, cooling unit.). By using guidewords to identify causes, consequences and safeguards, recommendations and conclusions are made according to if necessary safety is obtained. When actions are performed the HAZOP is completed.
(e.g. "No flow", cause: the pipe is deformed, consequence: pump runs hot, precaution: measurement of flow with a link to the emergency or if the consequence is not critical used manual monitoring and are written into the operational procedure.)

7.2 Flammable, reactive and pressurized substances and gas.
According to the Regulations for handling of flammable, reactive and pressurized substances and equipment and facilities used for this:

Flammable material: Solid, liquid or gaseous substance, preparation, and substance with occurrence or combination of these conditions, by its flash point, contact with other substances, pressure, temperature or other chemical properties represent a danger of fire.

Reactive substances: Solid, liquid, or gaseous substances, preparations and substances that occur in combinations of these conditions, which on contact with water, by its pressure, temperature or chemical conditions, represents a potentially dangerous reaction, explosion or release of hazardous gas, steam, dust or fog.

Pressurized : Other solid, liquid or gaseous substance or mixes having fire or hazardous material response, when under pressure, and thus may represent a risk of uncontrolled emissions

Further criteria for the classification of flammable, reactive and pressurized substances are set out in Annex 1 of the Guide to the Regulations "Flammable, reactive and pressurized substances"
http://www.dsb.no/Global/Publikasjoner/2009/Veiledning/Generell%20veiledning.pdf
http://www.dsb.no/Global/Publikasjoner/2010/Tema/Temaveiledning_bruk_av_farlig_stoff_Del_1.pdf

Experiment setup area should be reviewed with respect to the assessment of Ex zone
• Zone 0: Always explosive atmosphere, such as inside the tank with gas, flammable liquid.
• Zone 1: Primary zone, sometimes explosive atmosphere such as a complete drain point
• Zone 2: secondary discharge could cause an explosive atmosphere by accident, such as flanges, valves and connection points

7.4 Effects on the environment

With pollution means: bringing solids, liquid or gas to air, water or ground, noise and vibrations, influence of temperature that may cause damage or inconvenience effect to the environment.

Regulations: http://www.lovdata.no/all/hl-19810313-006.html#6

NTNU guidance to handling of waste:http://www.ntnu.no/hms/retningslinjer/HMSR18B.pdf

7.5 Radiation

Definition of radiation

Ionizing radiation: Electromagnetic radiation (in radiation issues with wawelength <100 nm) or rapid atomic particles (e.g. alpha and beta particles) with the ability to stream ionized atoms or molecules.
Non ionizing radiation: Electromagnetic radiation (wavelength >100 nm), og ultrasound[1] with small or no capability to ionize.
Radiation sources: All ionizing and powerful non-ionizing radiation sources.
Ionizing radiation sources: Sources giving ionizing radiation e.g. all types of radiation sources, x-ray, and electron microscopes.
Powerful non ionizing radiation sources: Sources giving powerful non ionizing radiation which can harm health and/or environment, e.g. class 3B and 4. MR[2] systems, UVC[3] sources, powerful IR sources[4].
[1]Ultrasound is an acoustic radiation ("sound") over the audible frequency range (> 20 kHz). In radiation protection regulations are referred to ultrasound with electromagnetic non-ionizing radiation. [2]MR (e.g. NMR) - nuclear magnetic resonance method that is used to "depict" inner structures of different materials. [3]UVC is electromagnetic radiation in the wavelength range 100-280 nm. [4]IR is electromagnetic radiation in the wavelength range 700 nm - 1 mm.

For each laser there should be an information binder (HMSRV3404B) which shall include:
- General information
- Name of the instrument manager, deputy, and local radiation protection coordinator
- Key data on the apparatus
- Instrument-specific documentation
- References to (or copies of) data sheets, radiation protection regulations, etc.
- Assessments of risk factors
- Instructions for users
- Instructions for practical use, startup, operation, shutdown, safety precautions, logging, locking, or use of radiation sensor, etc.
- Emergency procedures
- See NTNU for laser: http://www.ntnu.no/hms/retningslinjer/HMSR34B.pdf

7.6 The use and handling of chemicals.

In the meaning chemicals, a element that can pose a danger to employee safety and health
See: http://www.lovdata.no/cgi-wift/ldles?doc=/sf/sf/sf-20010430-0443.html

Safety datasheet is to be kept in the HSE binder for the experiment set up and registered in the database for chemicals.

Chapter 8 Assessment of operational procedures.

Ensures that established procedures meet all identified risk factors that must be taken care of through operational barriers and that the operators and technical performance have sufficient expertise.

8.1 Procedure Hazop

Procedural HAZOP is a systematic review of the current procedure, using the fixed HAZOP methodology and defined guidewords. The procedure is broken into individual operations (nodes) and analyzed using guidewords to identify possible nonconformity, confusion or sources of inadequate performance and failure.

8.2 Procedure for running experiments and emergency shutdown.

Have to be prepared for all experiment setups.

The operating procedure has to describe stepwise preparation, startup, during and ending conditions of an experiment. The procedure should describe the assumptions and conditions for starting, operating parameters with the deviation allowed before aborting the experiment and the condition of the rig to be abandoned.

Emergency procedure describes how an emergency shutdown have to be done, (conducted by the uninitiated),

what happens when emergency shutdown, is activated. (electricity / gas supply) and

which events will activate the emergency shutdown (fire, leakage).

Chapter 9 Quantifying of RISK

Quantifying of the residue hazards, Risk matrix

To illustrate the overall risk, compared to the risk assessment, each activity is plotted with values for the probability and consequence into the matrix. Use task IDnr.

Example: If activity IDnr. 1 has been given a probability 3 and D for consequence the risk value become D3, red. This is done for all activities giving them risk values.

In the matrix are different degrees of risk highlighted in red, yellow or green. When an activity ends up on a red risk (= unacceptable risk), risk reducing action has to be taken

CONSEQUENSES	Catastrophic	E1	E2	E3	E4	E5
	Major	D1	D2	D3	D4	D5
	Moderate	C1	C2	C3	C4	C5
	Minor	B1	B2	B3	B4	B5
	Insignificant	A1	A2	A3	A4	A5
		Rare	Unlikely	Possible	Likely	Almost
				PROBABILITY		

Table 8. Risk's Matrix

Table 9. The principle of the acceptance criterion. Explanation of the colors used in the matrix

COLOUR		DESCRIPTION
Red		Unacceptable risk Action has to be taken to reduce risk
Yellow		Assessment area. Actions has to be considered
Green		Acceptable risk. Action can be taken based on other criteria

NTNU   **SINTEF**

Attachment to Risk Assessment report

Diffuser experiment with laminar airflow

Prosjektnavn	Characterization of the airflow distribution in close proximity to a patient in operating rooms with laminar airflow at St. Olavs Hospital
Apparatur	Klimarom VVS-lab
Enhet	NTNU
Apparaturansvarlig	Guangyu Cao
Prosjektleder	Guangyu Cao
HMS-koordinator	Morten Grønli
HMS-ansvarlig (linjeleder)	Olav Bolland
Plassering	Klimarom, Varmetekniske laboratorier
Romnummer	C247C, 2. etg i klimalab, Varmetekniske laboratorier
Risikovurdering utført av	Inge Håvard Rekstad

TABLE OF CONTENTS

NTNU

SINTEF

ATTACHMENT A: PROCESS AND INSTRUMENTATION DIAGRAM

NTNU   SINTEF

ATTACHMENT B: HAZOP TEMPLATE

Project:	Characterization of the airflow distribution in close proximity to a patient in operating rooms with laminar				Page
airflow at St. Olavs Hospital					
Node: 1					

Ref	Guideword	Causes	Consequences	Safeguards	Recommendations	Action	Date/Sign
Not likely	No flow	Pipe blocked/bent	Fanwear. Will create under pressure in working part of pipe	Use flow meter by fan and at outlet. Make sure the flow levels are approximately the same	Check the duct setup before turning on the fan. Check flow meters.	Turn of the fan again and follow the recommendations	
Not likely	Reverse flow	Fan runs the wrong way	Faulty measurements during experiments	Check that the flow from the fan is correct.	Adjust the fan speed and direction of rotation to the desired setting	Turn off the fan again and follow the recommendations	
Low risk	More flow	The fan runs too fast	Faulty measurements during experiment		Adjust the fan speed to the correct speed	Adjust the fan speed to the correct speed	
Low risk	Less flow	The fan runs too slow	Faulty measurements during experiment		Adjust the fan speed to the correct speed	Adjust the fan speed to the correct speed	
Low risk	Higher or lower temperature in thermal manikin	Wrong current level for the heating system	Thermal manikin hotter than desired may cause fire or burns in extreme cases	Make sure the electrical equipment is set up correctly, following the equipment's guidelines	Follow the equipment's guidelines. Make sure the manikins material can stand high temperatures	Adjust input watt level to adjust temperature of heating system	
Low risk							

2

NTNU ⬤ **SINTEF**

Project: Characterization of the airflow distribution in close proximity to a patient in operating rooms with laminar airflow at St. Olavs Hospital

Node: 1

Page

Ref	Guideword	Causes	Consequences	Safeguards	Recommendations	Action	Date/Sign

◘ NTNU　　　　　　　　**◉ SINTEF**

ATTACHMENT C: TEST CERTIFICATE FOR LOCAL PRESSURE TESTING

Trykkpåkjent utstyr:	
Benyttes i rigg:	
Design trykk for utstyr (bara):	
Maksimum tillatt trykk (bara): (i.e. burst pressure om kjent)	
Maksimum driftstrykk i denne rigg:	

Prøvetrykket skal fastlegges i følge standarden og med hensyn til maksimum tillatt trykk.

Prøvetrykk (bara):			
X maksimum driftstrykk: I følge standard			
Test medium:			
Temperatur (°C)			
Start tid:		Trykk (bara):	
Slutt tid:		Trykk (bara):	
Maksimum driftstrykk i denne rigg:			

Eventuelle repetisjoner fra atm. trykk til maksimum prøvetrykk:……………

Test trykket, dato for testing og maksimum tillatt driftstrykk skal markers på (skilt eller innslått)

_____　　　_____

Sted og dato　　　　　　　　　　　Signatur

NTNU   SINTEF

ATTACHMENT D: HAZOP PROCEDURE (TEMPLATE)

Project:

Node: 1

Page

Reff#	Guideword	Causes	Consequences	Safeguards	Recommendations	Action	Date/Sign
	Not clear procedure	Procedure is to ambitious, or confusingly					
	Step in the wrong place	The procedure can lead to actions done in the wrong pattern or sequence					
	Wrong actions	Procedure improperly specified					
	Incorrect information	Information provided in advance of the specified action is wrong					
	Step missing	Missing step, or step requires too much of operator					
	Step unsuccessful	Step has a high probability of failure					
	Influence and effects from other	Procedure's performance can be affected by other sources					

5

⊡ NTNU ⊙ SINTEF

ATTACHMENT E: PROCEDURE FOR RUNNING EXPERIMENTS

	Dato	Signatur
Prosjekt Characterization of the airflow distribution in close proximity to a patient in operating rooms with laminar airflow at St. Olavs Hospital		
Apparatur Diffuser experiment with laminar airflow		
Prosjektleder Guangyu Cao	15.5.2017	*Gyu Ceo*

	Conditions for the experiment:	Completed
	Experiments should be run in normal working hours, 08:00-16:00 during winter time and 08.00-15.00 during summer time. Experiments outside normal working hours shall be approved.	✓
	One person must always be present while running experiments, and should be approved as an experimental leader.	✓
	An early warning is given according to the lab rules, and accepted by authorized personnel.	✓
	Be sure that everyone taking part of the experiment is wearing the necessary protecting equipment and is aware of the shut down procedure and escape routes.	✓
	Preparations	**Carried out**
	Post the "Experiment in progress" sign.	✓
	Turn on the fan to supply air through the diffuser nozzle, and check outlet velocity at different locations that the flow is evenly distributed	
	Measure initial air temperature in the room. Check at 3-4 different heights to be sure there is little thermal stratification	✓
	Measure all wall surface temperatures in case of radiation influence on the thermal manikin	✓
	Place anemometers and manikin at starting locations	✓
	Heat up manikin to the correct surface temperature. Turn on the ventilation, heat it to 22 °C (room temp.) and adjust it to have a velocity of 0.3 m/s at the outlet	✓
	During the experiment	
	Velocity measurements at all relevant locations and chosen points	✓
	Check the temperature from the diffuser. Is it the same as in the room?	
	End of experiment	
	Turn off fans and heat source	✓
	Remove all obstructions/barriers/signs around the experiment.	✓
	Tidy up and return all tools and equipment.	✓
	Tidy and cleanup work areas.	✓
	Return equipment and systems back to their normal operation settings (fire alarm)	✓

NTNU   SINTEF

To reflect on before the next experiment and experience useful for others	
Was the experiment completed as planned and on scheduled in professional terms?	
Was the competence which was needed for security and completion of the experiment available to you?	✓
Do you have any information/ knowledge from the experiment that you should document and share with fellow colleagues?	✓

Operator(s):

Navn	Dato	Signatur
Madeleine Charlotte Storås	15. mai 2017	Madeleine C. Storås

NTNU   ◉ SINTEF

ATTACHMENT F: TRAINING OF OPERATORS

Prosjekt Characterization of the airflow distribution in close proximity to a patient in operating rooms with laminar airflow at St. Olavs Hospital	Dato	Signatur
Apparatur Klimalab		
Prosjektleder Guangyu Cao	15.5.20??	_signature_

	Knowledge about EPT LAB in general	
	Lab • Access • routines and rules • working hour	
	Knowledge about the evacuation procedures.	
	Activity calendar for the Lab	
	Early warning, **iept-experiments@ivt.ntnu.no**	
	Knowledge about the experiments	
	Procedures for the experiments	
	Emergency shutdown.	
	Nearest fire and first aid station.	

I hereby declare that I have read and understood the regulatory requirements has received appropriate training to run this experiment and are aware of my personal responsibility by working in EPT laboratories.

Operator(s):

Navn	Dato	Signatur
Madeleine Charlotte Storås	15. mai 2017	_Madeleine C. Storås_

NTNU　　　　　　　　**SINTEF**

ATTACHMENT G: FORM FOR SAFE JOB ANALYSIS

SJA name:	
Date:	Location:
Mark for completed checklist:	

Participators:		
SJA-responsible:		

Specification of work (What and how?):
Risks associated with the work:
Safeguards: (plan for actions, see next page):
Conclusions/comments:

Recommended/approved	Date/Signature:	Recommended/approved	Date/Signature:
SJA-responsible:		HSE responsible:	
Responsible for work:		Other, (position):	

HSE aspect	Yes	No	NA	Comments / actions	Resp.
Documentation, experience, qualifications					
Known operation or work?					
Knowledge of experiences / incidents from similar operations?					
Necessary personnel?					
Communication and coordinating					
Potential conflicts with other operations?					
Handling of an eventually incident (alarm, evacuation)?					
Need for extra assistance / watch?					
Working area					
Unusual working position					
Work in tanks, manhole?					
Work in ditch, shaft or pit?					
Clean and tidy?					
Protective equipment beyond the personal?					
Weather, wind, visibility, lighting, ventilation?					
Usage of scaffolding/lifts/belts/ straps, anti-falling device?					
Work at hights?					
Ionizing radiation?					
Influence of escape routes?					
Chemical hazards					
Usage of hazardous/toxic/corrosive chemicals?					
Usage of flammable or explosive chemicals?					
Risk assessment of usage?					
Biological materials/substances?					
Dust/asbestos/dust from insulation?					
Mechanical hazards					
Stability/strength/tension?					
Crush/clamp/cut/hit?					
Dust/pressure/temperature?					
Handling of waste disposal?					
Need of special tools?					
Electrical hazards					
Current/Voltage/over 1000V?					
Current surge, short circuit?					
Loss of current supply?					
Area					
Need for inspection?					
Marking/system of signs/rope off?					
Environmental consequences?					
Key physical security systems					
Work on or demounting of safety systems?					
Other					

NTNU
SINTEF

APPARATURKORT / UNITCARD

Dette kortet SKAL henges godt synlig på apparaturen!
This card MUST be posted on a visible place on the unit!

Apparatur (Unit)	
Diffuser experiment with laminar airflow and thermal manikin	
Prosjektleder (Project Leader)	**Telefon mobil/privat** (Phone no. mobile/private)
Guangyu Cao	+47 91897689
Apparaturansvarlig (Unit Responsible)	**Telefon mobil/privat** (Phone no. mobile/private)
Guangyu Cao	+47 47361023
Sikkerhetsrisikoer (Safety hazards)	
Do not touch the thermal manikin while it's plugged in	
Sikkerhetsregler (Safety rules)	
Fans and manikin should be switched off when not in use	
Nødstopp prosedyre (Emergency shutdown)	
Switch off fans and unplug the thermal manikin	

Her finner du (Here you will find):

Prosedyrer (Procedures)	In the room
Bruksanvisning (Users manual)	In the room

Nærmeste (Nearest)

Brannslukningsapparat (fire extinguisher)	First floor VVSlab (syd)
Førstehjelpsskap (first aid cabinet)	First floor VVSlab (syd)

NTNU
Institutt for energi og prosessteknikk

SINTEF Energi
Avdeling energiprosesser

Dato

Dato

_____

_____

Signert

Signert

_____

_____

FORSØK PÅGÅR /EXPERIMENT IN PROGRESS

Dette kortet SKAL henges opp før forsøk kan starte!
This card MUST be posted on the unit before the experiment startup!

Apparatur (Unit)	
Diffuser experiment with laminar airflow and thermal manikin	
Prosjektleder (Project Leader)	**Telefon mobil/privat** (Phone no. mobile/private)
Guangyu Cao	+47 91897689
Apparaturansvarlig (Unit Responsible)	**Telefon mobil/privat** (Phone no. mobile/private)
Guangyu Cao	+47 47361023
Godkjente operatører (Approved Operators)	**Telefon mobil/privat** (Phone no. mobile/private)
Madeleine Charlotte Storås	+47 95308899

Prosjekt (Project)
Characterization of the airflow distribution in close proximity to a patient in operating rooms with laminar airflow at St. Olavs Hospital

Forsøkstid / Experimental time (start - stop)
16.05.2017-10.08.2017

Kort beskrivelse av forsøket og relaterte farer (Short description of the experiment and related hazards)
Measuring the velocity- and temperature distribution in close proximity to the thermal manikin, under the influence of laminar airflow from the diffuser (low velocities, 0.3 m/s). The door should be closed during the experiment. Do not touch the manikin while it is plugged in, as there may be a risk of electrical shock from the heating method of the manikin.

NTNU
Institutt for energi og prosessteknikk

SINTEF Energi
Avdeling energiprosesser

Dato

Dato

_____

_____

Signert

Signert

_____

_____

D   Results

D.1   Scenario 1

The average standard deviation (SD) at each measuring point for all of the five cases is presented in this sub chapter. The standard deviation is given in m/s.
Case 1:   The standard deviation for Case 1 is given in Table 10.

Table 10: Standard deviation for Case 1 [m/s]

Height	Table length	Table width				
		7.50	17.50	27.50	37.50	47.50
h=100 cm	40	0.021166667	0.0171	0.014066667	0.0103	0.006666667
	80	0.0071	0.005766667	0.005633333	0.005533333	0.0072
	120	0.020366667	0.021033333	0.0238	0.014	0.009833333
	160	0.02	0.026	0.021	0.016	0.009
	200	0.013	0.005	0.014	0.014	0.026
h=110 cm	40	0.006866667	0.0046	0.004166667	0.004733333	0.007633333
	80	0.005933333	0.0051	0.004866667	0.0046	0.004433333
	120	0.019666667	0.016233333	0.023633333	0.011933333	0.010366667
	160	0.024033333	0.020733333	0.020466667	0.013833333	0.007733333
	200	0.017166667	0.015233333	0.012433333	0.011866667	0.018566667
h=120 cm	40	0.006866667	0.005866667	0.005533333	0.007266667	0.005666667
	80	0.006933333	0.0064	0.005966667	0.004966667	0.007933333
	120	0.024766667	0.017533333	0.0212	0.0075	0.006
	160	0.021266667	0.0173	0.0158	0.008833333	0.009766667
	200	0.014033333	0.0147	0.013166667	0.009166667	0.0131

Case 2:   The standard deviation for Case 2 is given in Table 11.

Table 11: Standard deviation for Case 2 [m/s]

Height	Table length	Table width				
		7.50	17.50	27.50	37.50	47.50
h=100 cm	40	0.0057	0.004133333	0.005333333	0.005966667	0.004433333
	80	0.005366667	0.005666667	0.0055	0.0047	0.007833333
	120	0.0228	0.019933333	0.0274	0.0194	0.010866667
	160	0.027666667	0.0223	0.0219	0.015566667	0.011766667
	200	0.023133333	0.019566667	0.0122	0.007066667	0.007133333
h=110 cm	40	0.0068	0.004466667	0.004566667	0.0043	0.007966667
	80	0.012966667	0.011533333	0.0104	0.007033333	0.007933333
	120	0.024033333	0.026033333	0.025166667	0.012466667	0.006333333
	160	0.068633333	0.042133333	0.0281	0.014266667	0.009666667
	200	0.020233333	0.014	0.019766667	0.0132	0.010466667
h=120 cm	40	0.005866667	0.004366667	0.005333333	0.005166667	0.0043
	80	0.006666667	0.004633333	0.0053	0.004833333	0.008066667
	120	0.024066667	0.020966667	0.013733333	0.006466667	0.007566667
	160	0.065066667	0.041	0.032333333	0.0179	0.011566667
	200	0.015933333	0.0143	0.011533333	0.0058	0.0116

Case 3: The standard deviation for Case 3 is given in Table 12.

Table 12: Standard deviation for Case 3 [m/s]

Height	Table length	Table width				
		7.50	17.50	27.50	37.50	47.50
h=100 cm	40	0.0082	0.007466667	0.0098	0.006466667	0.0062
	80	0.025366667	0.012366667	0.011933333	0.010266667	0.008866667
	120	0.040066667	0.0206	0.023933333	0.0226	0.011866667
	160	0.0288	0.028	0.0279	0.020066667	0.014566667
	200	0.0115	0.0106	0.012966667	0.0133	0.009733333
h=110 cm	40	0.007066667	0.007233333	0.0076	0.006033333	0.007733333
	80	0.024666667	0.0088	0.0086	0.006566667	0.0058
	120	0.0364	0.022866667	0.025633333	0.024966667	0.008366667
	160	0.0224	0.025866667	0.028633333	0.017666667	0.041466667
	200	0.009833333	0.008366667	0.009166667	0.009	0.0102
h=120 cm	40	0.007833333	0.006966667	0.007	0.006466667	0.0073
	80	0.0165	0.01	0.005733333	0.0049	0.008766667
	120	0.015266667	0.017766667	0.0206	0.0096	0.007466667
	160	0.020266667	0.016	0.0208	0.0142	0.0157
	200	0.0073	0.006866667	0.0102	0.007866667	0.015

Case 4:   The standard deviation for Case 4 is given in Table 13.

Table 13: Standard deviation for Case 4 [m/s]

| Height	Table length	Table width				
		7.50	17.50	27.50	37.50	47.50
h=100 cm	40	0.0252	0.020333333	0.028633333	0.030233333	0.034333333
	80	0.0404	0.033166667	0.031733333	0.029733333	0.032733333
	120	0.0344	0.030533333	0.0341	0.0273	0.032566667
	160	0.037466667	0.023866667	0.0322	0.036966667	0.034866667
	200	0.03	0.029566667	0.034233333	0.037	0.0406
h=110 cm	40	0.0233	0.021633333	0.033033333	0.043	0.053733333
	80	0.035733333	0.030633333	0.030833333	0.0249	0.022166667
	120	0.040366667	0.026466667	0.031866667	0.0232	0.023566667
	160	0.0396	0.056066667	0.035066667	0.038233333	0.038066667
	200	0.023033333	0.028566667	0.039966667	0.0365	0.0311
h=120 cm	40	0.020433333	0.0152	0.020433333	0.029266667	0.041633333
	80	0.027966667	0.023266667	0.031366667	0.027766667	0.033366667
	120	0.023866667	0.026566667	0.029866667	0.0288	0.026433333
	160	0.0482	0.061333333	0.0403	0.0273	0.028466667
	200	0.0227	0.0248	0.029766667	0.0333	0.0332

Case 5:   The standard deviation for Case 5 is given in Table 14.

Table 14: Standard deviation for Case 5 [m/s]

| Height	Table length	Table width				
		7.50	17.50	27.50	37.50	47.50
h=100 cm	40	0.0348	0.026966667	0.031733333	0.0296	0.024833333
	80	0.039533333	0.0349	0.028733333	0.0291	0.0208
	120	0.0407	0.039733333	0.039533333	0.048233333	0.041333333
	160	0.0564	0.042433333	0.055	0.059466667	0.048066667
	200	0.040266667	0.031233333	0.032	0.0387	0.032666667
h=110 cm	40	0.047233333	0.0308	0.0323	0.035166667	0.033633333
	80	0.032866667	0.033266667	0.032166667	0.0388	0.041333333
	120	0.049466667	0.044666667	0.045433333	0.063833333	0.037433333
	160	0.062866667	0.043833333	0.043	0.039733333	0.033333333
	200	0.0274	0.0339	0.036666667	0.040366667	0.037733333
h=120 cm	40	0.031433333	0.025733333	0.035433333	0.033933333	0.0393
	80	0.039933333	0.034533333	0.0422	0.040666667	0.031366667
	120	0.047966667	0.0433	0.0433	0.0563	0.063966667
	160	0.052233333	0.052633333	0.0551	0.046366667	0.0432
	200	0.526066667	0.029033333	0.032566667	0.0308	0.053133333

D.1.1 Draft rate

Figure 48, 49 and 50 shows the draft rate at a height 100 cm, 110 cm and 120 cm above the floor, respectively.
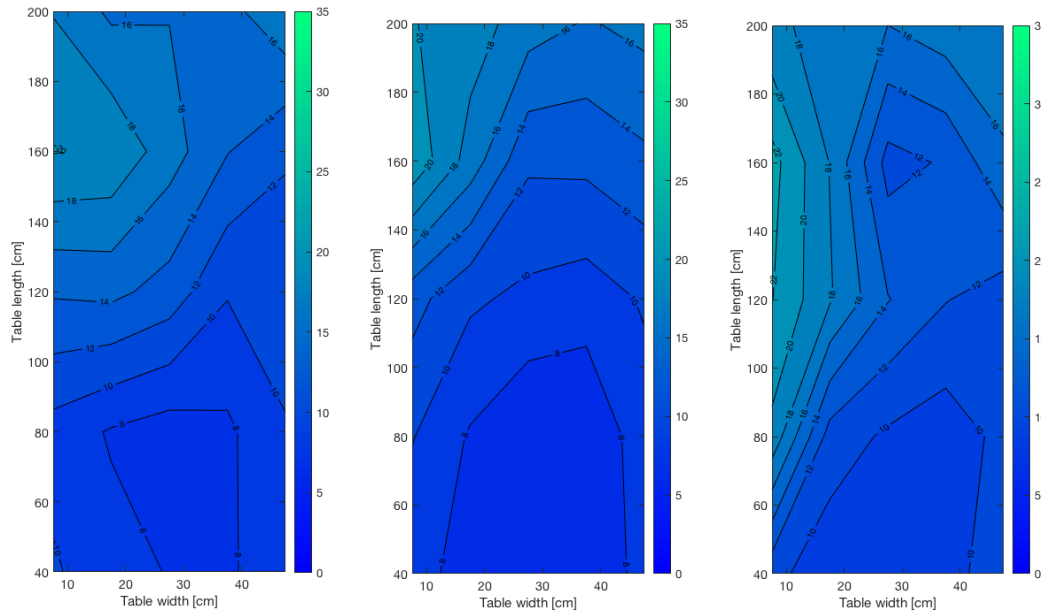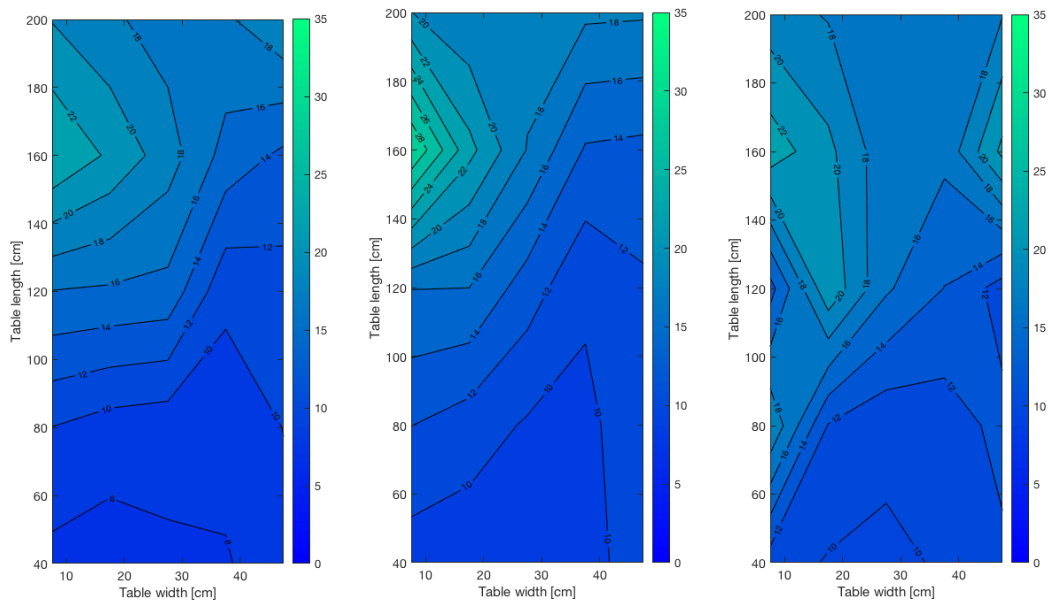

(a) Case 1   **(b)** Case 2   **(c)** Case 3
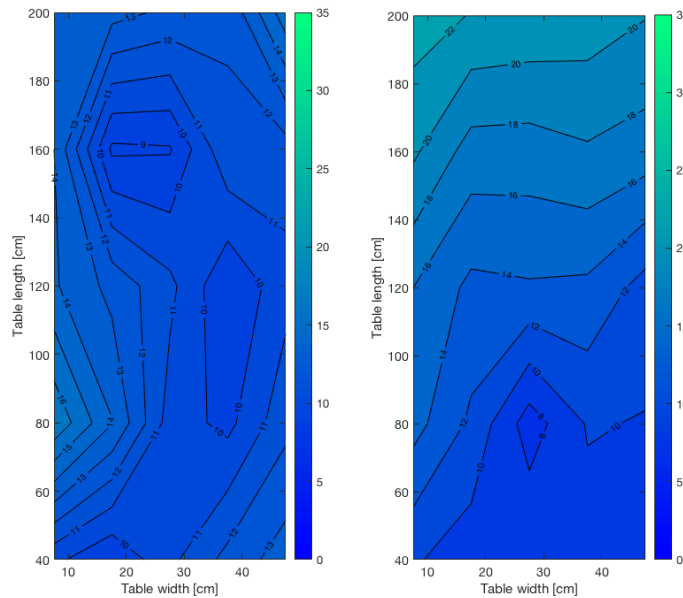
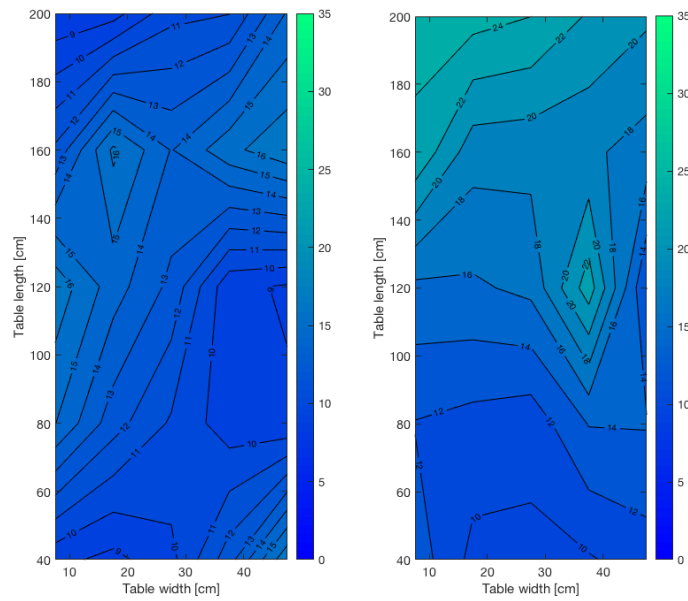**(d)** Case 4   **(e)** Case 5

Figure 48: Draft rate at 100 cm above the floor

(a) Case 1   (b) Case 2   (c) Case 3

(d) Case 4   (e) Case 5

Figure 49: Draft rate at 110 cm above the floor
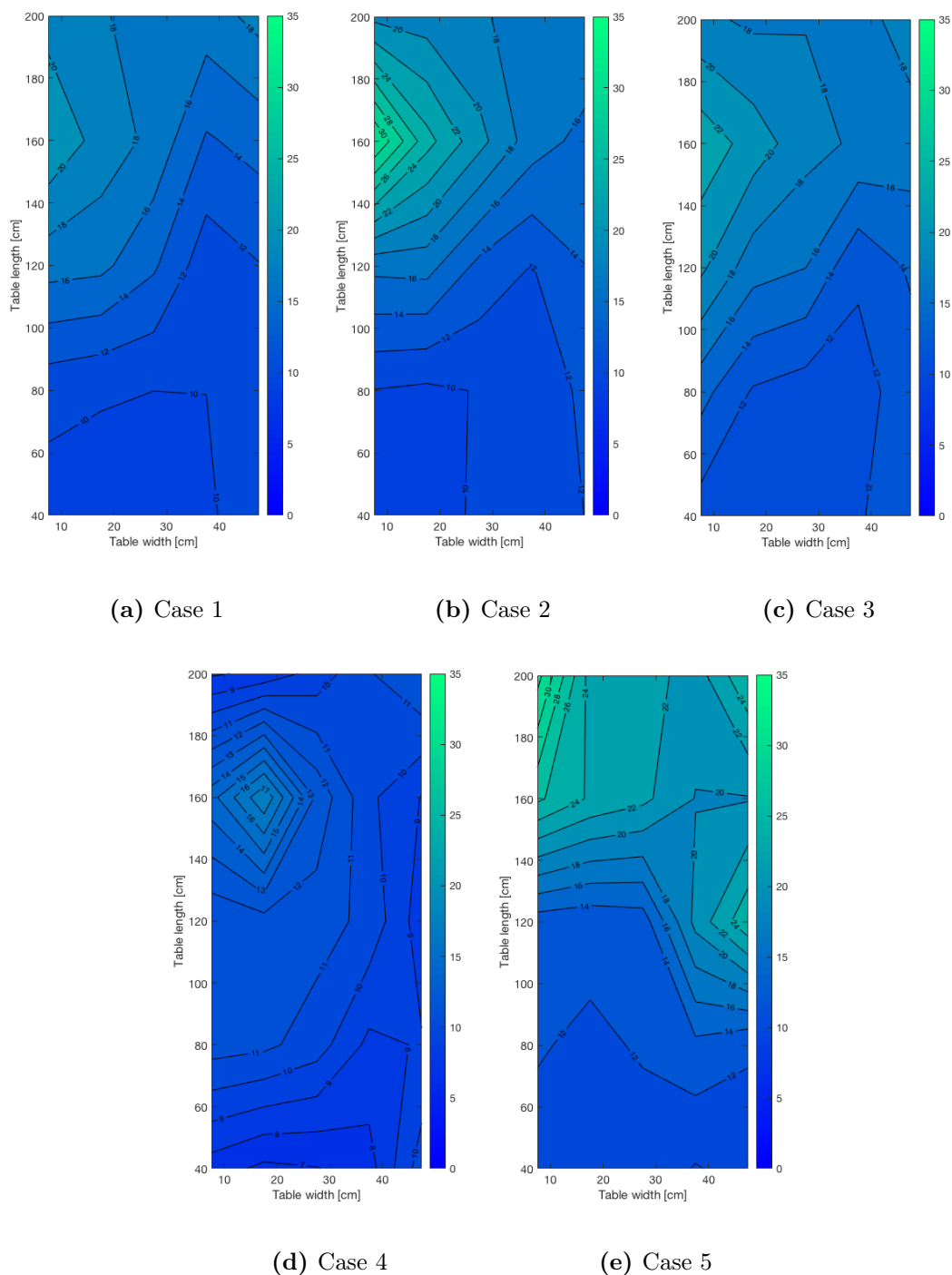
(a) Case 1 **(b)** Case 2 **(c)** Case 3

(d) Case 4 **(e)** Case 5

Figure 50: Draft rate at 120 cm above the floor

D.2 Scenario 2

D.2.1 Thermal manikin

The heating wire that is used for the thermal manikin is given by the following link: http: //no.rs-online.com/web/p/trace-heating-cable/0379744/ (downloaded at 05. june 2017).

A picture of the control panel for the manikin is given in Figure 51.

Figure 51: Control panel for the surface temperature of the manikin

Thermodetector Bosch PTD 1: The technical specification for the thermodetector is given in the following link: http://www.bosch-ptd1.com/no/no/product/ptd+1.html (downloaded 29. June 2017).

D.2.2   Results, plume modelling

From Figure 52 it is evident that the plume boundaries are not possible to be presented by a fitted line, and does therefore not give any applicable result. The fitted line which is presented in the figure gives a spread angle of 19.7 °and consequentially a C_b=0.357.
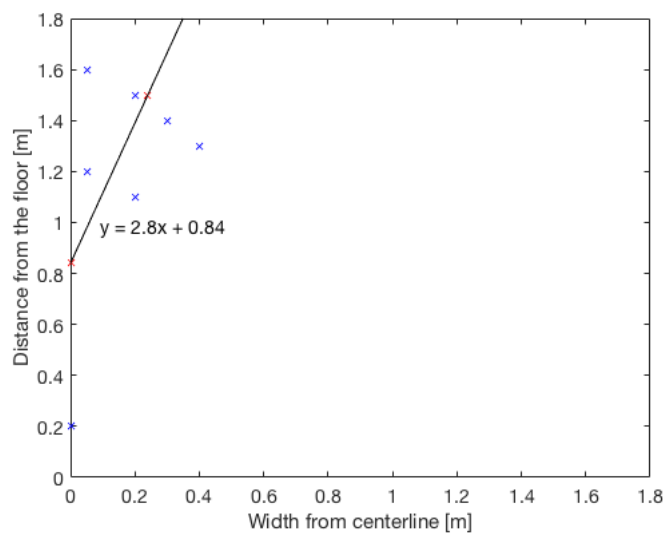

Figure 52: Spread angle for velocities above the head, modelled as a point source

D.3   Scenario 3

Ventilation system in resting mode: First the air velocity were measured for a patient below an LAF system in resting mode. The objective with studying this mode was to see the interaction between the plume and low airflow velocity ventilation. This should give an overview of the development of the plume disturbed by low velocities. A ventilation system

in full speed should manage to counteract the development of the plume. In this mode, the velocity at 108 different points were measured. Some of them were outside of the table width, but as the plume is most likely to develop in a greater area this was necessary. The plume were measured for five different heights as shown in Figure 53b Measuring setup as for plume.

The measuring point for each height are shown in Figure 53a. The distance between the measuring points in x-direction is 5 cm, while the distance between the measuring points in y-direction is 30 cm.

(a) Measuring points at each height

(b) Seven measuring heights
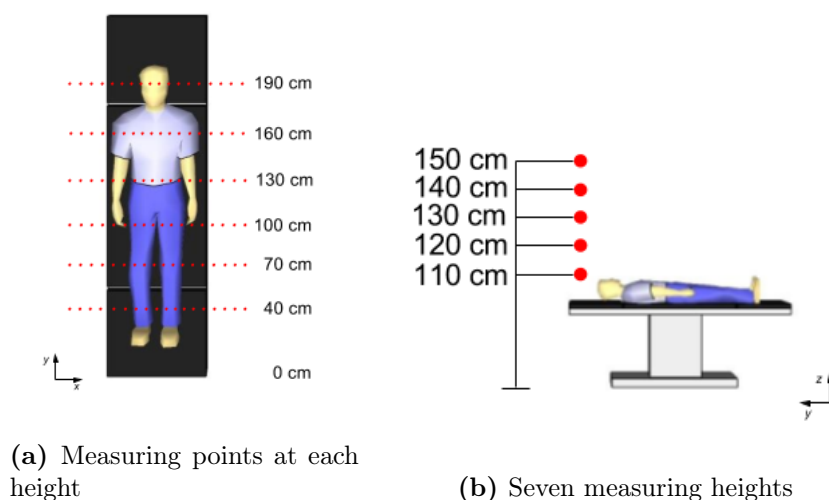
Figure 53: Sketch of measuring points for ventilation in resting mode

For the operating theatre at St. Olavs Hospital a ventilation mode named "Resting mode" is possible to chose. As the ventilation' air handling unit for the operating theatre is connected to the other operating theatres in the area, this mode will give the lowest possible LAF ventilation that will maintain balanced ventilation for the system in total, and the outlet velocities from the LAF was measured to have between 0.05 and 0.01 m/s within the ultra clean zone. In this mode, an increased airflow of the mixing kind of ventilation is measured elsewhere in the room, around the ultra clean zone. The objective with these measurements are to establish information about the development of plume in a mixing ventilation environment. A picture of the experimental setup is given in Figure 54.


Figure 54: Experimental setup for ventilation in resting mode

Figure 55 shows the velocity contours above and around the operating table for the ventilation

system in resting mode. The table width extends from width from 15 cm to 70 cm, as marked by the dotted lines on each sub-figure. The first height, 110 cm above the floor presented in Figure 55a, is measured right above the thermal manikin.

Equal for all the heights in Figure 55 the velocity at each height vary a lot, and that the left side of the contours have in general higher velocities than the right side. The velocity level is also in general much higher than for the ventilation in full mode used for Scenario 1. As the velocities from the LAF is measured to be at a minimum, the relatively high velocities has to come from the mixing ventilation around the ultra clean zone.
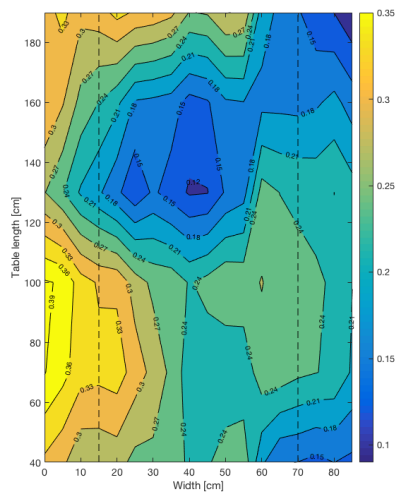
(a) 110 cm above the floor
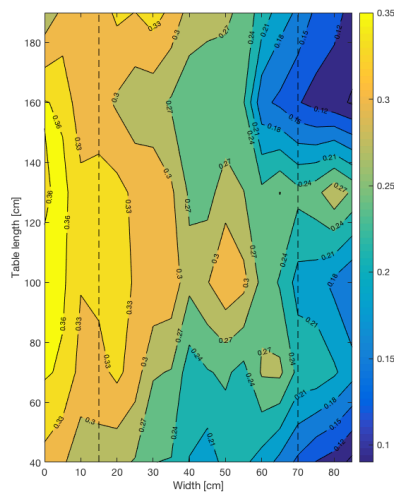
(b) 120 cm above the floor
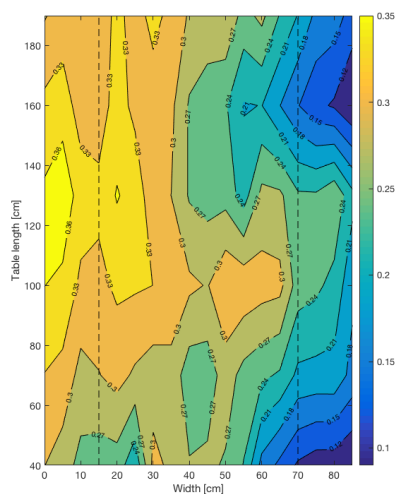
(c) 130 cm above the floor
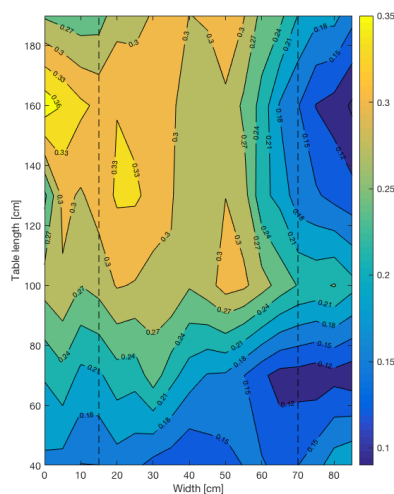
(d) 140 cm above the floor
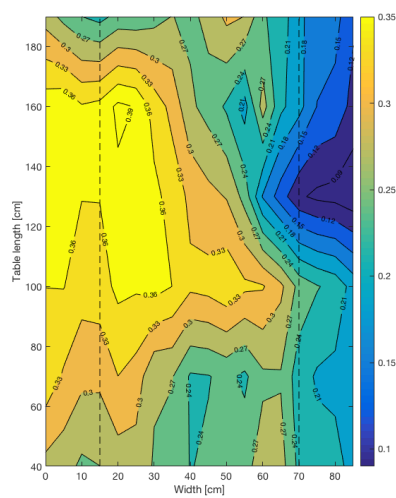
(e) 150 cm above the floor

Figure 55: Horizontal speed contours for five different heights

Vertical velocity contours has been made for each of the 18 points for the widths in Figure 55. These velocity contours are made to show the velocity distribution above the table length, and see if a development of thermal plume can be shown above the manikins surface in a room with less ventilation. The total series of 18 vertical contour plots are presented in the following figure. The operating table is placed from x=15 to x=70.

(a) x=0

(b) x=5

(c) x=10

(d) x=15

(e) x=20

(f) x=25

(g) x=30

(h) x=35

(i) x=40

(j) x=45

(k) x=50

(l) x=55

(m) x=60

(n) x=65

(o) x=70

(p) x=75

(q) x=80

(r) x=85
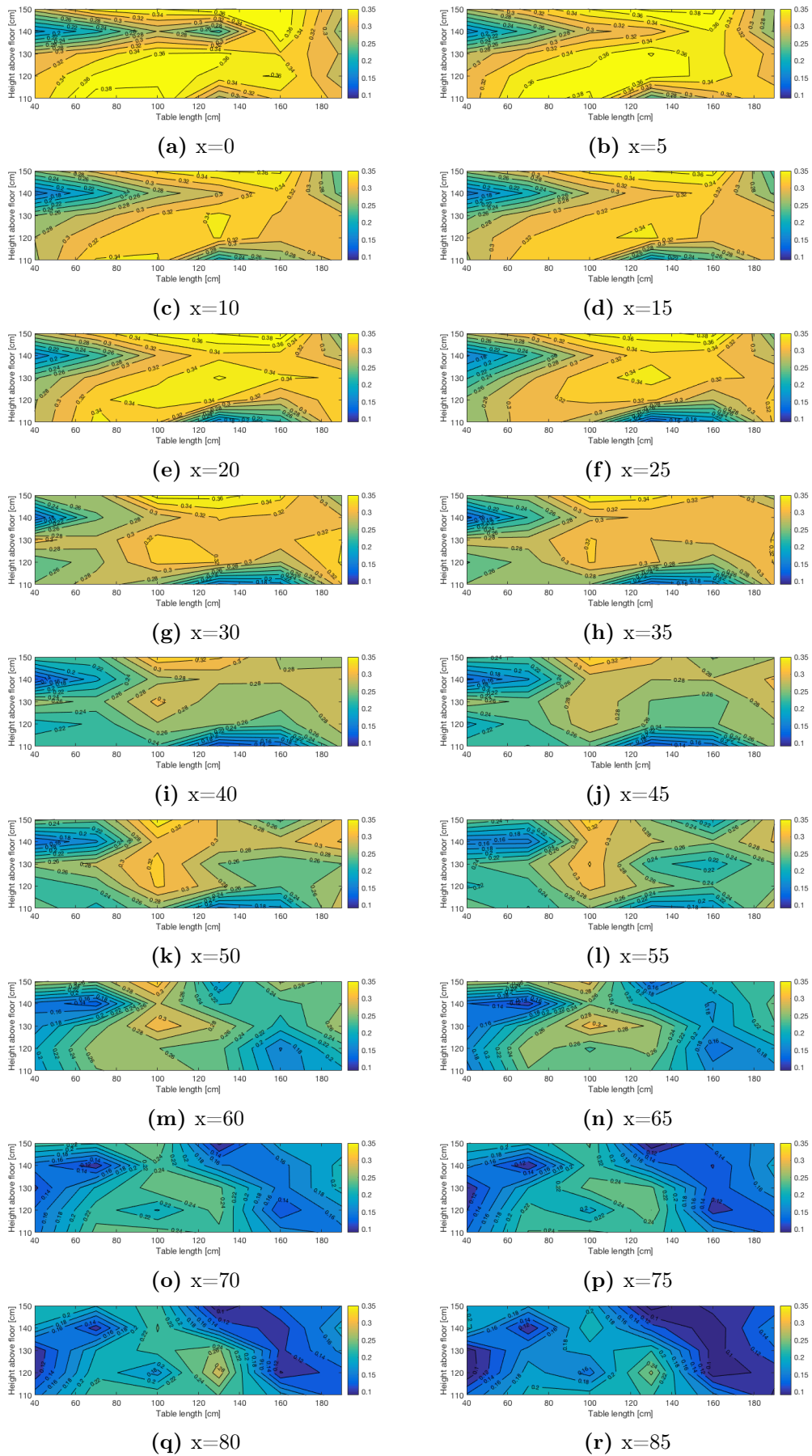
Figure 56: Vertical speed contours for each point for ventilation syste in resting mode

From Figure 56 is can be seen that the plume has a greatest impact in the abdominal/chest area, see from 100cm to 180 cm on the figures.

Velocity profile above different parts of the body is also found. Objective with this is to analyse the development of thermal plume and how it is influenced by mixing ventilation. In Figure **??** the table placed for distance from 15 cm to 70 cm.

(a) Legs

(b) Knees

(c) Upper thigh

(d) Stomach

(e) Chest

(f) Head
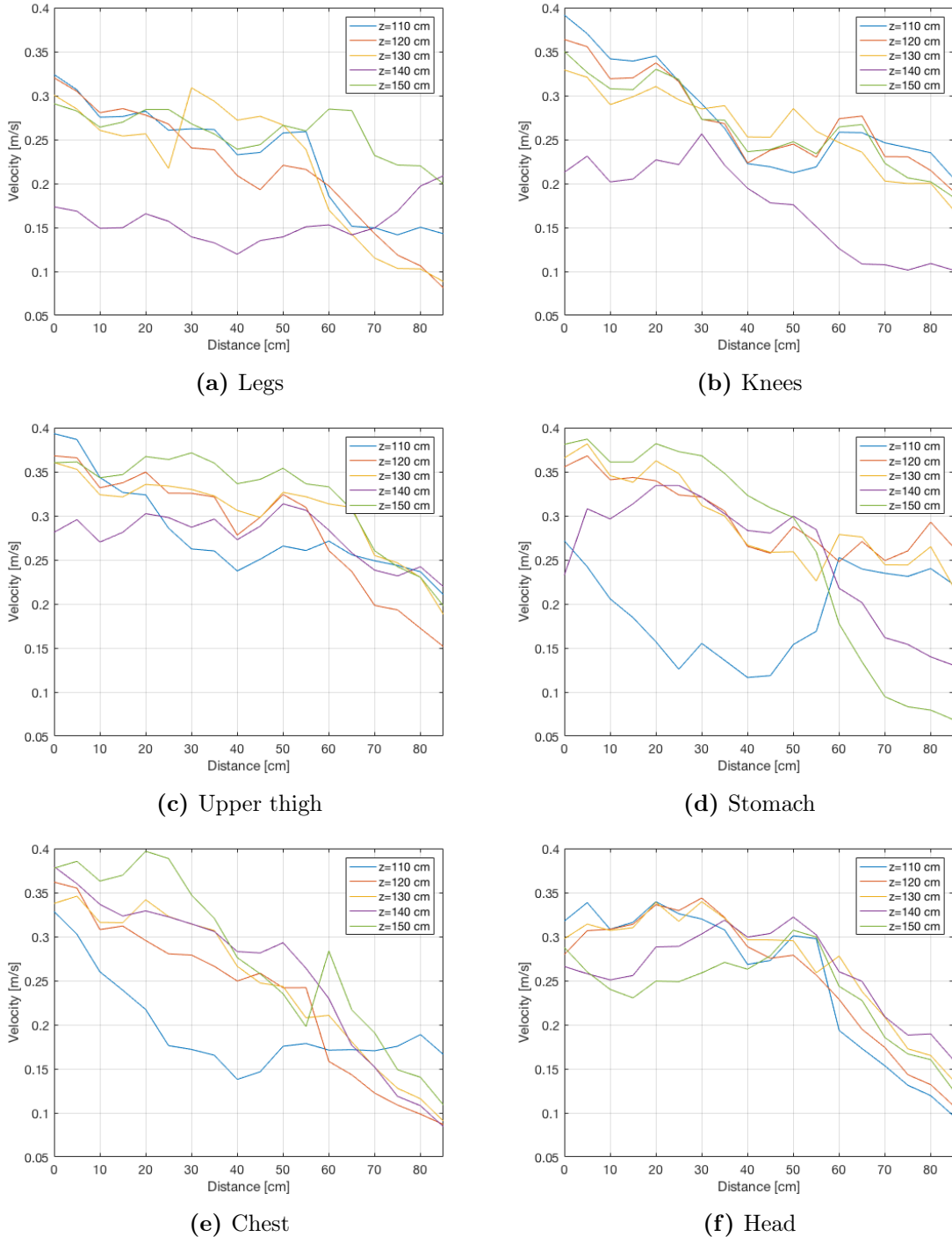
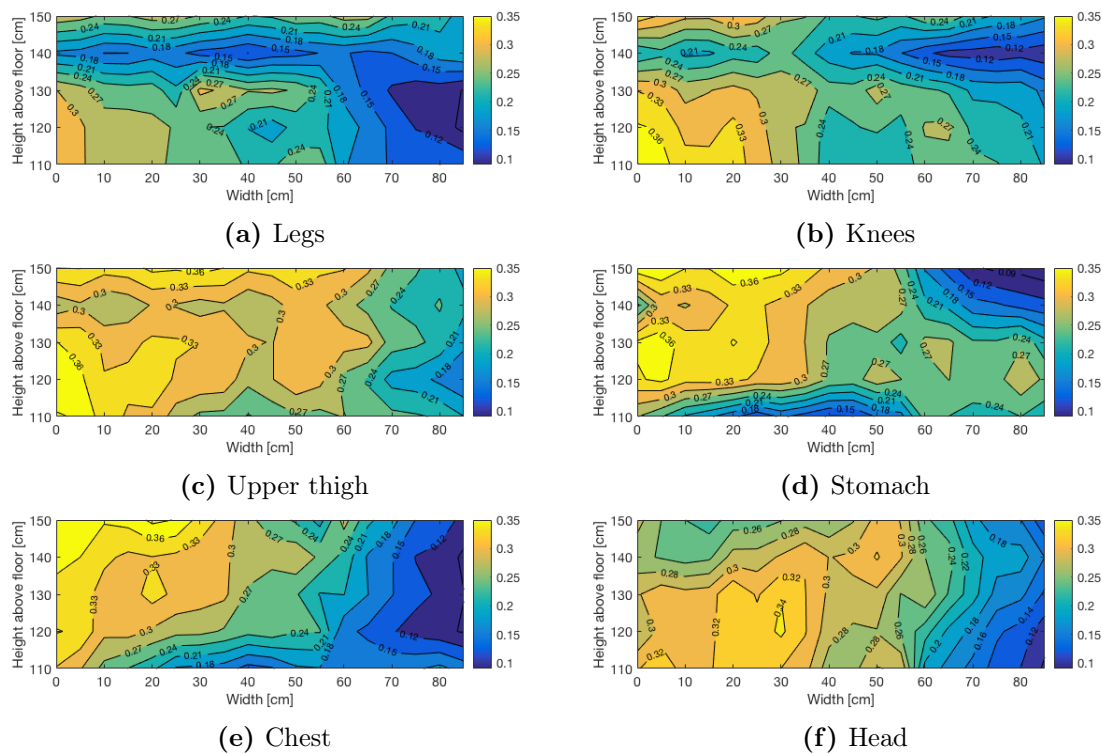**Figure 57:** Velocity plots for the six different places above the thermal manikin

From Figure 57 the most interesting graphs to study is Figure 57c, 57d and 57e as they say something about the interaction of the plume and ventilation. This is because the velocity

profile closest to the thermal manikin (most likely to be most influenced by thermal plume), pictured by the blue lines, are smaller than the other velocity profiles above the same place. This may be caused by interaction between plume and ventilation system. The presence of a thermal plume is most evident at the stomach area as shown in Figure 56, which support the statement of plume interaction in that area.

To dig deeper into the velocity profile and interaction of plume and ventilation vertical velocity contours are made and presented in Figure 58. The table is also here placed from width equal to 15 cm to 70 cm.

(a) Legs

(b) Knees

(c) Upper thigh

(d) Stomach

(e) Chest

(f) Head

Figure 58: Speed contour plots for the six different places above the thermal manikin

E   Matlab

This section is including the Matlab-scripts that were used to find the plume boundary. The boundary-script were originally created by Marie Steffensen, but were adapted to my measurements. All the other scripts were developed by myself.

- Speed contours for Scenario 1:

```
1  %Velocity
2  clear all
3  clc
4
5  xax=[7.50 17.50 27.50 37.50 47.50];
6  yax=[40
7  80
8  120
9  160
10  200];
```

```matlab
11
12  width=5.50;
13  height=21.00;
14
15  A1=load('case1v.txt');
16
17  f1=figure('units','inches','position',[1 1 width height]);
18  contourf(xax, yax, A1(1:5,1:5),'ShowText','on');
19  colorbar
20  caxis([0.09 0.35]);
21  xlabel('Table width [cm]');
22  ylabel('Table length [cm]');
23  %figure('units','inches','position',[1 1 width height]);
24  set(gca,'fontsize',14);
25  %set(gcf,'units','inches','position',[xax yax width height])
26
27
28  f2=figure('units','inches','position',[1 1 width height]);
29  contourf(xax, yax, A1(6:10,1:5),'ShowText','on');
30  colorbar
31  caxis([0.09 0.35]);
32  xlabel('Table width [cm]');
33  ylabel('Table length [cm]');
34  set(gca,'fontsize',14);
35
36  f3=figure('units','inches','position',[1 1 width height]);
37  contourf(xax, yax, A1(11:15,1:5),'ShowText','on');
38  colorbar
39  caxis([0.09 0.35]);
40  xlabel('Table width [cm]');
41  ylabel('Table length [cm]');
42  set(gca,'fontsize',14);
43  %————————
44  A2=load('case2v.txt');
45
46  f4=figure('units','inches','position',[1 1 width height]);
47  contourf(xax, yax, A2(1:5,1:5),'ShowText','on');
48  colorbar
49  caxis([0.09 0.35]);
50  xlabel('Table width [cm]');
51  ylabel('Table length [cm]');
52  set(gca,'fontsize',14);
53
54  f5=figure('units','inches','position',[1 1 width height]);
55  contourf(xax, yax, A2(6:10,1:5),'ShowText','on');
56  colorbar
57  caxis([0.09 0.35]);
58  xlabel('Table width [cm]');
59  ylabel('Table length [cm]');
60  set(gca,'fontsize',14);
61
```

```matlab
62  f6=figure('units','inches','position',[1 1 width height]);
63  contourf(xax, yax, A2(11:15,1:5),'ShowText','on');
64  colorbar
65  caxis([0.09 0.35]);
66  xlabel('Table width [cm]');
67  ylabel('Table length [cm]');
68  set(gca,'fontsize',14);
69  %————————————
70  A3=load('case3v.txt');
71
72  f7=figure('units','inches','position',[1 1 width height]);
73  contourf(xax, yax, A3(1:5,1:5),'ShowText','on');
74  colorbar
75  caxis([0.09 0.35]);
76  xlabel('Table width [cm]');
77  ylabel('Table length [cm]');
78  set(gca,'fontsize',14);
79
80  f8=figure('units','inches','position',[1 1 width height]);
81  contourf(xax, yax, A3(6:10,1:5),'ShowText','on');
82  colorbar
83  caxis([0.09 0.35]);
84  xlabel('Table width [cm]');
85  ylabel('Table length [cm]');
86  set(gca,'fontsize',14);
87
88  f9=figure('units','inches','position',[1 1 width height]);
89  contourf(xax, yax, A3(11:15,1:5),'ShowText','on');
90  colorbar
91  caxis([0.09 0.35]);
92  xlabel('Table width [cm]');
93  ylabel('Table length [cm]');
94  set(gca,'fontsize',14);
95  %————————————
96  A4=load('case4v.txt');
97
98  f10=figure('units','inches','position',[1 1 width height]);
99  contourf(xax, yax, A4(1:5,1:5),'ShowText','on');
100 colorbar
101 caxis([0.09 0.35]);
102 xlabel('Table width [cm]');
103 ylabel('Table length [cm]');
104 set(gca,'fontsize',14);
105
106 f11=figure('units','inches','position',[1 1 width height]);
107 contourf(xax, yax, A4(6:10,1:5),'ShowText','on');
108 colorbar
109 caxis([0.09 0.35]);
110 xlabel('Table width [cm]');
111 ylabel('Table length [cm]');
112 set(gca,'fontsize',14);
```

```matlab
113
114 f12=figure('units','inches','position',[1 1 width height]);
115 contourf(xax, yax, A4(11:15,1:5),'ShowText','on');
116 colorbar
117 caxis([0.09 0.35]);
118 xlabel('Table width [cm]');
119 ylabel('Table length [cm]');
120 set(gca,'fontsize',14);
121 %—————————
122 A5=load('case5v.txt');
123
124 f13=figure('units','inches','position',[1 1 width height]);
125 contourf(xax, yax, A5(1:5,1:5),'ShowText','on');
126 colorbar
127 caxis([0.09 0.35]);
128 xlabel('Table width [cm]');
129 ylabel('Table length [cm]');
130 set(gca,'fontsize',14);
131
132 f14=figure('units','inches','position',[1 1 width height]);
133 contourf(xax, yax, A5(6:10,1:5),'ShowText','on');
134 colorbar
135 caxis([0.09 0.35]);
136 xlabel('Table width [cm]');
137 ylabel('Table length [cm]');
138 set(gca,'fontsize',14);
139
140 f15=figure('units','inches','position',[1 1 width height]);
141 contourf(xax, yax, A5(11:15,1:5),'ShowText','on');
142 colorbar
143 caxis([0.09 0.35]);
144 xlabel('Table width [cm]');
145 ylabel('Table length [cm]');
146 set(gca,'fontsize',14);
```

- Plume spread for the line source:

```matlab
1 %plume spread, line source
2 clear all
3 clc
4 z=[1.10 1.20 1.30 1.40 1.50 1.60 1.70 1.80];
5 A=load('casePVa.txt');
6 V110=A(1:18, 1);
7 V120=A(19:36, 1);
8 V130=A(37:54, 1);
9 V140=A(55:72, 1);
10 V150=A(73:90, 1);
11 V160=A(91:108, 1);
12 V170=A(109:126, 1);
13 V180=A(127:144, 1);
14 %V120=load('casePVa120.txt');
15 %V130=load('casePVa130.txt');
```

```
16 %V140=load('casePVa140.txt');
17 %V150=load('casePVa150.txt');
18 %V160=load('casePVa160.txt');
19 %V170=load('casePVa170.txt');
20 %V180=load('casePVa180.txt');
21 x=load('xplume.txt');
22
23 V=[V110 V120 V130 V140 V150 V160 V170 V180];
24 %X=[x2, x2, x2, x2, x2, x2, x2, x2 x2 x2 x2 x2 x2 x2 x2 x2 x2];
25 %x=[0 5 10 15 20 25 30 35 40 45 50 55 60 65 70 75 80 85];
26
27 Um=[max(V110) max(V120) max(V130) max(V140) max(V150) max(V160) max(V170)
       max(V180)];
28 Uw=Um/2.71828183;
29 Uw_upper=Um/2;
30 Uw_lower=Um/3;
31
32 n=8;
33 k_w=zeros(1,n);
34 k_m=zeros(1,n);
35 for i=1:n
36     vn=V(:,i);              %<- a vector with all velocities for one height is
         searched under each loop (6 heights = 6 loops)
37     for j=1:18
38     if Uw_lower(i)<vn(j) && Uw_upper(i)>vn(j)       %Searches for Uc-point.
       Must be within set interval.
39         k_w(i)=j;                          %The found index-value j of the Uc-
       point is saved in a vector k_c
40     end
41     end
42     for j=1:18
43     if vn(j)==max(vn)                 %The index-value j of the maximum
       velocity point is saved in a vector k_m
44         k_m(i)=j;
45     end
46     end
47 end
48 disp(k_w)
49 disp(k_m)
50
51 vw_num=[V110(k_w(1)) V120(k_w(2)) V130(k_w(3)) V140(k_w(4)) V150(k_w(5))
       V160(k_w(6)) V170(k_w(7)) V180(k_w(8))]  %makes a vector of the Uc-
       point's location in the room, the x-value of the point
52 xw_loc=[x(k_w(1)) x(k_w(2)) x(k_w(3)) x(k_w(4)) x(k_w(5)) x(k_w(6)) x(k_w
       (7)) x(k_w(8))]
53 xm_loc=[x(k_m(1)) x(k_m(2)) x(k_m(3)) x(k_m(4)) x(k_m(5)) x(k_m(6)) x(k_m
       (7)) x(k_m(8))] %same wit h Um-point's location.
54
55
56 xw=xm_loc-xw_loc;        %Finding the distance between the centerline and the
         location of xc
```

```
57  xw=abs(xw);
58  xw=[0 xw]                %v_num is the respective velocity of the Ind_b at
        the x−values of b_num
59  y1=[0.2 z];
60  y2=[180 z−0.1];
61  b_l=[0.37 0];            %These two points were made to make the linear line
        −fitting pass through the source of the jet/plume.
62  y_l=[1.65 0.34];                %Curve fitting can be found at tools>basic
        fitting in the plot window.
63
64  figure(1)
65  plot(xw,y1,'xb',b_l,y_l,'xr')
66  xlabel('Width from centerline [m]');
67  ylabel('Distance from the floor [m]');
68  set(gca,'fontsize',14);
```

- Script for finding the plume boundary for the head modelled as a point source.

```
1   %point source, head
2   clear all
3   clc
4
5   z=[1.10 1.20 1.30 1.40 1.50 1.60];
6   A=load('point.txt'); %y=150 for alle h?yder
7   V110=A(1:18, 1);
8   V120=A(19:36, 1);
9   V130=A(37:54, 1);
10  V140=A(55:72, 1);
11  V150=A(73:90, 1);
12  V160=A(91:108, 1);
13  V170=A(109:126, 1);
14  V180=A(127:144, 1);
15
16  B=load('xplume.txt');
17  x=B(1:18,1);
18
19  V=[V110 V120 V130 V140 V150 V160];
20  X=[x, x, x, x, x, x];
21  %x=[0 5 10 15 20 25 30 35 40 45 50 55 60 65 70 75 80 85];
22
23  Um=[max(V110) max(V120) max(V130) max(V140) max(V150) max(V160)];
24  Uw=Um/2.71828183;
25  Uw_upper=Um/1;
26  Uw_lower=Um/10;
27
28  n=6;
29  k_w=zeros(1,n);
30  k_m=zeros(1,n);
31  for i=1:n
32      vn=V(:,i);             %<− a vector with all velocities for one height is
            searched under each loop (6 heights = 6 loops)
33      for j=1:18
```

131

```matlab
34       if Uw_lower(i)<vn(j) && Uw_upper(i)>vn(j)      %Searches for Uc−point.
      Must be within set interval.
35           k_w(i)=j;                          %The found index−value j of the Uc−
      point is saved in a vector k_c
36       end
37       end
38       for j=1:18
39       if vn(j)==max(vn)                %The index−value j of the maximum
      velocity point is saved in a vector k_m
40           k_m(i)=j;
41       end
42       end
43 end
44 disp(k_w)
45 disp(k_m)
46
47 vw_num=[V110(k_w(1)) V120(k_w(2)) V130(k_w(3)) V140(k_w(4)) V150(k_w(5))
      V160(k_w(6))]  %makes a vector of the Uc−point's location in the room,
       the x−value of the point
48 xw_loc=[x(k_w(1)) x(k_w(2)) x(k_w(3)) x(k_w(4)) x(k_w(5)) x(k_w(6))]
49 xm_loc=[x(k_m(1)) x(k_m(2)) x(k_m(3)) x(k_m(4)) x(k_m(5)) x(k_m(6))] %same
       wit h Um−point's location.
50 vv=[V110(k_m(1)) V120(k_m(2)) V130(k_m(3)) V140(k_m(4)) V150(k_m(5)) V160(
      k_m(6))]
51
52
53 xw=xm_loc−xw_loc;      %Finding the distance between the centerline and the
       location of xc
54 xw=abs(xw);
55 xw=[0 xw]              %v_num is the respective velocity of the Ind_b at
      the x−values of b_num
56 y1=[0.2 z];
57 y2=[180 z−0.1];
58 b_l=[0.24 0];          %These two points were made to make the linear line
      −fitting pass through the source of the jet/plume.
59 y_l=[1.5 0.84];               %Curve fitting can be found at tools>basic
      fitting in the plot window.
60
61 figure(1)
62 hold on
63 plot(xw,y1,'xb',b_l,y_l,'xr')
64 xlabel('Width from centerline [m]');
65 ylabel('Distance from the floor [m]');
66 set(gca,'fontsize',14);
67 hold off
68
69 y=[0.8 0.9 1.0 1.1 1.2 1.3 1.4 1.5 1.6 1.7 1.8];
70 figure(2)
71 %plot(vw_num,z)
72 %plot(vv,z)
73 hold on
```

```
74  plot(Um,z)
```

- Plume boundary above the stomach done by Method 1:

```
1  %spreading angle for thermal plume at y=90
2  clear all
3  clc
4  z=[1.10 1.20 1.30 1.40 1.50 1.60 1.70 1.80];
5  A=load('casePy90source.txt');
6  V110=A(1:18, 1);
7  V120=A(19:36, 1);
8  V130=A(37:54, 1);
9  V140=A(55:72, 1);
10 V150=A(73:90, 1);
11 V160=A(91:108, 1);
12 V170=A(109:126, 1);
13 V180=A(127:144, 1);
14 %V120=load('casePVa120.txt');
15 %V130=load('casePVa130.txt');
16 %V140=load('casePVa140.txt');
17 %V150=load('casePVa150.txt');
18 %V160=load('casePVa160.txt');
19 %V170=load('casePVa170.txt');
20 %V180=load('casePVa180.txt');
21 x=load('xplume.txt');
22
23 V=[V110 V120 V130 V140 V150 V160 V170 V180];
24 %X=[x2, x2, x2, x2, x2, x2, x2, x2 x2 x2 x2 x2 x2 x2 x2 x2 x2];
25 %x=[0 5 10 15 20 25 30 35 40 45 50 55 60 65 70 75 80 85];
26
27 Um=[max(V110) max(V120) max(V130) max(V140) max(V150) max(V160) max(V170)
      max(V180)];
28 Uw=Um/2.71828183;
29 Uw_upper=Um/1.4;
30 Uw_lower=Um/4;
31
32 n=8;
33 k_w=zeros(1,n);
34 k_m=zeros(1,n);
35 for i=1:n
36     vn=V(:,i);            %<- a vector with all velocities for one height is
        searched under each loop (6 heights = 6 loops)
37     for j=1:18
38     if Uw_lower(i)<vn(j) && Uw_upper(i)>vn(j)    %Searches for Uc-point.
        Must be within set interval.
39         k_w(i)=j;                        %The found index-value j of the Uc-
        point is saved in a vector k_c
40     end
41     end
42     for j=1:18
43     if vn(j)==max(vn)              %The index-value j of the maximum
        velocity point is saved in a vector k_m
```

133

```
44          k_m( i )=j ;
45      end
46      end
47 end
48 disp ( k_w )
49 disp ( k_m )
50
51 vw_num=[V110(k_w(1)) V120(k_w(2)) V130(k_w(3)) V140(k_w(4)) V150(k_w(5))
      V160(k_w(6)) V170(k_w(7)) V180(k_w(8))]  %makes a vector of the Uc−
      point's location in the room, the x−value of the point
52 xw_loc=[x(k_w(1)) x(k_w(2)) x(k_w(3)) x(k_w(4)) x(k_w(5)) x(k_w(6)) x(k_w
      (7)) x(k_w(8))]
53 xm_loc=[x(k_m(1)) x(k_m(2)) x(k_m(3)) x(k_m(4)) x(k_m(5)) x(k_m(6)) x(k_m
      (7)) x(k_m(8))] %same wit h Um−point's location .
54
55
56 xw=xm_loc−xw_loc;       %Finding the distance between the centerline and the
          location of xc
57 xw=abs (xw) ;
58 xw=[0 xw]              %v_num is the respective velocity of the Ind_b at
      the x−values of b_num
59 y1=[0.2 z ];
60 y2=[180 z −0.1];
61 b_l=[0.5 0];            %These two points were made to make the linear line−
      fitting pass through the source of the jet/plume.
62 y_l=[1.6 0.055];              %Curve fitting can be found at tools>basic
      fitting in the plot window.
63
64 figure (1)
65 plot (xw, y1 , 'xb' , b_l , y_l , 'xr ' )
66 xlabel ( 'Width from centerline [m] ' ) ;
67 ylabel ( 'Distance from the floor [m] ' ) ;
68 set ( gca , 'fontsize ' ,14) ;
```

- Plume boundary above the stomach done by Method 2:

```
1 %model made from y=90
2 clear all
3 clc
4
5 z =[1.10 1.20 1.30 1.40 1.50 1.60 1.70 1.80];
6 b=[0.515738974 0.460541736 0.522745638 0.413239184 0.469677622 0.412471434
      0.417440729 0.425];
7 Umax=[0.094097222 0.109635417 0.091666667 0.131597222 0.109722222
      0.111284722 0.124131944 0.138715278];
8 figure (1)
9
10 %figure (2)
11 y1=[0.2 z ];
12 b_l=[0.5 0];
13 y_l=[1.55 0.055];
14 hold on
```

```
15  scatter(b,z,'xb')
16  scatter(b_l,y_l,'xr');
17  %plot(xw,y1,'xb',b_l,y_l,'xr')
18  xlabel('Width from centerline [m]');
19  ylabel('Distance from the floor [m]');
20  set(gca,'fontsize',14);
21  hold off
22
23  figure(2)
24  %centerline velocity
25  plot(Umax,z);
26
27  figure(4)
28  A=load('cbgc.txt');
29  zax=A(1,1:17);
30  tp110=A(2,1:17);
31  tp120=A(3,1:17);
32  tp130=A(4,1:17);
33  tp140=A(5,1:17);
34  tp150=A(6,1:17);
35  tp160=A(7,1:17);
36  tp170=A(8,1:17);
37  tp180=A(9,1:17);
38  figure(4)
39  plot(zax, tp110)
40  hold on
41  plot(zax, tp120)
42  plot(zax, tp130)
43  plot(zax, tp140)
44  plot(zax, tp150)
45  plot(zax, tp160, 'c')
46  plot(zax, tp170, 'r')
47  plot(zax, tp180, 'm')
48
49  axis([-0.4 0.4 0.05 0.15]);
50  grid
51  set(gca,'fontsize',14);
52  xlabel('Distance [m]');
53  ylabel('Velocity [m/s]');
54  legend('z=110 cm','z=120 cm', 'z=130 cm', 'z=140 cm', 'z=150 cm', 'z=160
        cm', 'z=170 cm', 'z=180 cm');
55  hold off
```

- Comparison of different methods and formulas:

```
1  %centerline velocity for mine formmler og m?lt. over mage
2  %Felles konstanter
3  g=9.81; %[m/s^2]
4  cp=1; %specific heat of air [kJ/kgK]
5  rho=1.2; %density [kg/m^3]
6  b=1/300; %volumetrisk termisk utvidelseskoeffisient
7  T0=273+25; %ambient temperature [K]
```

```
 8 Ta=273+32; %body surface temperature [K]
 9 W=80; %human body weight [kg]
10 H=180; %human height [cm]
11 l=0; %lenght of the source
12 %z=1; %height
13 z0=0; %virtual origin above the source, negative
14 %z=[0 0.2 0.4 0.6 0.8 1 1.2 1.4];
15 %z0=[0 0 0 0 0 0 0 0];
16
17 %DuBois and DuBois surface area
18 A=0.007184*(W^0.425)*(H^0.725);
19
20 %Convective surface area of a person in supine position
21 Ac=0.811*1.98;
22
23 %Heat transfer coefficient for a supine body innatural convection
24 hc=0.881*(Ta-T0)^0.368;
25
26 %Convective heat release for a supine body[kW]
27 Qc=hc*Ac*(Ta-T0)/1000;
28 Qk=hc*Ac*(Ta-T0);
29 %
     _____

30 %Point source
31 z=[0:0.005:2];
32 %m? lt
33 Umalt=[0.094097222 0.109635417 0.091666667 0.131597222 0.109722222
       0.111284722 0.124131944 0.138715278];
34 zax=[1.045 1.145 1.245 1.345 1.445 1.545 1.645 1.745];
35 figure(1);
36 scatter(Umalt,zax);
37 hold on
38 Ucb1=3.31*(g*b)^(1/3)*(rho*cp)^(-1/3)*(Qc^(1/3))*((z+z0).^(-1/3));
39 plot(Ucb1,z);
40 Ucb2=3.39*(g*b)^(1/3)*(rho*cp)^(-1/3)*(Qc^(1/3))*((z+z0).^(-1/3));
41 plot(Ucb2,z);
42 u0=3.4*(g/(cp*rho*T0))^(1/3)*(Qc)^(1/3)*(z-z0).^(-1/3);
43 plot(u0,z);
44 um=1.28*(Qc^(1/3))*((z+z0).^(-1/3));
45 plot(um,z);
46 v_yo=0.128*(Qk^(1/3))*z.^(-1/3);
47 %plot(v_yo,z);
48
49 ylabel('Height above point source [m]');
50 xlabel('Velocity [m/s]');
51 legend('Measured U0', 'Method 1', 'Method 2', 'Heskestad (1984)','Skaaret
       (2000)', 'Mierzwinski (1981)/Popiolek (1981)');
52 set(gca,'fontsize',14);
53 grid
```